A role for *diaphanous homolog 3* in the mammalian auditory system

by

Cynthia J. Schoen

A dissertation submitted in partial fulfillment
of the requirements for the degree of
Doctor of Philosophy
(Neuroscience)
in The University of Michigan
2012

Doctoral Committee:

Professor Margit Burmeister, Chair
Professor Marci M. Lesperance
Professor Miriam H. Meisler
Professor Yehoash Raphael
Associate Professor Robert K. Duncan

Dedication

To my husband, George, from whom I learn daily

Acknowledgements

Dr. Margit Burmeister has guided me well through these last years. Although I did not join her lab with the intention of studying hearing, I am very glad she suggested this challenging and highly rewarding project and field. I am grateful for everything she has taught me.

I would also like to thank Dr. Marci Lesperance, who has supported this project—and me—in so many ways.

I have learned a lot from interacting with my committee members, Margit, Marci, Dr. Miriam Meisler, Dr. Yehoash Raphael, and Dr. Keith Duncan. They have all helped me to become a better and more confident presenter and researcher, and they have all shown their support in important ways.

The members of the Burmeister lab have been a wonderful support system, and I would like to thank all of the past and present members, but especially Ela Sliwerska, Dr. Viktoriya Strumba, Kristine Sikora, Randi Burns, and Dr. Sandra Villafuerte. Each of them has helped me in big and small ways, and they have become my friends in the process.

Thank you to Sarah Emery, who worked tirelessly on this project before graciously letting me take it in a new direction.

In addition to everyone mentioned above, there have been numerous people who have helped me scientifically in the last years. To mention just a few: I would like to thank Yehoash again; he was always willing to share his time and knowledge. Ariane

Kanicki and Lisa Beyer have both given me lessons, tips, and suggestions for preparing, staining, and visualizing mouse cochleae. I am grateful to Dr. Mirna Mustapha, who was the first person to show me how to separate a mouse from its cochleae. Dr. Gustavo Patino gave me lessons on Northern blotting (and also happens to be a wonderful friend).

Dr. Bill Freed and Dr. Joe Sanchez at the National Institute on Drug Abuse in Baltimore, Maryland, let me into the lab and taught me so much about doing research and enjoying life. It was a wonderful introduction to a new world.

I would not have been here without the encouragement of my friend, Dr. Jennifer Snyder-Cappione, whom I followed, with her help and support, into the wonderful and frustrating world of science.

Special thanks to Dr. Adrienne Wang and Dr. Elizabeth Gibbs. They made the time pass much more quickly and much more slowly, whatever the moment called for.

My parents, Vulgens and Betty Schoen, are not scientists by training, but I see now that they have always had the hearts of scientists and have always approached problems scientifically. I owe to them my abiding curiosity in almost everything. Thanks, also, to Luise, the family artist and comedienne, and Walter, the family mathematician and, in many ways, my Doppelgänger.

Finally, I would like to thank Dr. George Mashour, who has been with me through this from (almost) the beginning. He has supported and encouraged me all along—but especially when I needed it most.

Table of Contents

List of Figures

List of Tables

List of Appendices

List of abbreviations

ABR	auditory brainstem response
AUNA1	autosomal dominant, auditory neuropathy 1
Ct	threshold cycle
CtBP2	C-terminal Binding Protein 2
DAD	diaphanous autoregulatory domain
DFNA	deafness, autosomal dominant
DFNB	deafness, autosomal recessive
DID	diaphanous inhibitory domain
DPOAE	distortion product otoacoustic emissions
DRF	diaphanous-related formin
FDR	false discovery rate
GBD	GTPase-binding domain
IHC	inner hair cell
JO	Johnston's organ
LCL	lymphoblastoid cell line
MET	mechanoelectrical transduction
OAE	otoacoustic emissions
OHC	outer hair cell
SAM	Significance Analysis of Microarray
SGC/SGN	spiral ganglion cell/neuron

Chapter 1
Introduction

The mammalian peripheral auditory system

The Italian anatomist Alfonso Corti first described the anatomy of the inner ear organ that bears his name in 1851[1]. In the 160 years that have followed, we have begun to develop an understanding of how the organ of Corti functions to allow mammals to process sound waves. What follows is an abbreviated description of the hearing process, with emphasis on the subjects that will be relevant for later discussions.

The cascade of events that accompany the perception of sound begins when sound waves are directed by the pinnae toward the outer ear canal and transmitted by the ossicles of the middle ear to the spiral shaped cochlea that houses the organ of Corti (Figure 1-1). The organ of Corti, in which the primary sensory cells, neurons, and various supporting cells of the auditory system are located, is situated on top of the basilar membrane (Figure 1-2A). The sound waves that are transmitted to the cochlea perturb the basilar membrane at positions along the organ of Corti that correspond to the frequency of the sound waves, with higher frequencies perturbing the membrane at the base of the cochlea and lower frequencies at the apex. The primary sensory cells consist of one row of inner hair cells (IHCs) and three rows of outer hair cells (OHCs) (Figure 1-2A). Hair cells (HCs) typically have three rows comprised of dozens of actin-rich stereocilia protruding from their apical surfaces into the endolymph of the cochlea's middle chamber (of three). The perturbations of the basilar membrane lead to the deflection of the

stereocilia toward the tallest row, or toward the stria vascularis (Figure 1-2B). Each row of stereocilia is connected to the adjacent row by tip links (Figure 1-3) that are linked to gating springs (currently unidentified) that gate mechanoelectrical transduction (MET) channels on the two shorter rows of stereocilia[2-4]. Deflection of the stereocilia increases tension on the tip links and opens the channels by pulling on the gating springs[5]. Opening of the channels results in depolarization and subsequent release of neurotransmitter vesicles from the synapse at the basal end of the hair cell.

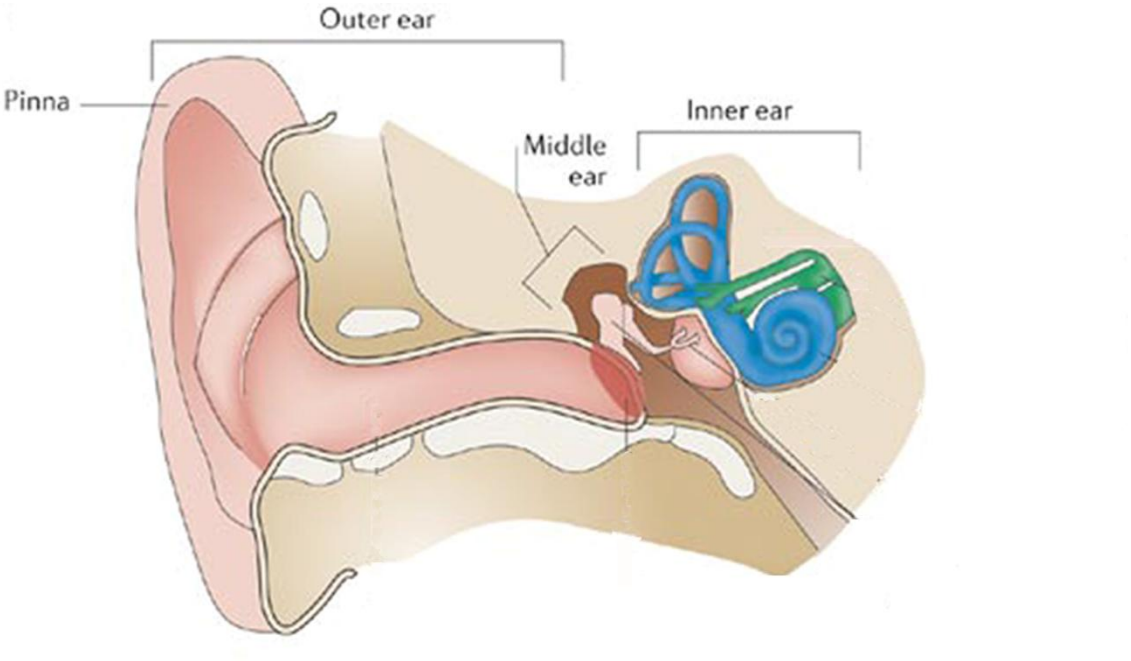

Figure 1-1. A schematic of the major structures of the human outer, middle, and inner ear. The cochlea is shown in blue. Modified from (Kelley, 2006)[6].

The IHCs and OHCs are anatomically and molecularly similar in many ways but there are important distinctions that confer differential functionality. The primary difference, and the one most relevant to this discussion, is that approximately 90-95% of the afferent fibers of the auditory system synapse on the IHCs, while the OHCs,

conversely, are primarily the target for efferent fibers[7,8]. IHCs, therefore, provide the main input to the auditory cortex. The OHCs act as cochlear amplifiers by expanding and contracting the shape of their somata[9]. Each IHC synapses with approximately 10-30 type I afferent spiral ganglion neurons (SGN), while each type I afferent SGN synapses on only one IHC[7]. These synapses, called ribbon synapses, are specialized to provide sustained neurotransmitter release and are named for their appearance in transverse sections, in which a central, often elongated, density is surrounded on all sides by tethered vesicles[10] (schematic shown in Figure 1-4). It is believed that this tethering of multiple vesicles at the pre-synaptic site allows for precisely timed release of vesicles, graded responses, and continuous activity[10]. As suggested by the diverse and heterogeneous genes and mutations that have been identified as responsible for hearing loss, disruption of any of the structures and processes of the initial stages of hearing briefly described above may result in deafness.

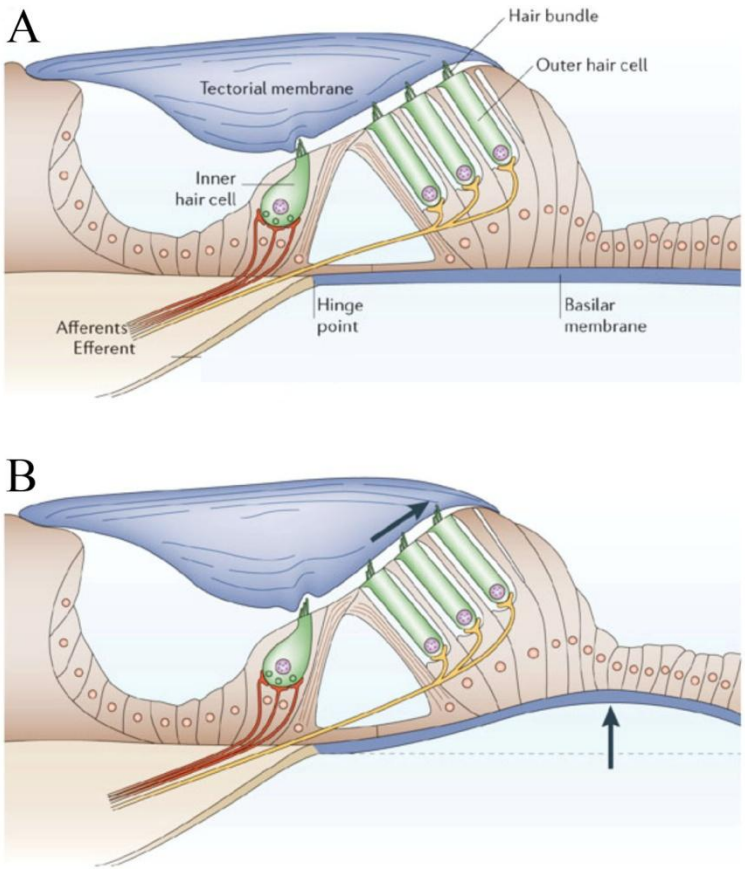

Figure 1-2. A cross section of the organ of Corti. (A) The IHCs and OHCs are the primary sensory cells of the cochlea. (B) Stimulation of hair cells is initiated by movement of the basilar membrane. The stereocilia are deflected toward the direction of the stria vascularis, not shown, which would be distal to the OHCs. Modified from (Fettiplace and Hackney, 2006)[11].

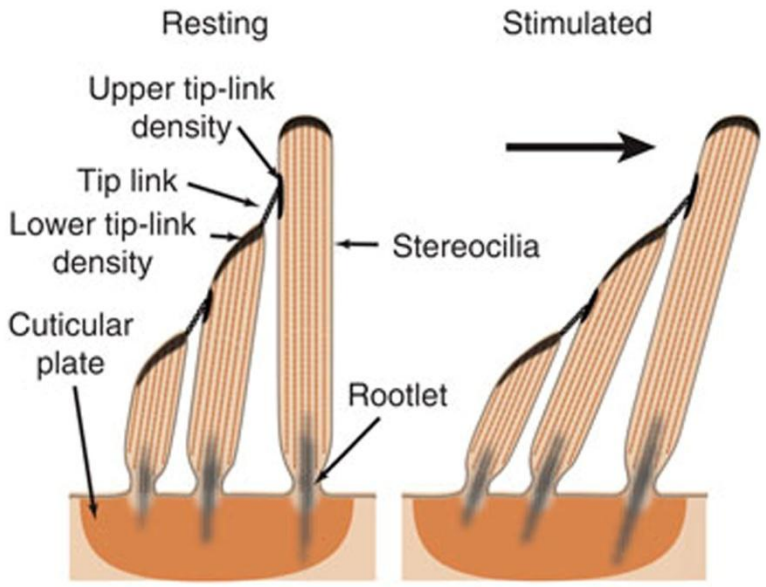

Figure 1-3. Three rows of stereocilia extend from the apical surface of auditory hair cells. Deflection of stereocilia results in the opening of MET channels at the lower end of the tip links that adjoin each row of stereocilia. The stereocilia are anchored to the cuticular plate at the apical surface of the hair cell via rootlets. From (Peng et al., 2011)[12].

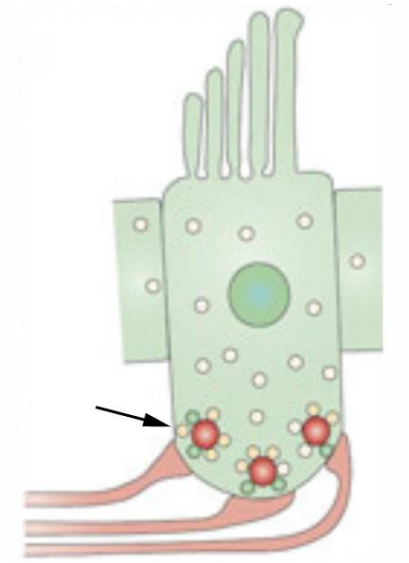

Figure 1-4. Schematic of an inner hair cell. Ribbons (an arrow points to one of three shown here) are structures at the base of the IHC from which neurotransmitter is released. The red center represents a central density to which multiple neurotransmitter-filled vesicles are tethered. Modified from (Matthews and Fuchs, 2010)[10].

Overview of deafness

According to a governmental national household survey, 20.3 million individuals, or 8.6% of the United States population, experience some degree of hearing loss[13]. This loss results in a decreased ability to communicate and interact with others and, often, a decreased quality of life. Estimates suggest that approximately 1 out of every 1000 infants in the United States is born with hearing loss[14]. Approximately 50% of these cases are due to gene mutations[15]. Monogenic forms of deafness can be recessive (which account for 77% of genetic deafness), dominant (22%), sex-linked (1%), or mitochondrial (<1%)[15]. The majority of cases of recessive deafness is congenital or prelingual, while most cases of dominant deafness are postlingual and progressive[16]. Surprisingly little is known about the epidemiology of postlingual or progressive hearing loss; household surveys generally do not differentiate between hearing loss acquired through noise trauma or ototoxic drug exposure and genetic hearing loss[15]. Non-genetic causes of hearing loss include environmental noise exposure, infection, and exposure to ototoxic drugs, such as aminoglycoside antibiotics or certain chemotherapeutic agents[17]. Age-related hearing loss is a complex disorder, thought to be the result of a combination of genes and environment, and the relative contribution of each of these elements is highly variable[18]. Although, based on chromosome map positions, more than 100 non-syndromic deafness loci are known to exist, only approximately half of the responsible genes have been identified (hereditaryhearingloss.org; accessed March 31, 2012).

Genetic, nonsyndromic, auditory neuropathy

Hearing loss generally can be classified as conductive, sensorineural, or both. Conductive hearing loss involves a defect of the sound conduction mechanism or the outer and/or middle ear, while sensorineural hearing loss involves the cochlea and/or auditory nerve[16]. Sensorineural hearing loss can be further classified as sensory, a disorder of the IHCs and OHCs of the cochlea, or neural, a disorder of the auditory nerve. Auditory neuropathy is a form of neural deficit defined by normal OHC function but absent or abnormal auditory brainstem response[19].

In auditory neuropathy, the OHCs function normally as evidenced by the presence of otoacoustic emissions (OAEs), while the deficit lies in the IHCs, the auditory nerve, or the intervening synapse[19]. In cases of selective IHC dysfunction, the term auditory neuropathy may be considered a misnomer. In human subjects, however, current technology does not allow us to differentiate easily between hearing loss due to an IHC deficit (pre-synaptic) and hearing loss due to a defect of the nerve (post-synaptic).

Auditory brainstem responses (ABRs) are the evoked potentials derived from the polysynaptic auditory processing pathway in response to acoustic input. This input may be, for example, a series of tones played at various frequencies at various sound intensities. In humans, these are measured by placing recording electrodes on the scalp, while in mice they are measured with needle electrodes. When comparing two subjects, a subject who has poorer hearing and therefore requires louder intensities to elicit a brainstem response at a given frequency will have a higher auditory threshold. Distortion product otoacoustic emissions (DPOAEs) are generated by functional OHCs when two tones of certain relative frequency are presented simultaneously to the ear canal of a subject; healthy OHCs generate additional components (OAEs) that can be recorded from

the ear canal[20]. Neither ABRs nor DPOAEs requires the subject to be conscious or able to respond, and both may be performed on newborns or anesthetized laboratory animals to screen hearing. For humans, often only one of these tests is used, despite the fact that measuring ABRs alone does not provide sufficient information to differentiate between auditory neuropathy and sensory hearing loss, a useful distinction when planning genetic testing.

There is a limited number of genes associated with auditory neuropathy. Some of these are responsible for syndromic auditory neuropathy[21], but only two are commonly associated with nonsyndromic auditory neuropathy. Mutations in *OTOF*, which encodes the calcium-sensing protein otoferlin, result in impaired exocytosis at the ribbon synapse of the IHC of mice[22,23]. Mutations in *PJVK*, which encodes pejvakin, was initially identified as *DFNB59* and subsequently localized exclusively to auditory neurons in mouse models[24]. Others, however, have identified pejvakin in the hair cells of the vestibular and auditory systems (both IHCs and OHCs) of mouse models, which would suggest a role for this protein in cochlear processes in addition to its unidentified role in the auditory nerve[25]. Human mutations identified in *PJVK* confirm that this gene may cause either auditory neuropathy or sensory hearing loss[24,26]. The specific roles of pejvakin in the inner ear, however, have not yet been elucidated.

AUNA1 family

In addition to the two genes described above, another auditory neuropathy locus, autosomal dominant 1 (*AUNA1*), was identified in a large family in 2004[27,28]. There is a wide age range of hearing loss onset (7 to 45 years, often based on self-report) with *AUNA1*, but the average age of onset is 18.6 years[28]. Hearing loss in this family is

progressive, and individuals become profoundly deaf within approximately 20 to 30 years of disease onset[27]. Patients initially present with normal DPOAEs and elevated ABR thresholds, but at later time points OAEs are no longer present[27]. Higher frequencies are affected to a greater extent than lower frequencies[27], as is typical of the majority of forms of hearing loss[16]. Patients were examined for additional peripheral neuropathies but none were identified[27].

Three individuals with *AUNA1* who had received cochlear implants were tested for electrically evoked ABR, and in each case cochlear implantation restored a peak at Wave V (thought to reflect activity at the inferior colliculus)[27]. Additionally, two of the three subjects showed improved speech recognition at the time of formal testing, and the authors note that the third also reported improvement in speech comprehension at a later point[27]. The efficacy of cochlear implants in individuals with *AUNA1* has significant implications for the possible mechanism of hearing loss. The electrodes of cochlear implants stimulate different populations of SGNs[29,30], and when significant numbers of SGNs or their myelin sheaths are absent or ineffective due to dysfunction or disease, cochlear implants become less effective[31]. Successful use of cochlear implants, then, suggests that the cell bodies and axons of the SGCs are relatively healthy. The site of the lesion in this case, therefore, is likely to be localized to the IHCs, the terminal dendrites of the auditory nerve, or the synapses between them, but not to the SGC bodies[19].

The locus containing the gene mutation responsible for *AUNA1* was determined by linkage analysis to map to an 18 Mb interval on chromosome 13q14-q21[28]. Genomic DNA from 33 affected individuals, 10 unaffected family members, and 4 unrelated spouses was used to identify differences in microsatellite markers in order to identify

regions of DNA that were shared by all affected individuals but not by unaffected individuals[28]. Although the interval contains approximately 40 genes, there were several that stood out as interesting biological candidates. Only *diaphanous homolog 3* will be discussed here.

Diaphanous homologs 1, 2, and *3*

Like the protocadherins, *diaphanous homolog 3*, or *DIAPH3*, was identified as a biological candidate of interest because there is precedent for the involvement of a related gene in hearing loss. A mutation in *DIAPH1*, another diaphanous-related formin, was identified as the cause of dominant, nonsyndromic *DFNA1* deafness[32]. The mutation in *DIAPH1* leads to a frameshift and insertion of 21 amino acids before encountering a stop codon; in addition to inserting 21 aberrant amino acids, 32 of the wild-type C-terminal amino acids are not incorporated into the mutant protein[32]. A *Diap1* knockout mouse is afflicted with splenomegaly and myelodysplasia, but no auditory phenotypes or other abnormalities are observed[33]. *DIAPH2* and *DIAPH3* have also been implicated in human disorders. A translocation breakpoint that interrupts *DIAPH2* on the X chromosome has been associated with human premature ovarian failure[34]. Finally, a recent paper suggests that mutations in *DIAPH3* may confer susceptibility to autism in humans[35].

Drosophila diaphanous (*dia*) was initially identified in 1993 in a screen of *Drosophila* spermatogenesis mutants to identify genes important for germ cell meiosis and mitosis[36]. A year later, the same group showed that *dia* is required for cytokinesis in both somatic and germline cells as well as both mitosis and meiosis[37]. It was also noted that two of the dia protein domains were similar to murine formin proteins[37].

While *Drosophila* has only a single *diaphanous* gene, mammals have three orthologs. *DIAPH3* and its paralogs, *DIAPH1* and *DIAPH2*, encode diaphanous-related formins, a family of proteins that is involved in actin regulation both through nucleation of *de novo* unbranched actin filaments[38,39] and control of the elongation rate of existing unbranched actin filaments[40]. These formins are also known to be involved in microtubule stabilization[41]. Because of their fundamental roles in cytoskeleton dynamics, these proteins are involved in many cellular processes, including cell division[42,43], endosome trafficking[44], and cell migration and motility[45,46], among others.

The protein product of *DIAPH3*, somewhat confusingly called mDia2, consists of several regulatory and binding domains (Figure 1-5). The GTPase-binding domain (GBD), the diaphanous inhibitory domain (DID), and the diaphanous autoregulatory domain (DAD) interact to either inhibit or activate mDia2 homodimers. Binding of Rho-GTPases to the GBD interrupts the inhibitory interaction of the DID and DAD, allowing the protein to become activated[47]. A dimerization domain (DD) and coiled-coil region (CC) have been suggested to be involved in both homodimerization and autoinhibition[48,49]. Finally, the formin homology 1 and 2 (FH1 and FH2) domains mediate the effect of the protein on actin and microtubules[48]. The FH1 domain contains multiple regions of consecutive prolines and has been shown to bind profilin in a number of systems[50-52]. The FH2 domain is the most highly conserved of the diaphanous domains, and it binds to the barbed, fast-growing ends of actin filaments[53,54]. In addition to their effects on actin, mDia2 FH1 and FH2 also bind and stabilize microtubules[41].

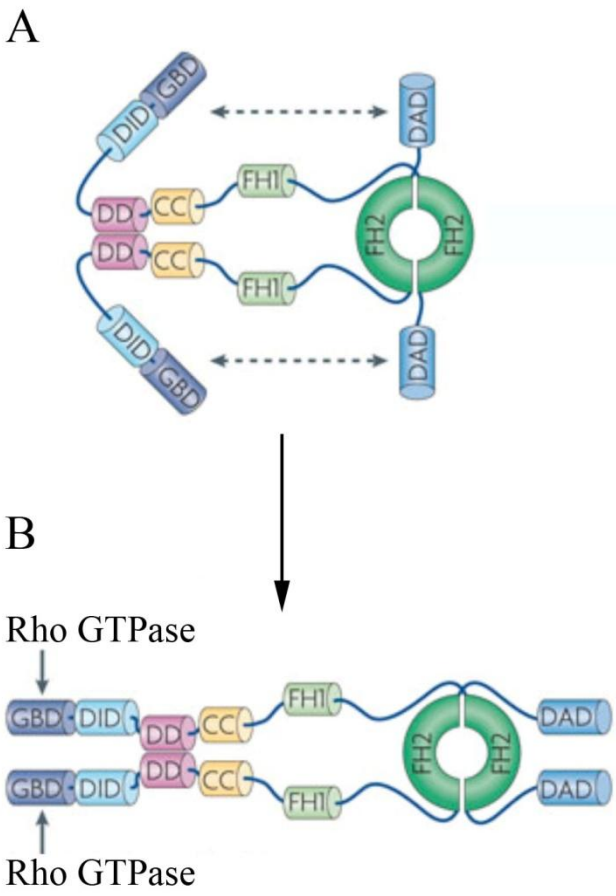

Figure 1-5. Autoinhibited and activated mDia2, the protein product of *DIAPH3*. (A) DAD interacts with DID to prevent mDia2 homodimers from nucleating and polymerizing actin. (B) Binding of Rho-GTPases to the GBD relieves autoinhibition. GBD, GTPase-binding domain; DID, Diaphanous inhibitory domain; DD, dimerization domain; CC, coiled-coil region; FH1, Formin homology 1 domain; FH2, Formin homology 2 domain; DAD, Diaphanous autoregulatory domain. Modified from (Campellone and Welch, 2010)[49].

Because of its roles in cytoskeleton dynamics, mDia2 is an attractive candidate for a role in hearing loss. Actin and microtubules play major, but often underappreciated, roles in pre-synaptic and post-synaptic cytoskeleton dynamics[55,56], either of which may be at work in the IHC synapses of individuals with *AUNA1*. Additionally, the apical end

of the IHC is rich in actin and microtubules; actin and tubulin are major components of the cuticular plate, and the stereocilia are themselves actin-filled structures[57,58].

Mouse and *Drosophila* models of hearing loss

Generating animal models of human disorders, and of deafness disorders in particular, has proven to be extremely useful. First, animal models of human disorders provide additional evidence that a suspected mutation is in fact responsible for the human disorder. Although there may be very strong evidence that an identified mutation is the causative factor, the strongest evidence, perhaps, is a mouse model of a single gene mutation that recapitulates the phenotype of interest. Second, mouse models of human disorders provide a source of tissue that can be used to study the consequences of the mutation morphologically, molecularly, and physiologically. This is particularly important in systems of the human body that are not easily accessible to researchers, including the peripheral auditory system. Third, tissues and organs from these mouse models can be used to study the downstream consequences of the primary genetic alteration. They can, for example, be used in microarray expression analyses to identify genes that are affected by dysregulation of the gene of interest. Finally, mouse models of human disorders can be used to test potential therapeutic interventions, and preventing or reversing human disease is generally considered to be the ultimate goal of all biomedical research.

Mouse models of human deafness disorders have proved to be excellent tools for elucidating the normal and pathological molecules involved in sound transduction. Many genes important for human hearing have been identified by comparing wild-type mice to mice that have hearing deficits due to random mutagenesis (e.g. naturally occurring or

ENU-induced). Conversely, mutations initially identified in humans can be genetically manipulated in mice to generate models that can be used to identify the molecular mechanisms responsible for hearing loss, which further illuminates our understanding of normal hearing.

There is a limited number of models of genetic or chemically-induce auditory neuropathy in which ABRs are normal but OAEs are absent or abnormal. In addition to the *Otof* and *Pjvk* mouse models discussed above, a null allele of *Slc17a8* results in elevated ABR thresholds but preserved OAEs in mice due to defective glutamate release at the IHC synapse[59]. The IHCs of the Bronx waltzer mouse selectively degenerate during development[60]. In a somewhat unusual model, *Slc19a2* knockout mice selectively lose IHCs with relative preservation of OHCs when fed a thymine deficient diet[61]. Among the most common chemically-induced mouse models are administration of carboplatin or ouabain; intravenous carboplatin administration in chinchilla selectively damages IHCs[62], while ouabain exposure in gerbils damages type I SGNs[63,64].

Mammalian models of hearing loss have been joined by other models, such as *Drosophila melanogaster*. Most *Drosophila* genes can be knocked out, knocked down, overexpressed, or mutated[65], and it has been estimated that as many as 75% of genes that cause disorders in humans have related genes in *Drosophila*, including a number of deafness genes[66].

One powerful tool of *Drosophila* genetics is the UAS-Gal4 system, which allows researchers to drive expression of a gene of interest in restricted cell types (reviewed in Muqit and Feany, 2002[67]). In this system, two fly lines are created and crossed. In the so-called driver line, the GAL4 yeast transcriptional activator is placed downstream of a

tissue- or cell-specific promoter. GAL4 is then expressed in those tissues or cells with no effect on the organism. In the transgene line, the gene of interest is placed downstream of an upstream activating sequence (UAS), which has binding sites for GAL4. The gene of interest will not be expressed unless GAL4 is present. When the driver and transgene lines are crossed, the offspring will express the gene of interest in those cells in which GAL4 is also expressed. Many different driver lines have been generated and are available for use, including driver lines for the Drosophila auditory organ, the Johnston's organ (JO).

Using this system, researchers have demonstrated that mutant alleles of mammalian deafness gene homologs, including *diaphanous, forked* (homolog of espin), and *crinkled* (homolog of myosin VIIA), also result in hearing loss in *Drosophila*[68,69]. Although the *Drosophila* hearing system is anatomically very different from the mammalian auditory system (compare Figure 1-6 to 1-1 and 1-2), it is thought to have evolved from a common primitive sensory apparatus[70]. Johnston's organ is a chordotonal organ that is housed in the second antennal segment (Figure 1-7). Chordotonal organs function as stretch receptors and are able to transduce various stimuli[71]. In *Drosophila*, motion generated by sound waves is transferred by the arista through the third antennal segment from which the arista protrudes, to the JO in the second antennal segment. The joint shared by the two antennal segments is rotated in one of two directions, and displacement in one direction stretches the cilia of the chordotonal neurons, which results in an action potential[71]. One significant difference between the mammalian cochlea and the JO is the composition of the structural core of the sensory receptors. Unlike the stereocilia of mammalian hair cells, which are composed of bundled, unbranched, actin

filaments (and are therefore more closely related to microvilli than to cilia), the cilia of the JO sensory units are true cilia, composed of microtubules[72].

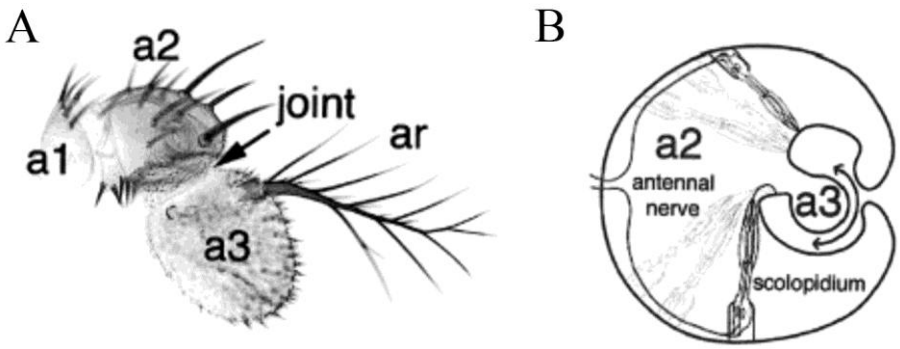

Figure 1-6. The sensory structures of the auditory system of *Drosophila melanogaster*. (A) The arista (ar), which transmits sound waves to the hearing organ, extends from the third antennal segment (a3). The joint that is displaced as a result of movement of the arista is indicated. Modified from (Boekhoff-Falk, 2005)[73]. (B) The *Drosophila* hearing organ, or Johnston's organ, is located in the second antennal segment (a2). The sensory units, or scolopidia, are stretched or relaxed when the joint between a2 and a3 is rotated in one direction or the other[70]. Stretching of the scolopidia is thought to open MET channels that result in an electrical signal that is propagated through the antennal nerve[73]. Only a few of the 150-200 scolopida are shown. Modified from (Caldwell and Eberl, 2002)[70].

In addition to the hearing loss genes mentioned above, the *Drosophila* genes *atonal* and *spalt* have been shown to be required for JO specification, and their mammalian homologs (atonal homolog 1 (*Drosophila*) and sal-like 1 (*Drosophila*)) are important to the development of the auditory system as well[73]. The number of similarities between the genetic programs of auditory system development in *Drosophila* and mammals suggests that useful information can be gained from evaluating *Drosophila* gene mutations of human deafness homologs.

Summary

Animal models are tools for evaluating and investigating the molecular mechanisms of auditory system development, function, and disease. The auditory system is complex and, due to its location and size, difficult to study. We have not yet identified many of the molecules involved in normal hearing, but by identifying and investigating those that are involved in hearing loss, we will elucidate important mechanisms. In this dissertation, I describe the identification of a mutation responsible for a form of human hearing loss. I then describe the generation and characterization of two mouse models of the hearing loss.

Chapter 2

Increased activity of *Diaphanous homolog 3* (*DIAPH3*)/*diaphanous* causes hearing defects in humans with auditory neuropathy and in *Drosophila*

Previously published in Proceedings of the National Academy of Sciences of the United States of America (Proc Natl Acad Sci USA 2010 Jul 27;107(30):13396-401.)

Cynthia J. Schoen, Sarah B. Emery, Marc C. Thorne, Hima R. Ammana, Elzbieta Sliwerska, Jameson Arnett, Michael Hortsch, Frances Hannan, Margit Burmeister, and Marci M. Lesperance

Introduction

Auditory neuropathy (AN) is a rare form of deafness resulting from a disorder of IHCs, their synapses with the auditory nerve (VIII nerve), or the auditory nerve itself. Auditory neuropathy is characterized by an absent or abnormal auditory brainstem response (ABR) with preservation of OHC function[19]. In contrast, most forms of deafness are associated with a loss of OHC function, as typically measured by otoacoustic emissions (OAEs). Although there are more than 60 genes for nonsyndromic deafness, the genetic architecture of nonsyndromic auditory neuropathy is not well understood. We now report the identification of *diaphanous homolog 3* (*DIAPH3*) as a gene responsible for a dominant form of nonsyndromic auditory neuropathy.

DIAPH3 is one of three human orthologs of *Drosophila diaphanous*. A mutation in *DIAPH1* underlies *DFNA1*, autosomal dominant nonsyndromic sensorineural hearing loss[32], whereas mutations in the X-linked *DIAPH2* cause premature ovarian failure[34]. These genes encode diaphanous-related formin (DRF) proteins, actin nucleation factors

involved in maintenance of cell polarity and cell shape, intracellular transport, and vesicular trafficking[74]. DRFs are maintained in an inactive state through an autoinhibitory interaction between the N-terminal GTPase-binding domain (GBD) and the C-terminal diaphanous autoinhibitory domain (DAD)[74]. Binding of Rho-GTP to the GBD activates DRFs through displacement of DAD, a process that is tightly regulated.

We previously mapped the nonsyndromic auditory neuropathy, autosomal dominant 1 (*AUNA1*) locus to chromosome 13q21-q24 in an American family of European descent[28]. Affected individuals in this family develop hearing loss in the second decade of life that rapidly progresses to profound deafness. OHC function as measured by OAEs is preserved until approximately the fifth decade of life. Electrically evoked responses of the auditory nerve return to normal after cochlear implantation, suggesting that the defect resides in the IHCs, the afferent synapses, or the terminal dendrites of the auditory nerve[27]. Except for the possibility of slightly earlier onset in homozygotes, no phenotypic differences between homozygotes and heterozygotes were observed in this family.

Materials and methods

Human subjects

Informed consent was obtained from participants, and studies were approved by the Institutional Review Board of the University of Michigan Medical School. DNA was extracted from peripheral venous blood samples and/or saliva. Epstein-Barr Virus (EBV) transformation of peripheral lymphocytes was performed to create lymphoblastoid cell lines (LCLs). RNA was isolated from LCLs with RNeasy Plus Mini Kit (Qiagen). DNA

samples not previously available were genotyped for markers linked to the *AUNA1* locus as described[28]. All sequencing and genotyping was performed using dye-terminator cycle sequencing on a 3730*xl* DNA analyzer (Applied Biosystems) at the University of Michigan DNA Sequencing Core.

Gene expression analysis

Total RNA was isolated from LCLs derived from five control subjects and four affected family members (two homozygotes and two heterozygotes) and was prepared and hybridized to Illumina Human-6 v2 Expression BeadChips (Illumina) per the manufacturer's instructions. The chip was scanned on an Illumina BeadStation using Bioinformatics software, and data were downloaded to Illumina BeadStudio.

DNA and cDNA sequencing of *DIAPH3*

Primers for PCR were designed to amplify *DIAPH3* cDNA and all exons and intron-exon junctions for DNA. For cDNA, reverse transcription was done with SuperScript III First Strand Synthesis Supermix (Life Technologies) on LCL RNA from a homozygote and from controls, using the manufacturer's recommended conditions for random hexamers. PCR was done with Failsafe (Epicenter Biotechnologies) according to the manufacturer's instructions. Sequence data were compared with the *DIAPH3* reference sequence NM_001042517 with Lasergene software (DNAStar).

Detected variants were screened using a custom probe (Custom TaqMan SNP Genotyping Assay, Applied Biosystems) or by DNA sequencing in 379 DNA samples (758 chromosomes) from controls consisting of 2 from unrelated spouses, 90 from the DNA Polymorphism Discovery Resource, 200 from the Caucasian Panel, and 87 from Human Variation Panels (10 Northern European, 10 Czechoslovakian, 10 African

American, 10 South American, 9 Chinese, 10 Mexican, 10 Southeast Asian, 2 Middle Eastern, 9 South Saharan, and 7 Ashkenazi samples) (Coriell Cell Repositories).

Multiple sequence alignment

A multiple sequence alignment of the region that maps to the 5' end of a variety of orthologs for the human *DIAPH3* gene was performed with the Multiple Alignment based on Fast Fourier Transform (MAFFT) program[75]. The analysis was limited to vertebrate species, which have 3 diaphanous genes.

Quantitative RT-PCR

A probe and primer set was selected for *DIAPH3* exons 19-20 from existing Taqman Gene Expression Assays (Applied Biosystems, LIFE Technologies Corporation). Samples included RNA from LCLs of two heterozygotes, two homozygotes, and two controls. Cells were grown three times, and each batch was tested at four RNA concentrations (150, 125, 100, and 75 ng of RNA) in triplicate.

Real-time PCR was done with Taqman FAM-labeled MGB probe and primer sets (Applied Biosystems, LIFE Technologies Corporation) on a 7900HT Fast Real-Time PCR System using the manufacturer's recommended conditions. *GUSB* (β-glucuronidase) was selected from a panel of endogenous controls (Applied Biosystems, LIFE Technologies). Sequence Detection Systems 2.2.1 software (Applied Biosystems, LIFE Technologies) was used to determine threshold cycle. The *DIAPH3* threshold cycle (Ct) was normalized to the Ct of the housekeeping gene *GUSB* to determine ΔC (Ct *GUSB* – Ct *DIAPH3*) for each individual. The marginal mean for ΔC with a 95% confidence interval was estimated and compared for homozygotes, heterozygotes, and

controls. Fold change was calculated by raising 2 to the power of the difference (ΔC controls - ΔC homozygotes or heterozygotes).

Protein electrophoresis and immunoblotting

Four batches of LCLs, each consisting of two heterozygotes, two homozygotes, and two controls, were cultured for 2 to 3 weeks, and lysate was prepared in RIPA buffer containing HALT protease inhibitor mixture (Thermo Scientific). Equal amounts of protein (50-100 µg per batch) were electrophoresed on 4-20% gradient Tris•HCl-ready gels (Bio-Rad) and transferred to PVDF membranes (GE Healthcare Biosciences). Blots were blocked with 5% nonfat dry milk in TBS-T (Tris-buffered saline/0.1% Tween-20, pH 8). For *DIAPH3* we used primary antibody DT154 at a dilution of 1:2,000[46,76]; the secondary antibody was HRP-conjugated antibody against rabbit IgG diluted 1:10,000 (NA934V; GE Healthcare). Reactions were visualized using Supersignal West Femto Maximum Sensitivity Substrate (Thermo Scientific) and FluorChem SP imager (Cell Biosciences). Blots were stripped with Restore Western Blot Stripping Buffer (Thermo Scientific) and reprobed with primary antibody GAPDH (sc-25778; Santa Cruz Biotechnology) at a dilution of 1:1,000 using the same secondary antibody and Pierce ECL Western Blotting Substrate (Thermo Scientific).

Chemiluminescent detection was done on an Alpha Innotech imager (Cell Biosciences), and densitometry measurements for DIAPH3 and GAPDH were done with Alpha Ease software (Cell Biosciences). DIAPH3 measurements were normalized to bands detected by GAPDH in the sample to account for variability in amount loaded. The marginal mean for the ratio of DIAPH3/GAPDH was estimated, and fold change was

calculated by dividing the estimated mean for homozygotes or heterozygotes by the estimated mean for wild type.

Northern blotting

Poly(A)+ RNA was isolated from the LCLs of two controls, two heterozygotes, and two homozygotes using the Dynabeads mRNA Direct Kit (Invitrogen). An RNA probe amplified from *DIAPH3* exon 28 was labeled using the DIG Northern Starter Kit (Roche Applied Science). *GAPDH* was used as a control probe.

Sequence analysis of minor transcription products from *DIAPH3* exons 1-5

Total RNA prepared from the LCLs of one homozygote, two heterozygotes, and one unaffected individual was reverse transcribed using a combination of oligo $(dT)_{20}$ and random hexamer primers and SuperScriptase II (Invitrogen). To amplify the minor transcripts preferentially, the cDNA template was digested before PCR with *Ssp*I (New England Biolabs, Ipswich, MA, USA).

Luciferase assay

A 256-bp region 21bp upstream from the start of *DIAPH3* was identified as a putative promoter with PROSCAN Version 1.7 software[77]. DNA from a homozygous affected individual (IV:9)[28] and a Centre d'Etude du Polymorphisme Humain (CEPH) control DNA (NA10846, Coriell Cell Repositories) were used as templates. For reporter constructs, PCR primers were designed to amplify the 256-bp putative promoter, the 21-bp linking region, and the 5' UTR of *DIAPH3*, with a *Nhe*I site in the forward primer and a *Hind*III site in the reverse primer. PCR was done using Failsafe reagents (Epicentre Biotechnologies) per the manufacturer's instructions and standard thermocycling

conditions including an annealing temperature of 58°C and 1 min extension for 32 cycles. The PCR product was isolated by agarose gel electrophoresis and purified with the MinElute Gel Extraction Kit (QIAGEN).

Purified PCR products and pGL3-basic firefly luciferase reporter vector (Promega) were digested with *Nhe*I and *Hind*III (New England Biolabs) and isolated and purified as outlined above. Vector and product were ligated with the Rapid DNA Ligation Kit (Roche) per the manufacturer's instructions and transformed into *Escherichia coli* DH5α-competent cells (Invitrogen). Plasmid preps for all three reporter constructs, pGL3-basic firefly luciferase reporter vector, and pRL-TK renilla luciferase control vector were done with the Qiaprep Spin Miniprep Kit (QIAGEN).

Transfection: For transfection, 1.2 x 10^5 NIH 3T3 cells were seeded in each well of a 24-well plate and cultured overnight in fully supplemented DMEM (Gibco). Cells were washed twice and then covered with 500 µL of DMEM without serum or antibiotics. A transfection mixture containing 100 µL OptiMEM, 1.1 µg of pGL3 firefly luciferase reporter construct or vector, 0.1 µg of pRL-TK renilla luciferase reporter vector (Promega), and 2.6 µL of lipofectamine 2000 (Invitrogen) was made per the manufacturer's protocol and added to each well for a 4-hour incubation at 37°C. Transfection medium was replaced with fully supplemented DMEM, and cells were grown for 20 hours. Cells were washed with PBS, and luciferase activity was determined for firefly and renilla luciferase using the Dual Luciferase Assay kit and the GloMax 96 Microplate Luminomenter (Promega).

Drosophila melanogaster studies

The expression pattern in the JO for the various JO-Gal4 driver lines used is described in Table 2-1. All flies were out-crossed for 5-10 generations to an isogenized line of wild-type control flies ($w^{118(isoCJ1)}$). JO15/TM3Ser flies were constructed using standard genetic crosses. Flies were raised on sucrose/cornmeal medium at 25^{o}C on a 12-hour light/dark cycle.

Recordings of SEPs were made from the antennae of female mutant and control flies as described previously[68]. Control flies included wild-type (+/+) as well as parental control flies (UAS-diaphanous^{CA}/+, and JO-Gal4/+). Twenty to 30 flies of each genotype were assayed in a blind fashion. Responses to 10 stimulus presentations were averaged, and the maximum amplitude of the peak response was recorded (peak amplitude; SEP) (Figure 2-8) and used to calculate mean, SEM, and median SEP values (Table 2-2).

Statistical analysis

We used the Illumina BeadStudio software to analyze the gene expression data. Data from affected individuals were compared with data from control samples in a two-group differential expression using the Illumina rank invariant normalization and custom error model. For quantitative PCR, a linear mixed-models analysis was used to estimate marginal means for ΔC of wild-type, homozygous, and hetereozygous samples and differences of marginal means for wild type vs. homozygotes vs. heterozygotes (SAS 9.2; SAS Institute). The 95% confidence intervals and *p* values were calculated with Tukey-Kramer adjustment for multiple testing. The linear mixed models analysis with Tukey-Kramer adjustment for multiple testing also was used to estimate the marginal mean for the DIAPH3/GAPDH ratio as measured by band density of immunoblots. For luciferase

assays, significance was determined with an unpaired *t* test. For SEPs in *Drosophila*, statistical significance was calculated by nonparametric Mann-Whitney analysis of median peak amplitudes using GraphPad Prism v5.0b statistical software (GraphPad Software).

Results

Genotyping of additional short tandem repeat markers as well as single nucleotide polymorphisms in the linkage region refined the telomeric boundary of *AUNA1* to D13S1309, excluding the protocadherin 9 gene (*PCDH9*)[78]. Genotyping of a DNA sample from a distantly related affected family member revealed a recombination event at marker D13S1492, which redefined the centromeric end of the *AUNA1* interval (Figure 2-1). The refined *AUNA1* interval spans an 11-Mb, 3.28-cM genomic region containing only four genes: protocadherin 17 (*PCDH17*), protocadherin 20 (*PCDH20*), Tudor domain-containing 3 (*TDRD3*), and *DIAPH3*.

DNA sequencing of all exons and intron-exon junctions of *DIAPH3* demonstrated a point mutation in the 5' UTR, c. -172G>A, g.48G>A, occurring within a consensus GC box DNA recognition site[79]. The 5' UTR DNA sequence is highly conserved in the vertebrate orthologs of the human *DIAPH3* gene (Figure 2-2). The mutation is absent in 379 controls (758 control chromosomes), segregates with deafness, and, as predicted by the linkage analysis[28], is homozygous in two affected subjects. DNA sequencing of *PCDH17*, *PCDH20*, and *TDRD3* revealed no novel variants from the reference sequences (data not shown).

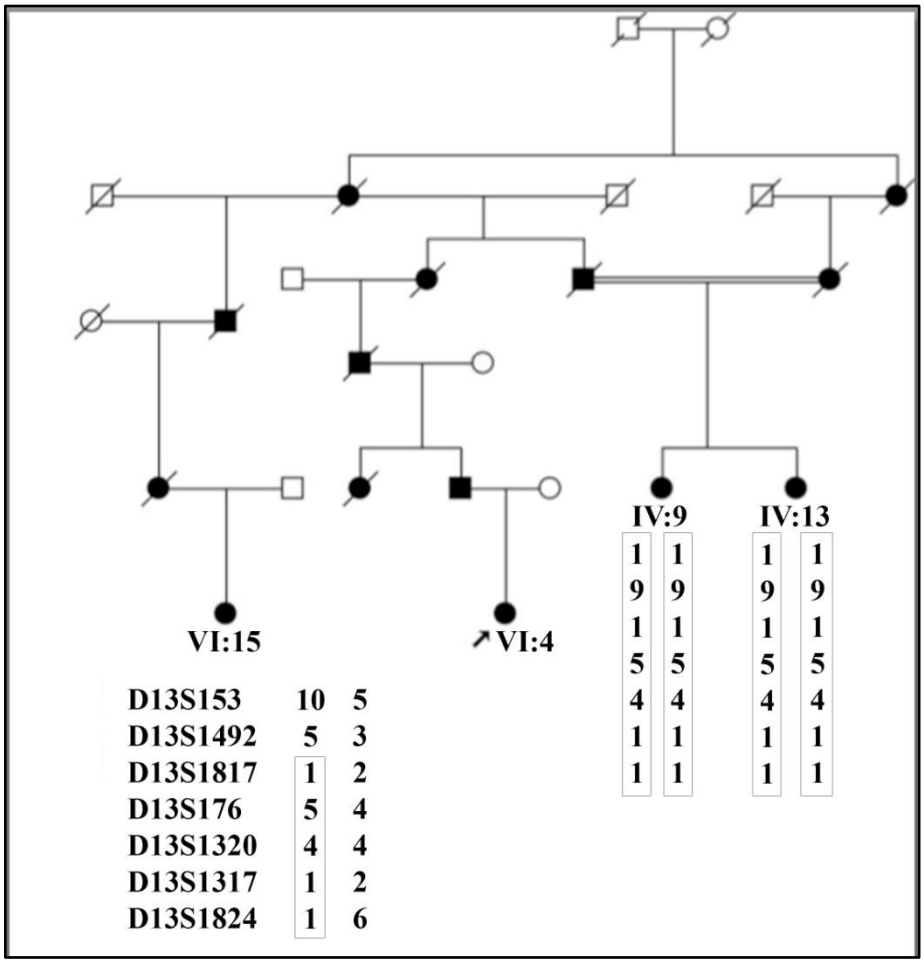

Figure 2-1. Haplotype analysis of nonsyndromic auditory neuropathy, autosomal dominant 1 (*AUNA1*) interval. Squares indicate males; circles indicate females; slashes indicate deceased individuals; darkened symbols indicate affected individuals; double line indicates consanguineous marriage; arrow indicates proband VI:4 (after (Kim et al., 2004)[28]). DNA samples from individuals VI:15 and homozygous individuals IV:9 and IV:13 were genotyped for short tandem repeat markers as shown. Boxed haplotype segregates with affected status. Recombination event occurs at marker D13S1492 in individual VI:15.

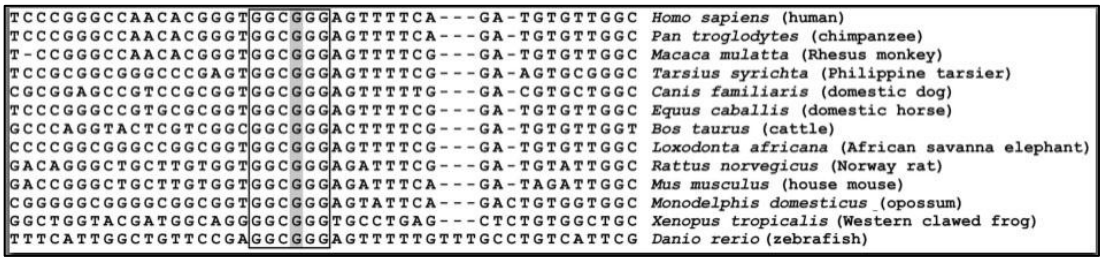

Figure 2-2. The c.-172G>A mutation occurs within a GC box element. Multiple sequence alignment of the region that maps to the 5' end of the human *Diaphanous homolog 3* (*DIAPH3*) orthologs in a variety of vertebrate species was performed with the

MAFFT program[75]. c.-172G (gray shading) occurs within the minimal consensus sequence GGGCGG (indicated by box), which functions in both directions of mRNA synthesis[79]. Accession numbers for the sequences are as follows: *Homo sapiens*, AADB02015980; *Pan troglodytes*, AACZ03093315; *Macaca mulatta*, AANU01126478; *Tarsius syrichta*, ABRT010091844; *Canis familiaris*, AAEX02017151, *Equus caballis* AAWR02010753; *Bos Taurus*, AAFC03095308; *Loxodonta Africana*, AAGU03045871; *Rattus norvegicus*, AABR05052693; *Mus musculus*, AAHY01116079; *Monodelphis domesticus*, AAFR03045720; *Xenopus tropicalis*, AAMC01064078; *Danio rerio*, CAAK05032804.

Whole-genome expression arrays were used to identify genes that are differentially expressed in mRNA from lymphoblastoid cell lines (LCLs) from affected individuals and controls. Signal intensity was 2- to 3-fold higher in affected individuals than in controls for two probes representing the *DIAPH3* gene (*Hs*. 576922 and *DIAPH3*, p=0.000029 and p=0.000713, respectively). To confirm and quantify the expression changes seen on microarrays, the threshold cycle (Ct) for *DIAPH3*, as compared with the Ct for a housekeeping gene, ß-glucuronidase (*GUSB*), was determined for controls, heterozygotes, and homozygotes by quantitative RT-PCR of mRNA from LCLs. The estimated difference of marginal means for ΔC (Ct *GUSB* – Ct *DIAPH3*) was significant for controls vs. heterozygotes (-0.4285 vs. 0.6496, p=0.0028) and controls vs. homozygotes (-0.4285 vs. 1.1466, p<0.001) (Figure 2-3). Expression was increased 2.11-fold in heterozygotes compared with controls and 2.98-fold in homozygotes compared with controls, as reflected by an increase in ΔC values (Figure 2-3). Results for homozygotes were not significantly different from those for heterozygotes (p=0.2641).

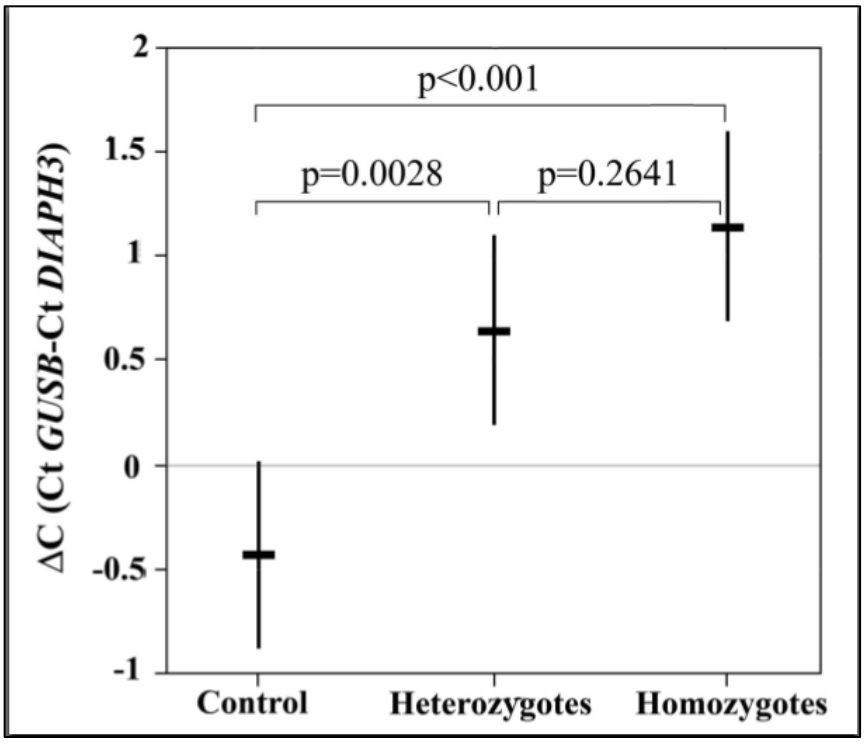

Figure 2-3. *DIAPH3* is significantly overexpressed in mRNA from heterozygotes and homozygotes as compared with controls. Relative *DIAPH3* gene expression in mRNA extracted from LCLs of wild-type, homozygous, and heterozygous individuals was assessed using quantitative RT-PCR amplifying exons 19-20. The *DIAPH3* Ct was normalized to the Ct of the housekeeping gene *GUSB* to determine ΔC (Ct *GUSB* – Ct *DIAPH3*) for each sample. Estimated marginal means for ΔC (control = -0.4285; heterozygotes = 0.6496; homozygotes = 1.1466) are indicated by bold horizontal lines, with 95% confidence intervals represented by vertical lines. *P* values for significance of difference of marginal means are indicated by brackets.

To determine the effect of increased mRNA expression on levels of protein expression, we used immunoblotting to compare relative amounts of DIAPH3 protein in LCL lysates from controls, heterozygotes, and homozygotes (Figure 2-4A). GAPDH was used as a loading control, and the DIAPH3/GAPDH ratio was calculated. There was a significant difference in the estimated marginal means for the DIAPH3/GAPDH ratio in controls vs. heterozygotes (4.83 vs. 7.14, p=0.045) and controls vs. homozygotes (4.83 vs. 7.85, p=0.0093) (Figure 2-4B). Protein levels were increased 1.48-fold in

heterozygotes and 1.62-fold in homozygotes relative to controls (Figure 2-4B). There was no significant difference in protein levels between homozygotes and heterozygotes (p=0.68).

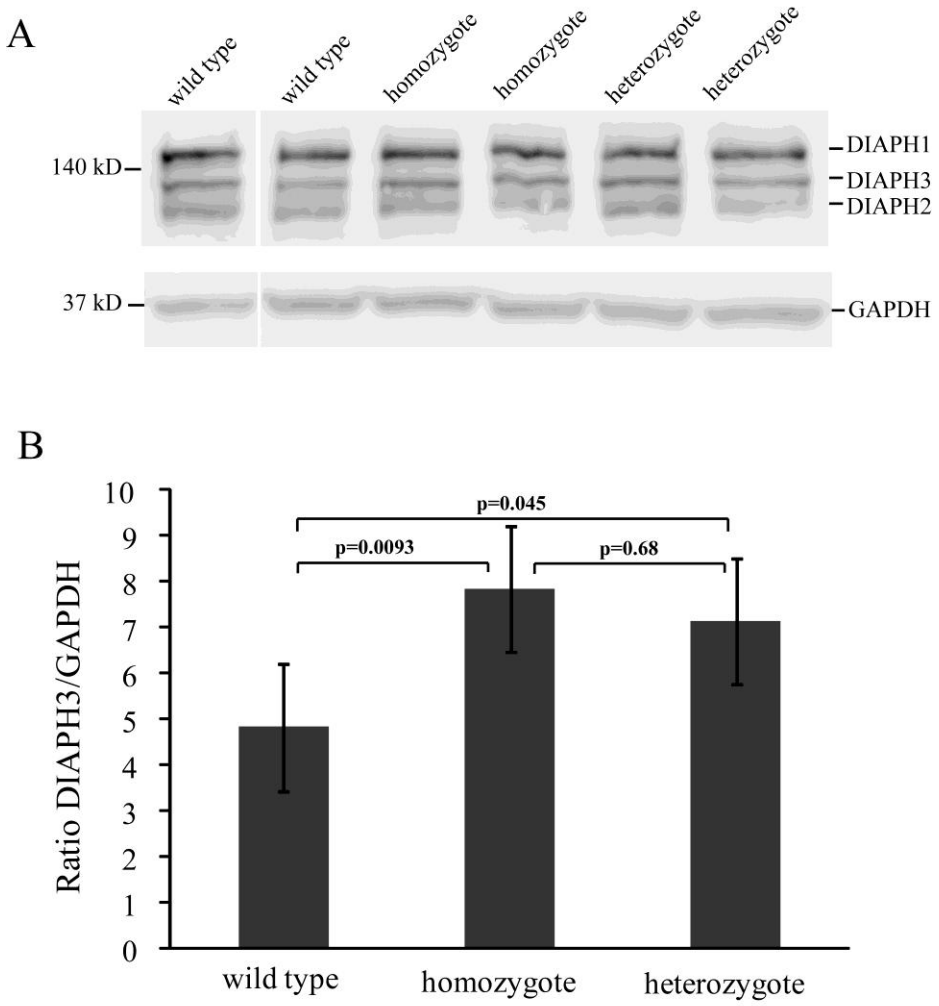

Figure 2-4. Expression of DIAPH3 protein is significantly increased in lysates from LCLs from heterozygotes and homozygotes vs. controls. (A) Immunoblot of LCL lysates from two wild types, two homozygotes, and two heterozygotes using DT154 antibody[46,76]. The DIAPH3 band is at 137 kDa (UniProt database); cross-reactivity is seen with DIAPH1 (140 kDa) and DIAPH2 (126 kDa). GAPDH was used as a loading control, and DIAPH3 densitometry was normalized to GAPDH densitometry. (B) Estimated marginal means and SE for the DIAPH3/GAPDH ratio for wild types, homozygotes, and heterzygotes tested in four batches of cells. There was a significant difference between controls and heterozygotes (4.83 vs. 7.14, P=0.045, a 1.48-fold increase) and between controls and homozygotes (4.83 vs. 7.85, p=0.0093, a 1.62-fold

increase). There was no significant difference in protein levels between homozygotes and heterozygotes (p=0.68).

Given the increased expression of *DIAPH3* observed in mRNA from affected family members, we investigated whether increased expression could be explained by the presence of the 5' UTR mutation. Although promoter and/or enhancer sequences for *DIAPH3* have not yet been identified, we hypothesized that the 5' UTR sequence plays a role in controlling the expression of *DIAPH3*. Therefore, the putative promoter and the 5' UTRs (mutant and wild-type) were cloned into a luciferase reporter vector to determine the effect of the c.-172G>A mutation on gene expression. When compared to the wild-type *DIAPH3* 5' UTR, the c.-172G>A mutation up-regulates the expression of a luciferase reporter gene significantly, ≈ 2-to 3-fold (p<0.001) (Figure 2-5). These data show that the c.-172G>A mutation is sufficient to cause the observed overexpression of *DIAPH3*.

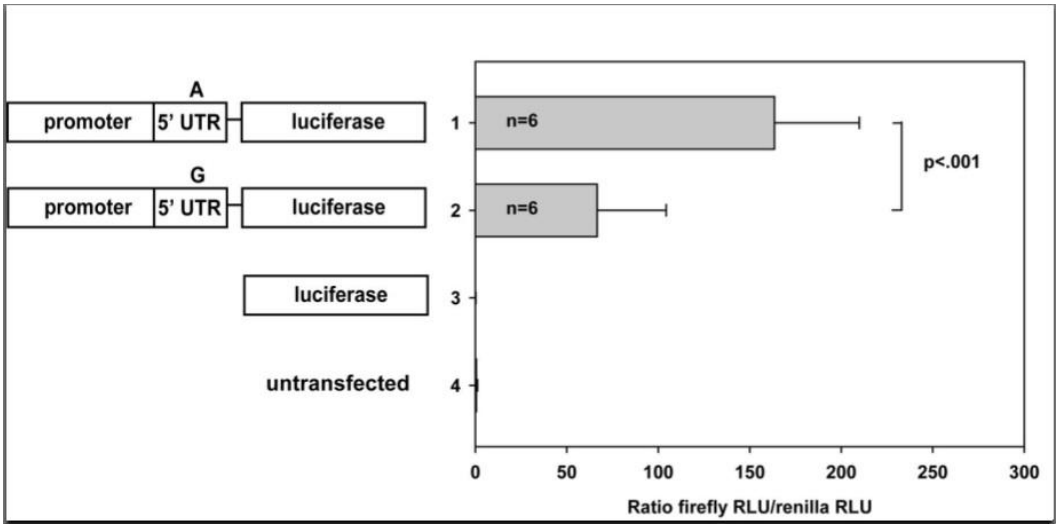

Figure 2-5. Effect of base substitution in *DIAPH3* 5' UTR on luciferase reporter gene expression. (*Left*) Three constructs of the pGL3-basic luciferase reporter vector were tested, as were nontransfected cells: (1) promoter with mutant 5' UTR (c.-172G>A) from affected homozygote; (2) promoter and wild-type 5' UTR from CEPH DNA NA10846 (Coriell Cell Repositories); (3) no promoter or UTR; (4) untransfected cells.

(*Right*) Normalized luciferase units are shown as mean ± SD with $n = 6$. Expression from construct of DNA from affected individuals with mutant 5' UTR (line 1) is significantly higher than that of the wild-type 5' UTR (line 2) (unpaired t test, $p<0.001$). No expression was seen in construct lacking promoter and 5' UTR (line 3) or in untransfected cells (line 4).

Additional investigations of *DIAPH3* were performed to determine whether variations in splicing, differential abundance of normal transcripts, and/or novel transcripts caused by exon-skipping or rearrangements accounted for the observed change in *DIAPH3* expression. Comparison of PCR products spanning the *DIAPH3* cDNA shows no discernable difference in size or sequence variations between homozygote and control cDNA (data not shown). Similarly, Northern blots show no novel transcripts in samples from affected individuals (Figure 2-6). Finally, there was no difference in the relative abundance of any of the various *DIAPH3* transcripts in RNA from mutant LCLs as compared with controls (Figure 2-7).

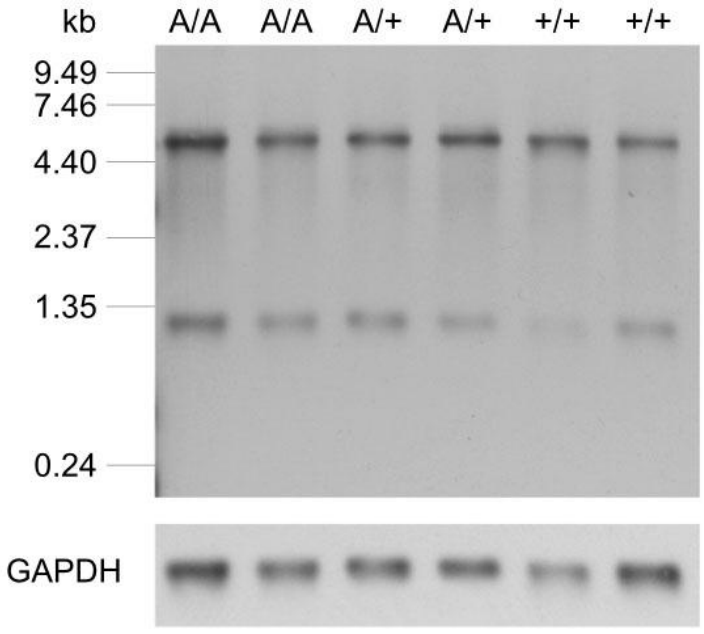

Figure 2-6. Northern blot demonstrates similar banding patterns among affected individuals and controls. (Upper) mRNA from lymphoblastoid cell lines of four

affected individuals (homozygotes = A/A; heterozygotes = A/+) and two control individuals (+/+) show the same banding pattern, with a primary band at the predicted size of 4.7 kb and a band at ≈1 kb representing an uncharacterized major isoform. (Lower) The blot shown in (upper) hybridized with a *GAPDH* control probe.

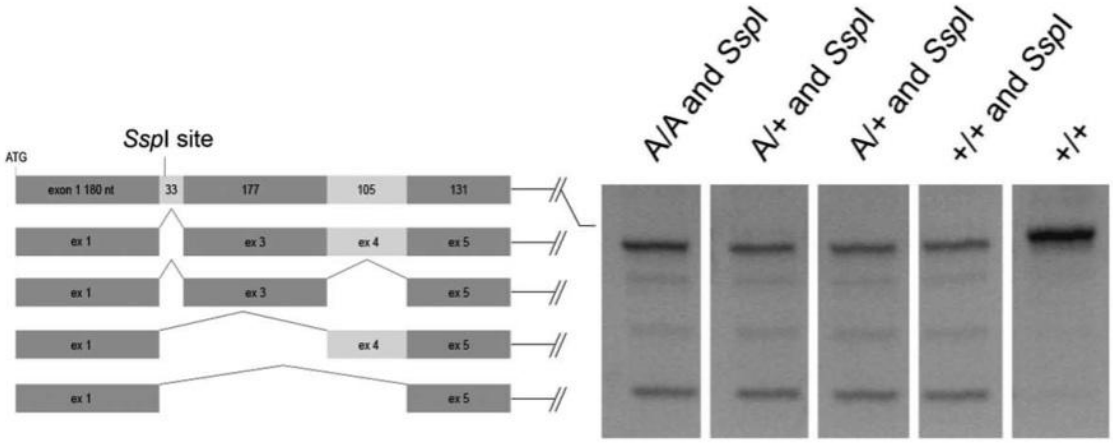

Figure 2-7. Analysis of *DIAPH3* splice products using RT-PCR. (Left) *DIAPH3* has two documented major isoforms, a ubiquitous long form encoding a full-length protein encoded by exons 1-28, and a testis-specific short isoform encoded by alternative exon 1b and exons 8-28 (UCSC Genome Browser). In addition, there are several minor isoforms (UCSC Genome Browser). Line 1: ubiquitous major transcript (exons 6-28 are not shown, because these exons are common to all depicted variants). Lines 2-5: minor isoforms. Because exon 2 is lacking from all four minor isoforms and contains a unique *Ssp*I site, *Ssp*I selectively digests the major isoform. (Right) RT-PCR using primers in exons 1 and 5. For lanes 1-4, template cDNA was digested with *Ssp*I before PCR. In lane 1, A/A = homozygote; in lanes 2 and 3, A/+ = heterozygote; in lanes 4 and 5, +/+ = control. Lane 5 demonstrates major transcript (exons 1-28) in the absence of *Ssp*I. Comparison of banding patterns revealed no differences between affected and unaffected individuals.

To investigate the role of diaphanous proteins in the auditory function of a model organism, we created lines of flies (*Drosophila melanogaster*) that express a constitutively active form of diaphanous protein in the auditory organ (Johnston's organ, JO). Sound-evoked potentials (SEPs) were compared in affected flies versus parental and wild-type control flies. We used five different JO-Gal4 lines, each with a specific expression pattern in the JO (Table 2-1). In the Gal4-upstream activating sequence (UAS)

system, the yeast transcription activator protein Gal4 binds to the UAS to activate transcription of the transgene in a tissue- and temporally specific manner[80]. UAS-diaphanous^{CA} (UAS-diaCA) is a transgenic line that, in the presence of Gal4, expresses a mutant form of diaphanous protein, diaphanous^{CA} [81]. Diaphanous^{CA} was created by removing both the N-terminal Rho-binding domain and the C-terminal autoinhibitory domain of *Drosophila* diaphanous[81]; the lack of these regulatory domains results in a constitutively active protein. Expression of diaphanous^{CA} under control of the JO1-Gal4 driver was found to be lethal in the late pupal stage and semilethal for the JO2-Gal4 driver line, with only a few viable flies. For the four crosses generating viable flies, all those expressing diaphanous^{CA} exhibit significantly reduced SEPs in comparison with wild-type flies and parental control flies (Figure 2-8 and Table 2-2). The majority of responses of the wild-type flies and parental control flies fall in the range of 0.5-1.3 mV, whereas most flies with constitutive expression of diaphanous^{CA} exhibit responses in the range of 0.25-0.75 mV.

Table 2-1. Johnston's organ (JO)-Gal4 lines used in *Drosophila* experiments

Genotype of driver line	Synonyms	Areas of expression in the JO*	Percent of JO neurons labeled
JO1-Gal4	JO1, NP0761	JO-ABCDE[82]	94 ± 4
JO2-Gal4	JO2, NP1046	JO-B[82]	22 ± 3 (middle ring)†
JO3-Gal4	JO3, NP1245	JO-ABCDE[82]	67 ± 5 (distributed)†
JO4-Gal4	JO4, NP6303	JO-ACE[82]	38 ± 1 (posterior cluster)†
JO15-Gal4/TM3Ser	JO15	JO-AB[83]	30 ± 2 (anterior cluster)†

*Neuronal subgroups of Johnston's organ. Neurons in subgroups A and B respond to sound vibrations; subgroups C and E respond to wind and gravity; the function of subgroup D is unknown.
†Pattern of expression in the JO. JO neurons are organized in a bowl shape.

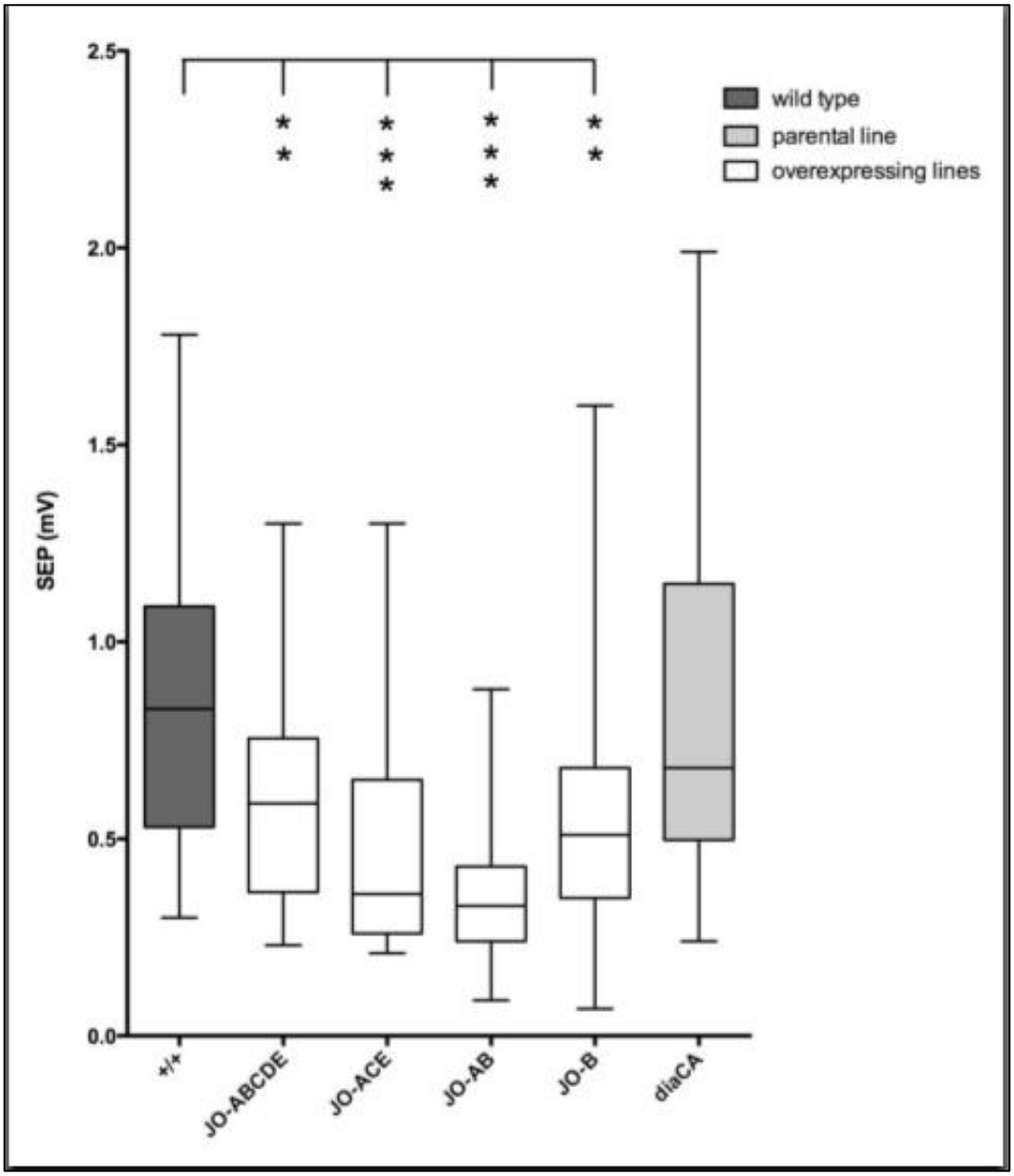

Figure 2-8. Flies expressing a constitutively active diaphanous protein demonstrate impaired response to sound. Peak amplitude of SEP is reduced in flies expressing UAS-diaphanous^{CA} in the JO auditory neurons (subgroups A, B, C, D, and/or E, as noted), (unshaded bars) as compared with wild-type flies (+/+, dark shaded bar) and diaphanous^{CA} parental control flies (light shaded bar). Box plots indicate median, 25th, and 75th percentiles and minimum-maximum whiskers. The majority of responses of wild-type flies and parental control flies fall in the range of 0.5-1.3 mV. In contrast, most flies with expression of constitutively active diaphanous protein exhibit responses in the range of 0.25-0.75 mV. SEPs are considerably lower in flies expressing diaphanous^{CA} than in wild-type flies (**$p < 0.005$; ***$p < 0.0001$; Mann-Whitney test) and in parental control flies (Table 2-2). Complete genotypes and expression patterns are shown in Table 2-1.

Table 2-2. Comparison of sound-evoked potentials in fly strains expressing mutant diaphanous protein (diaphanous^{CA}) vs. parental and wild-type controls

Genotype	N	Mean (mV)	SEM (mV)	Median (mV)	*p* value vs. wild type	*p* value vs. respective JO-Gal4 parental line	*p* value vs. UAS-diaCA parental line
Wild type	47	0.86	0.06	0.59	—	—	ns
JO2-Gal4	11	0.71	0.07	0.65	ns	—	ns
JO3-Gal4	13	1.05	0.16	1.06	ns	—	ns
JO4-Gal4	25	0.87	0.08	0.85	ns	—	ns
JO15-Gal4/TM3Ser	27	0.89	0.07	0.84	ns	—	ns
UAS-diaCA	20	0.85	0.11	0.68	ns	—	ns
JO2-Gal4/+; UAS-diaCA/+	27	0.58	0.07	0.51	0.0011	0.0459	0.0273
JO3-Gal4/+; UAS-diaCA/+	29	0.60	0.05	0.59	0.0032	0.0077	0.0598
JO4-Gal4/+; UAS-diaCA/+	23	0.48	0.06	0.36	<0.0001	0.0002	0.0033
JO15-Gal4/ UAS-diaCA	39	0.38	0.03	0.33	<0.0001	<0.0001	<0.0001

ns, not significant; *p* value, Mann-Whitney test; UAS-diaCA, upstream activating sequence-diaphanous^{CA}.

Discussion

We have identified a point mutation in the 5' UTR of the human *DIAPH3* gene that leads to overexpression of *DIAPH3* and causes a progressive nonsyndromic auditory neuropathy, *AUNA1*. The c.-172G>A substitution occurs within a GC box element consensus sequence (Figure 2-2) known to bind transcription factors of the Sp1 and Krüppel-like protein families, which may function either as activators or repressors[84]. We demonstrate that the mutant 5' UTR is sufficient to drive overexpression in a luciferase reporter vector, suggesting that this highly conserved sequence in the 5' UTR of *DIAPH3* may be important for its transcriptional regulation. Similar mutations in the 5' UTR of the ß-globin gene have been shown to result in thalassemia through a reduction of mRNA levels[85]. Given the observed effect of overexpression, we postulate that the c.-172G>A

mutation may decrease the binding of a transcriptional repressor. Other transcriptional mechanisms are possible, such as disruption of an internal ribosome entry site[86], increased binding of an activator, modification of the mRNA secondary structure, or alteration of microRNA binding.

A paralog of *DIAPH3*, *DIAPH1*, is responsible for *DFNA1* deafness, an autosomal dominant, progressive, low-frequency, sensorineural hearing loss[32]. A G→T substitution in a splice junction leads to a four-base insertion (TTAA), generating a frameshift that truncates the C terminus of the *DIAPH1* mRNA[32]. Given the proximity of the truncation to the C-terminal DAD domain, it has been suggested that the *DFNA1* mutation interferes with autoregulation of *DIAPH1*[87], resulting in a constitutively active protein. A knockout model of the mouse ortholog, *Diap1*, develops a myelodysplastic syndrome but has no apparent hearing defects[33]. Thus, although the exact mechanism of *DFNA1* hearing loss is still unknown, a gain of function appears more likely than a loss-of-function mechanism such as haploinsufficiency.

Similar to *DIAPH1* deafness, our data support a gain-of-function mechanism causing *AUNA1* deafness by the overexpression of *DIAPH3*. Gain-of-function mechanisms of dominance include increased gene dosage, increased and/or constitutive activity of the protein, and ectopic or temporally altered mRNA expression[88]. In LCLs, we demonstrate a significant 2- to 3-fold increase in mRNA expression over wild type by quantitative RT-PCR and an increase in protein levels of ≈1.5 fold by immunoblotting. Although *DIAPH3* is ubiquitously expressed, family members with the c.-172G>A mutation do not develop clinical manifestations other than delayed-onset, rapidly progressive profound deafness. The human auditory system may be specifically sensitive

to a 1.5-fold increase in DIAPH3 protein levels, or the 2- to 3-fold increase in mRNA expression may be amplified to a greater degree at the protein level in the inner ear. Alternatively, the c.-172G>A mutation may lead to a constitutively active protein, augmenting DIAPH3 activity beyond that expected from a mild increase in protein levels. Interestingly, a similarly modest (1.5- to 1.8-fold) level of overexpression in *MYO6*, a known deafness gene that is expressed in cochlear hair cells, also has been implicated in deafness[89].

Like *DIAPH1*, loss of function of *DIAPH3* is associated with neoplasia[90]. In contrast, haploinsufficiency of the single *diaphanous* gene in *Drosophila* leads to an impaired response to sound[68]. Redundant function of the three closely related DRF proteins in higher-order organisms such as humans and mice may account for decreased sensitivity of the auditory organs to the lack of *DIAPH1* and *mdia1*, respectively[91]. Knockdown of the zebrafish ortholog of *DIAPH3*, *zdia2*, by antisense morpholino oligonucleotides is lethal to the embryo before the formation of the auditory organ[92].

Formins are important in regulation of actin polymerization through effects on nucleation, elongation, and capping[48]. In addition to coordination of actin dynamics, DRF proteins play a role in binding and regulating microtubules[93]. In *Drosophila*, *diaphanous* is essential for the regulation of the presynaptic actin and microtubule cytoskeletons at the larval neuromuscular junction[94]. In the cochlea, through their interaction with Rho GTPases, DRF proteins may play a role in specifying the precise shape and polarity of hair bundles[95] or in regulating stereocilia length mediated by the treadmilling mechanism[96]. However, an abnormality of the stereocilia and/or bundles might be expected to affect IHCs and OHCs equally.

Alternatively, *DIAPH3* overexpression may cause deafness through a direct effect on the IHC synapse. Approximately 95% of afferent auditory nerve fibers innervate mammalian IHCs, whereas only 5% of afferents innervate the OHCs[97]. A recent study of mouse cortical and hippocampal neurons found that mDia2, the protein encoded by the gene orthologous to *DIAPH3*, is necessary for the function of dendritic spines, actin-rich structures arising from dendrites that house the post-synaptic components of excitatory synapses[98]. Thus, a defect in afferent auditory nerve fibers might be expected initially to have a greater effect on IHCs but over time eventually would affect OHCs as well.

We created *Drosophila* models of constitutively active diaphanous protein expressed in the auditory organ (the JO) that replicate the phenotype of hearing loss. Because *Drosophila* has only one *diaphanous* gene, these crosses serve as models for gain-of-function mutations in both *DIAPH3* and *DIAPH1*. The JO consists of an array of mechanosensory neurons that share many developmental and functional similarities with mammalian IHCs[71,72]. There are five neuronal subgroups in the JO: neurons of subgroups A and B are activated by sound vibrations and are essential for hearing, whereas neurons in subgroups C and E respond to gravity and wind movements[99,100]. The function of neurons in subgroup D is currently unknown.

Each of the JO-Gal4 lines used in our experiments expresses in about 30-60% of the total population of JO neurons, including both A and B neurons[82] (Table 2-1). The lethality of the JO1-Gal4/diaphanous^{CA} cross and the semilethality of the JO2-Gal4/diaphanous^{CA} cross cannot be explained by their expression pattern in the JO, but presumably are caused by expression in the *Drosophila* CNS outside of the JO. Qualitatively, the JO1-Gal4 line drives a higher level of CNS expression than do the JO2-

Gal4, JO3-Gal4, or JO4-Gal4 lines, and JO15-Gal4 has no detectable expression outside the JO[82,99].

The effect of expression of constitutively active diaphanous^{CA} in neurons essential for hearing in Drosophila leads to a statistically significant reduction in response to sound in all four crosses yielding viable flies (p<0.005 for JO-3 and JO-2, p<0.0001 for JO-4 and JO-15; Figure 2-4). The range of SEPs obtained from wild-type and parental control flies overlapped with those obtained from flies expressing diaphanous^{CA}, largely because of a greater variability of hearing responses in the control flies. This variability has been observed previously[68,99,100] and may result in part from the technical limitations of placing the electrode in a consistent location within the JO. In contrast, uniformly low response levels were observed in the affected flies, in particular the JO15-Gal4 cross, which has expression limited to the auditory system (subgroups A and B of the JO neurons).

Only two genes, the otoferlin gene *OTOF*[101] and pejvakin *PJVK*[24], have been implicated previously in human nonsyndromic auditory neuropathy. *OTOF* originally was identified as the cause of *DFNB9* recessive deafness[102] and appears to be a relatively common cause of recessive AN and sensorineural deafness in patients of Spanish descent[103,104]. Mutations in *PJVK* are reported in consanguineous families of Iranian descent, presenting either as autosomal recessive auditory neuropathy (*DFNB59*)[24] or sensorineural hearing loss[25]. Auditory neuropathy may be unrecognized if testing is not performed early in life, because ≈20-30% of AN subjects ultimately demonstrate loss of OHC function over time[105]. Furthermore, OAE testing is not performed routinely in all

patients with significant hearing loss. Thus, it is difficult to estimate the proportion of cases of auditory neuropathy caused by mutations in these genes.

Elucidation of the role of the diaphanous-related formins in the cochlea may provide insights into the biology of these proteins as well as into the mechanisms underlying delayed-onset hearing loss. In addition, the discovery of *DIAPH3* as an auditory neuropathy gene will facilitate genetic testing for individuals with dominant and recessive auditory neuropathy.

Acknowledgements

Additional experimental contributions: Marc Thorne performed the DNA sequencing. Sarah Emery performed the cDNA sequencing, quantitative RT-PCR, protein electrophoresis and immunoblotting, and luciferase assays. Marc and Sarah were formerly in Marci Lesperance's laboratory. Michael Hortsch generated the multiple sequence alignment. Hima Ammana in Frances Hannan's laboratory performed the *Drosophila melanogaster* studies.

We thank the family for their participation, James Chang for technical assistance, and the University of Michigan Center for Statistical Consultation and Research for statistical support for the quantitative RT-PCR and immunoblotting experiments. We thank Henry Higgs (Dartmouth Medical School) for providing the DT154 anti-DIAPH3 antibody. We thank Mark Peifer (University of North Carolina) for providing UAS-diaCA flies, Azusa Kamikouchi (Cologne, Germany) for providing JO1-Gal4, JO2-Gal4, JO3-Gal4 and JO4-Gal4 flies, Daniel Eberl (University of Iowa) for providing JO15/TM3Sb flies, and Jerry Yin (University of Wisconsin) for providing $w^{118(isoCJ1)}$

flies. This work was supported by National Institutes of Health Grants R01 DC007380 (to M.M.L.) and T32 DC000011-31 (to C.J.S.) and a grant from the Children's Hearing Institute of New York (to F.H.).

Chapter 3

Overexpression of murine *diaphanous homolog 3* (*Diap3*) results in inner hair cell defects in transgenic mice

Introduction

We have demonstrated that a mutation in the 5' UTR of *diaphanous homolog 3* (*DIAPH3*) results in 2 to 3-fold overexpression of the gene, both in mRNA from lymphoblastoid cell lines derived from affected individuals and in an *in vitro* luciferase reporter system[106]. This overexpression leads to *AUNA1* deafness in humans[106]. Furthermore, expression of constitutively active *diaphanous* in *Drosophila* results in a significant reduction of sound-evoked potentials (SEPs)[106].

Although these observations are strong evidence that overexpression of *DIAPH3* in humans results in auditory neuropathy, it is not direct evidence. In *Drosophila*, reduced SEPs have been demonstrated in flies with a *diaphanous* (*dia*) mutant allele[68] and in flies that express constitutively active *dia*[106]. The effect of wild-type *dia* overexpression in *Drosophila*, however, has not been studied. Furthermore, the Drosophila genome has only one *diaphanous* gene, compared to three diaphanous paralogs in mammals. It is possible that the role *dia* fills in the *Drosophila* hearing organ, Johnston's organ (JO), is filled by one of the other diaphanous genes in the mammalian cochlea. *DIAPH1*, for example, has been implicated in *DFNA1* deafness[32], and therefore appears to have an as-yet-unidentified role in the mammalian cochlea. In order to directly confirm that overexpression of wild-type *diaphanous homolog 3* results in hearing loss, therefore, it

was important to generate a model that overexpresses the wild-type gene in a model system that has all three diaphanous paralogs.

We generated two lines of transgenic mice, both of which overexpress *Diap3*, the murine ortholog of *DIAPH3*. Both lines demonstrate a delayed-onset, progressive hearing loss with preservation of OHC function, recapitulating *AUNA1* auditory neuropathy. We also identify several alterations to the inner hair cells (IHCs) that likely contribute to the increase in auditory threshold, including a specific defect of the IHC stereocilia. To our knowledge, this is the first mouse model of an IHC-specific stereocilia defect.

Materials and methods

Mouse care

All mice were cared for in accordance with institutional animal care standards, and all experiments were approved by the University Committee on Use and Care of Animals (UCUCA).

Transgenic DNA construct and generation of *Diap3*-overexpressing mice

No complete, full-length murine *Diap3* clone was commercially available, so two partial clones (IMAGE clone ID 6407081; and IMAGE clone ID 598489, Open Biosystems) were ligated. The clones were sequenced by the University of Michigan Sequencing Core to confirm the presence of the full coding region and to confirm consensus with the reference sequence (RefSeq NM_019670.1). To create a full-length cDNA of *Diap3*, clone 598489 was subcloned into the vector containing clone 6407081 using XbaI and NotI restriction sites (all restriction enzymes were purchased from New England BioLabs). To facilitate subcloning of the resulting full-length *Diap3* cDNA into the expression vector, and to create a marker to differentiate between endogenous and

exogenous *Diap3*, a synonymous mutation was introduced into the wild-type cDNA to eliminate a SalI restriction site (c.2898C>G) using the QuikChange II Site-Directed Mutagenesis Kit (Stratagene). To eliminate the SalI site, we mutated the final nucleotide of a triplet encoding the wild-type valine from the second most common valine triplet in the mouse genome (GUC) (kazusa.or.jp/codon) to the most common valine triplet (GUG). This mutated construct was digested with NotI, blunt-ended, and then digested with SalI.

The expression vector, pCAGGS (Belgian Coordinated Collections of Microorganisms/LMBP), includes the chicken beta-actin/rabbit beta-globin hybrid promoter along with the human CMV immediate early enhancer to drive strong, ubiquitous expression[107]. This vector was digested with MscI and XhoI, and the digested *Diap3* cDNA was subcloned into the digested pCAGGS vector. The final DNA construct (Figure 3-1) was sequenced by the University of Michigan Sequencing Core to confirm that no unintentional mutations had been introduced during the subcloning process. The construct was linearized with SalI-HF and SfiI. The *E. coli* lac operon promoter, which is downstream of the ß-globin 3' elements, is retained in the linearized construct as a consequence of the available restriction sites. The University of Michigan Transgenic Animal Model Core microinjected the linearized construct into fertilized FVB/NJ mouse eggs and transferred them into pseudopregnant FVB/NJ females.

Genotyping

Genomic DNA was obtained from tail biopsies using the Gentra Puregene Genomic DNA Purification Kit (Qiagen). Transgenic mice were identified by PCR amplification of a DNA sequence unique to the transgene. The forward primer matches

sequence in the exogenous promoter (F: 5'-TGG TTA TTG TGC TGT CTC ATC A-3'); the reverse primer matches sequence that spans the exon 2-3 junction (R: 5'-TTG TCC AGC ATA TCA TCT GTC A-3'). The locations of these primers ensure that only the transgene is amplified from genomic DNA. Sequence from the mouse beta-globin gene was amplified as a control for DNA quality (F: 5'-CCA ATC TGC TCA CAC AGG ATA GAG AGG GCA GG-3'; R: 5'-cct tga ggc tgt cca agt gat tca ggc cat ct-3'). All transgenic mice used in these experiments were hemizygous for the transgene.

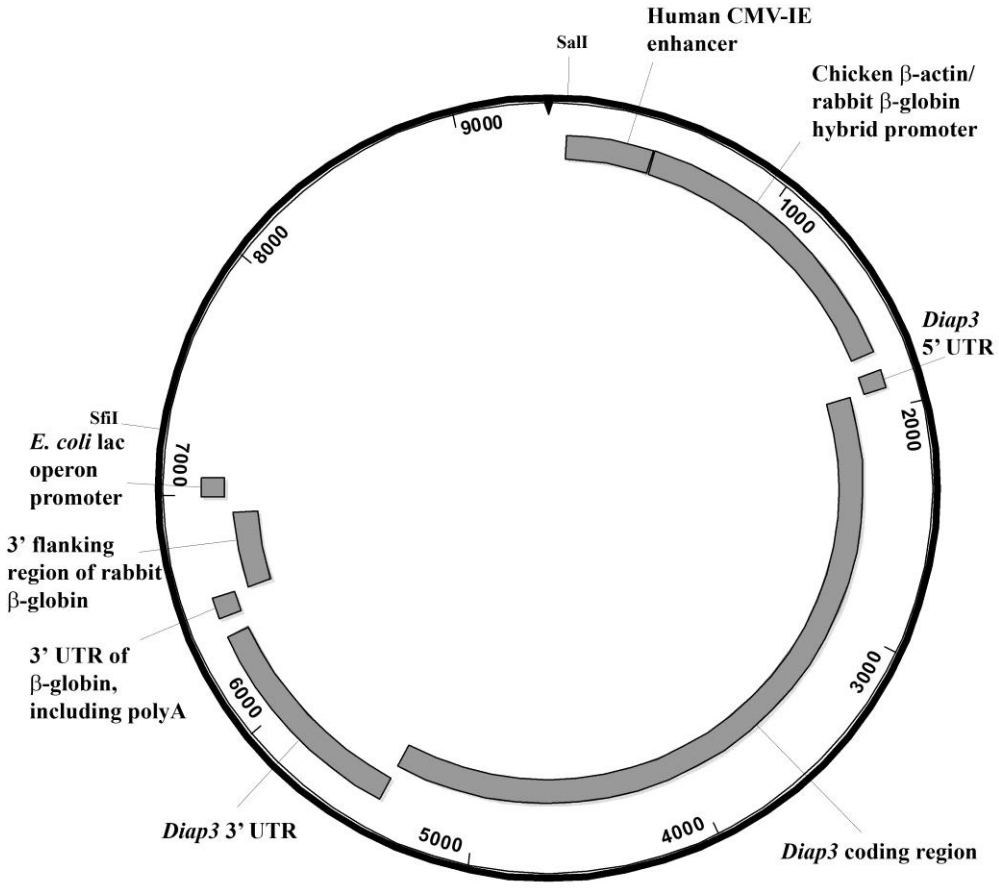

Figure 3-1. Schematic of the pCAGGS-*Diap3* DNA construct. The *Diap3* coding region and 5' and 3' UTRs, as well as all elements of the pCAGGS parent vector that were retained in the linearized plasmid, are shown. The SalI site, shown near nucleotide 1 in this schematic, and the SfiI site downstream of nucleotide 7000 indicate the ends of the

linearized plasmid that was used to generate the transgenic models. The lac operon promoter, an unnecessary element of the transgene, was retained in the linearized construct.

Transgene copy number estimation by quantitative PCR (qPCR)

We used qPCR to estimate the number of copies of *Diap3* in the two lines of transgenic mice versus wild-type mice. We performed qPCR reactions on serial dilutions of genomic DNA from tail biopsies to test primer efficiency and to identify an appropriate amount of DNA template to use for experimental reactions. Two ng of genomic DNA were used from 3 mice of each genotype (wild type, 771, and 924). Primers amplified *Diap3* sequence from exon 21 (F: 5'-GTA CTG CCT GCG AGG AGA TCA-3'; R: 5'-GAG CTA AGG TCA AAT CCG AAG G-3'). The reference gene, *GusB*, was amplified using a forward primer in exon 3 (5'-CCA TCG TCT ACA AGA CTG ACA CC-3') and a reverse primer in intron 3 (5'-gat cca gag cta gaa cca ttc tcc-3'). Primers and gDNA were mixed with 2X SYBR Green Supermix (Bio-Rad) in 20 ul reactions. Reactions were run in an iCycler iQ Real Time Thermal Cycler (BioRad). The iCycler iQ Real Time Detection System Software (BioRad) was used to determine Ct. Fold change was calculated using the ΔΔCt method[108]. Threshold cycles (Ct) were normalized to a reference gene, *GusB*, of which a stable number of copies (two) is present in both wild-type and *Diap3*-overexpressing mice. ΔCt was calculated for each sample as (Ct *GusB* – Ct *Diap3*). The mean of three technical replicates was calculated, and the means of three biological replicates were averaged. Fold increase was calculated as 2 raised to the power of the negative difference (ΔCt wild-type mice – ΔCt transgenic mice). The total number of copies of the *Diap3* gene in the chromosome of transgenic mice was calculated as the fold change multiplied by 2 (for the two copies in the

chromosome of wild-type mice). The number of inserted copies of the *Diap3* transgene was calculated as the total number of copies less 2 (for the two copies in the chromosome of wild-type mice).

Measurement of Auditory Brainstem Responses (ABRs)

ABRs were recorded by the University of Michigan Cochlear Physiology Core. Mice were anesthetized with ketamine/xylazine, and ABRs were recorded in an electrically and acoustically shielded chamber (Acoustic Systems). Needle electrodes were placed at vertex (active) and the test ear (reference) and contralateral ear (ground) pinnae. Tucker Davis Technologies (TDT) System III hardware and SigGen/BioSig software (TDT) were used to present the stimuli and record responses. Tones were delivered through an EC1 driver (TDT, aluminum enclosure made in-house), with the speculum placed just inside the tragus. Stimulus presentations were 15 ms tone bursts, with 1 ms rise/fall times, presented 10 per second. Up to 1024 responses were averaged for each stimulus level. Responses were collected for stimulus levels in 10 dB steps at higher stimulus levels, with additional 5 dB steps near threshold. Thresholds were interpolated between the lowest stimulus level where a response was observed, and 5 dB lower, where no response was observed. ABRs were measured for hemizygotes and wild-type littermates at 12, 24, and 48 kHz at 4, 8, 16, and 24 weeks of age. Statistical significance was determined using a linear mixed model, with threshold as the dependent variable, and genotype and age as fixed factors. All comparisons were made using age-matched wild-type littermates.

Measurement of Distortion Product Otoacoustic Emissions (DPOAEs)

DPOAEs were recorded by the University of Michigan Cochlear Physiology Core. DPOAEs were measured immediately following ABR testing, while mice were anesthetized. The primary tones, F1 and F2, were set at a ratio of F2/F1 = 1.2. The intensity of F1 (L1) was varied in 5 or 10 dB steps (with the intensity of F1 ranging from 10-80 dB SPL), with the intensity of F2 (L2) held at 10 dB quieter than L1. The DPOAE was measured at 2F1 – F2. Tones were presented via two EC1 drivers (TDT, aluminum-shielded enclosure made in house) connected through an Etymotic microphone (ER 10B+, Etymotic Research, Inc.). TDT System III hardware and SigGen/BioSig software were used to present the stimuli and record responses. DPOAEs were measured for hemizygotes and wild-type littermates at 12, 24, and 48 kHz at 16 and 24 weeks of age. Statistical significance was determined using repeated measures analysis of variance. All comparisons were made using age-matched wild-type littermates.

Gene expression analysis by quantitative reverse transcription PCR (qRT-PCR)

Mice were euthanized in a saturated CO_2 chamber. Cochlear tissue from a minimum of 4 ears (2 mice) was removed and immediately submerged in Trizol (Invitrogen), and RNA was isolated according to the manufacturer's instructions. Residual DNA was eliminated using TURBO DNA-free (Ambio) following the manufacturer's recommendations. Equal amounts of DNAse-treated RNA (typically 1 ug) was used to synthesize single-stranded cDNA with SuperScript II (Invitrogen), primed by oligo$(dT)_{12\text{-}18}$ (Invitrogen) according to the manufacturer's instructions. RNA was intermittently run on gels to assess RNA quality. We mixed 15% (per PCR reaction) of the first strand reaction with primers and 2X SYBR Green Supermix (BioRad).

Primers amplified sequence that spans exons 24 and 25 (F: 5'-TTA TCA GTG CGA ACG AGC A-3'; R: 5'-TAT CCT GGC ACG TTT CTC C-3'). Primers for the reference gene, beta-glucoronidase (*GusB*), spanned exons 10 to 12 (F: 5'-CCG ATT ATC CAG AGC GAG TAT G-3'; R: 5'-CTC AGC GGT GAC TGG TTC G-3'). The reference gene *GusB* was selected because we expected its expression to be unaltered by *Diap3* dysregulation, and indeed, equal amounts of template cDNA resulted in similar threshold cycles in both wild-type and transgenic animals. Reactions were run in an iCycler iQ Real Time Thermal Cycler (BioRad). The iCycler iQ Real Time Detection System Software (BioRad) was used to determine Ct. Negative control reactions without reverse transcriptase were regularly run to assess genomic DNA contamination, and no products were detected. We performed qRT-PCR reactions on serial dilutions of cDNA to test primer efficiency and to identify an appropriate amount of cDNA template to use for experimental reactions. As for qPCR, above, fold change was calculated using the ΔΔCt method[108]. Briefly, the Ct was normalized for each sample by subtracting the reference gene Ct from the gene of interest Ct (ΔCt = Ct *GusB* – Ct *Diap3*). The mean of three technical replicates was calculated, and the means of three biological replicates were averaged. The ΔΔCt was calculated as the difference between the mean ΔCt of the transgenic samples and the ΔCt of the wild-type samples (ΔΔCt = ΔCt wild-type mice – ΔCt transgenic mice). Fold increase was calculated as 2 raised to the power of the negative difference (ΔCt wild-type mice – ΔCt transgenic mice). Statistical significance was established by ANOVA, and a 95% confidence interval was established for the difference in means.

Spiral ganglion cell (SGC) counts

Mice were deeply anesthetized with sodium pentobarbital, and tissues were fixed by vascular perfusion with 4% paraformaldehyde (PFA). Cochleae were removed and post-fixed in 4% PFA for 4 hours, then decalcified in 5% EDTA for 1-2 days. Cochleae were embedded in JB-4 resin and sectioned to a thickness of 5 microns. For each mouse, SGNs were counted from six sections of the mid-modiolar plane. A SGC was included in the count if its cell body had a diameter between 12 and 25 μm and an area between 12 and 28 μm^2 and if the nucleus was visible with a diameter between 5 and 9 μm. Results are reported as mean SGCs per 10,000 μm^2. Statistical significance of the difference between means of the three genotypes was determined by ANOVA.

Immunohistochemistry

Mice were euthanized in a saturated CO_2 chamber. Cochleae were removed and fixed by local perfusion with 4% PFA for 2-4 hours, rinsed with PBS, then decalcified for 2 days in a 5% EDTA solution at room temperature. After decalcification, cochleae were further dissected to expose the organ of Corti. Exposed organs of Corti were incubated in 5% normal donkey serum diluted in 0.3% Triton X in PBS supplemented with Ca^{2+} and Mg^{2+} for 30 minutes at room temperature. Organs of Corti were incubated overnight at 4ºC with mouse anti-CtBP2 (BD Transduction Laboratories) primary antibody diluted in PBS supplemented with Ca^{2+} and Mg^{2+}. Specimens were rinsed with PBS, then incubated in Alexa Fluor donkey anti-mouse 488 secondary antibody (Life Technologies) for 1.5 hours at room temperature. After 45 minutes in secondary antibody, Alexa Fluor 568 Phalloidin (Life Technologies) was added to the incubation step. Specimens were rinsed

with PBS, then further dissected into separate apex, base, and hook segments. Segments were mounted on coverslips with Fluoromount-G (SouthernBiotech).

Confocal imaging

All confocal images were taken on an Olympus Fluoview FV1000 confocal microscope. Confocal z-stacks were obtained using either a 10X objective or a 60X oil immersion objective. Every attempt was made to take all images (including SEM) from the same approximate region of the organ of Corti, between approximately 15 to 40% of the distance from the apex to the base. This region is expected to correspond to the organ of Corti that is most responsive to the ~8 to 19 kHz range as described by Müller et al.[109]. Images were acquired with Olympus FV1000 ASW software and analyzed using ImageJ.

Counts of Ribeye-positive puncta

The antibody for C-terminal Binding Protein 2 (CtBP2) recognizes both the CtBP2 protein in the nucleus of cells, where it acts as a transcriptional repressor, and also the closely related protein Ribeye, a marker for ribbon synapses[110]. Thus this antibody can be used to identify the nuclei of individual IHCs as well as their punctate ribbons. During confocal image acquisition, the top and bottom of the z-stack were set as the points at which puncta first appeared and last disappeared. The z-stacks were maximum-projected onto a single plane using ImageJ software. Lines were drawn to estimate the borders of each IHC, and the number of ribeye-positive puncta per cell was counted. Puncta were counted by three evaluators blind to the genotypes of the specimens. The means of the three counts were averaged, and statistical significance between wild-type and transgenic mice was determined using Student's *t* test. Although it is common to use 3D reconstruction to count puncta, and there is concern that projecting the z-stack onto a

single plane may result in underestimation of the number of puncta, we have found that our wild-type ribbon counts per IHC (mean of ~15-16 per IHC; range of 10 to 30) agree with previously published studies in which a variety of methods have been used to count ribbons[22,111,112].

Scanning Electron Microscopy (SEM)

Mice were euthanized in a saturated CO_2 chamber. Cochleae were removed and locally perfused with 2.5% glutaraldehyde in 0.15M cacodylate buffer for 2 hours, then the sensory epithelium was exposed to reveal the stereocilia of the IHCs and OHCs. Samples were prepared for SEM using the OTOTO method[113], in which samples are alternately incubated in osmium tetroxide and thiocarbohydrozide. For dehydrating samples, specimens were immersed in increasing concentrations of ethanol from 30% to 100%, then immersed and incubated in 100% hexamethyldisilazane (HMDS). Images were captured on an AMRAY 1910 Field Emission Scanning Electron Microscope using X-Stream Image Capture software (SEMTech Solutions, Billerica, MA).

Results

Generation of *Diap3*-overexpressing transgenic mice

A pCAGGS vector and two partial clones of full-length *Diap3* were utilized, as no complete, full-length clones were commercially available. A point mutation was introduced into the coding region of one of the *Diap3* clones in order to eliminate a SalI restriction site, both to facilitate subcloning and to use as a means of differentiating between endogenous and exogenous *Diap3* sequence. The pCAGGS vector contains the chicken beta-actin/rabbit beta-globin hybrid promoter along with the human CMV

immediate early enhancer to drive strong, ubiquitous expression[107] of the full-length *Diap3* clone. The University of Michigan Transgenic Animal Model Core microinjected the DNA construct into fertilized FVB/NJ mouse eggs and implanted them into pseudopregnant FVB/NJ mice. Many of the mouse strains commonly used in transgenesis, such as C57Bl/6, experience age-related hearing loss. We selected FVB/NJ as the background strain because these mice have been shown to be resistant to age-related hearing loss[114], yet they produce large pronuclei for relatively easy microinjection, as well as frequent, large litters[115].

PCR genotyping of DNA isolated from tail biopsies revealed that 10 of 83 potential transgenic founders had integrated the transgene. One of these 10 mice lacked a Preyer reflex, the characteristic startle response to sudden loud sound presentations, but this mouse died prior to producing offspring. All nine surviving transgenic mice exhibited a Preyer reflex, a test that reveals only severe to profound hearing loss. These mice were mated to wild-type FVB/NJ mice, and six founders transmitted the transgene to their offspring. We used ABR to identify hearing loss in the F1 generation at 4, 8, and 16 weeks of age. Three founders were identified that both transmitted the transgene and experienced hearing loss within the first 16 weeks of life. These three lines presumably differ in the number of copies of the transgene and in the location of the transgene insertion site due to random integration during microinjection. From this point forward, these lines, FVB-Tg(CAG-Diap3)771Lesp, FVB-Tg(CAG-Diap3)924Lesp/J, and FVB-Tg(CAG-Diap3)946Lesp, will be called 771, 924, and 946, respectively.

Transgenic mice from lines 771 and 924 were born in expected Mendelian ratios, and these two lines are discussed here. Transgenic mice from the third line, 946, were not

born in Mendelian ratios and experienced a more severe, but not fully penetrant, phenotype. This line is discussed in Appendix B. A cardiac phenotype that was identified in *Diap3*-overexpressing mice is discussed in Appendix A.

In order to estimate the number of copies of transgene that were integrated into the genome, we used qPCR to amplify *Diap3* sequence from wild-type and transgenic genomic DNA template. An estimated 8 to 9 copies of transgene integrated into the genome of transgenic mice from line 771, and an estimated 6 copies of transgene integrated into the genome of transgenic mice from line 924 (data not shown).

Two lines of *Diap3* transgenic mice develop progressive hearing loss

We used ABR to assess hearing in lines 771 and 924 at 4, 8, 16, and 24 weeks of age. Line 771 manifested a mild hearing loss at 12 kHz at 4 and 8 weeks of age, with a mean threshold shift of 20 dB (Figure 3-2A). At 16 weeks of age, the hearing loss progressed to a 40 dB shift at both 12 and 24 kHz. The threshold shift progressed further by 24 weeks of age to 60 dB at both 12 kHz and 24 kHz. Auditory threshold differences at 48 kHz were not statistically significant at any time point (data not shown).

While there was no significant relationship of age and threshold for wild-type mice at 12 kHz (p=0.150) or 24 kHz (p=0.552), there was a significant relationship between age and threshold for transgenic mice of line 771 at 12 kHz (p=0.010) and at 24 kHz (p=0.001). The results were similar for line 924: there was no significant relationship of age with threshold for wild-type mice at 12 kHz (p=0.563) or 24 kHz (p=0.761), but there was a significant relationship between age and threshold for transgenic mice of line 924 at 12 kHz (p<0.001) and at 24 kHz (p<0.001).

Transgenic mice from line 924 had auditory thresholds that were indistinguishable from wild-type thresholds at 4 and 8 weeks of age, but by 16 weeks of age, threshold shifts of 35 dB at 12 and 24 kHz were recorded (Figure 3-2B and D). Similar to line 771, these threshold changes progressed by 24 weeks of age to severe hearing loss, with 50 dB threshold shifts at both 12 and 24 kHz. Auditory threshold differences at 48 kHz were not statistically significant at any time point (data not shown).

Both lines of transgenic mice retain otoacoustic emissions despite significant shifts in auditory thresholds.

DPOAE measurements at 24 weeks of age demonstrated that transgenic mice from lines 771 and 924 retain otoacoustic emissions at 12 kHz (Figure 3-3A and B) despite significantly increased auditory thresholds (Figure 3-2A and B). There was no significant difference between line 771 mice and wild-type littermates at 12 kHz at 24 weeks (p= 0.2136) or between line 924 mice and wild-type littermates (p=0.1094) (Figure 3-3A and B). Retention of emissions at 24 kHz was variable at 24 weeks for mice of each line, but while the difference between wild-type and transgenic mice was statistically significant for line 771 (p=0.0049), it was not significant for line 924 (p=0.105) (Figure 3-3C and D).

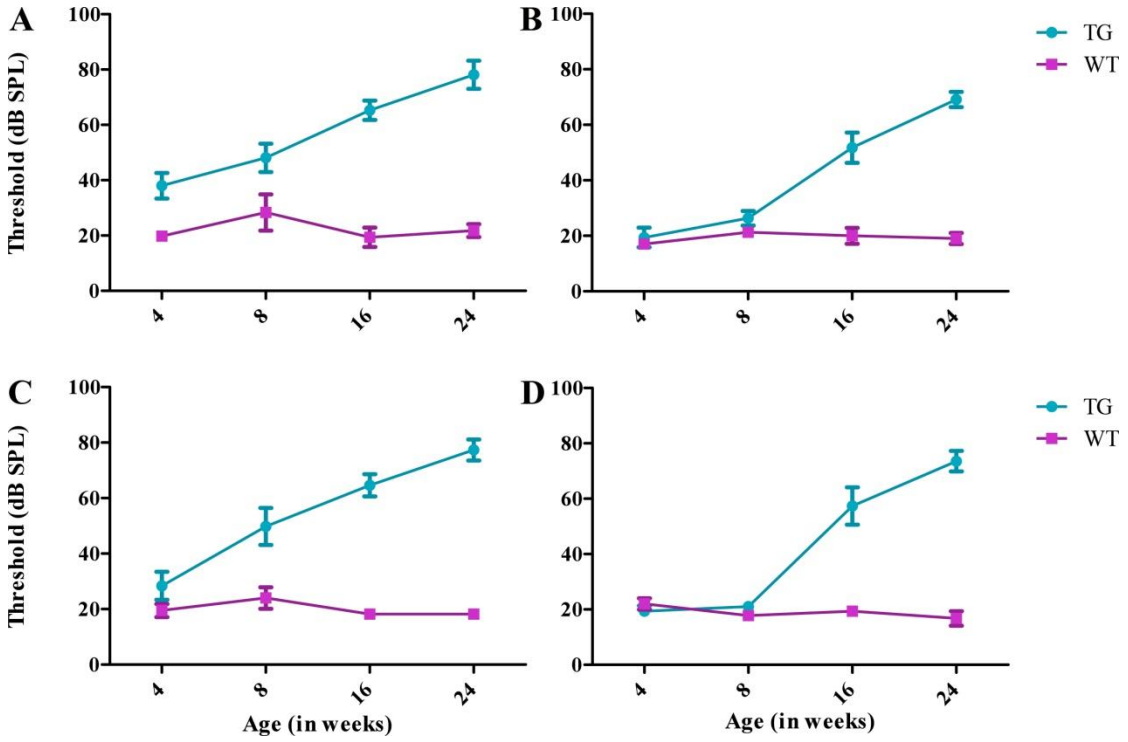

Figure 3-2. ABRs demonstrate that *Diap3*-overexpressing mice experience progressive hearing loss. Mean ABR thresholds (and mean ± SEM) are shown. Higher thresholds indicate that higher volumes are required to elicit a brainstem response. (A) At 12 kHz, line 771 mice exhibited an ~20 dB increase in auditory thresholds at 4 and 8 weeks that continued to increase at 16 and 24 weeks (blue circles, *n*=5-11) compared to wild-type littermates (purple squares, *n*=4-6). (C) At 24 kHz, hearing deteriorated from wild-type levels at 4 weeks of age to a difference of ~60 dB by 24 weeks of age. (B and D) At both 12 and 24 kHz, auditory thresholds for transgenic mice from line 924 (*n*=5-8) were indistinguishable from wild-type mice (*n*=3-5) at 4 and 8 weeks of age. Over the next 16 weeks, thresholds of transgenic mice increased significantly, compared to those of wild-type littermates. TG, transgenic; WT, wild type.

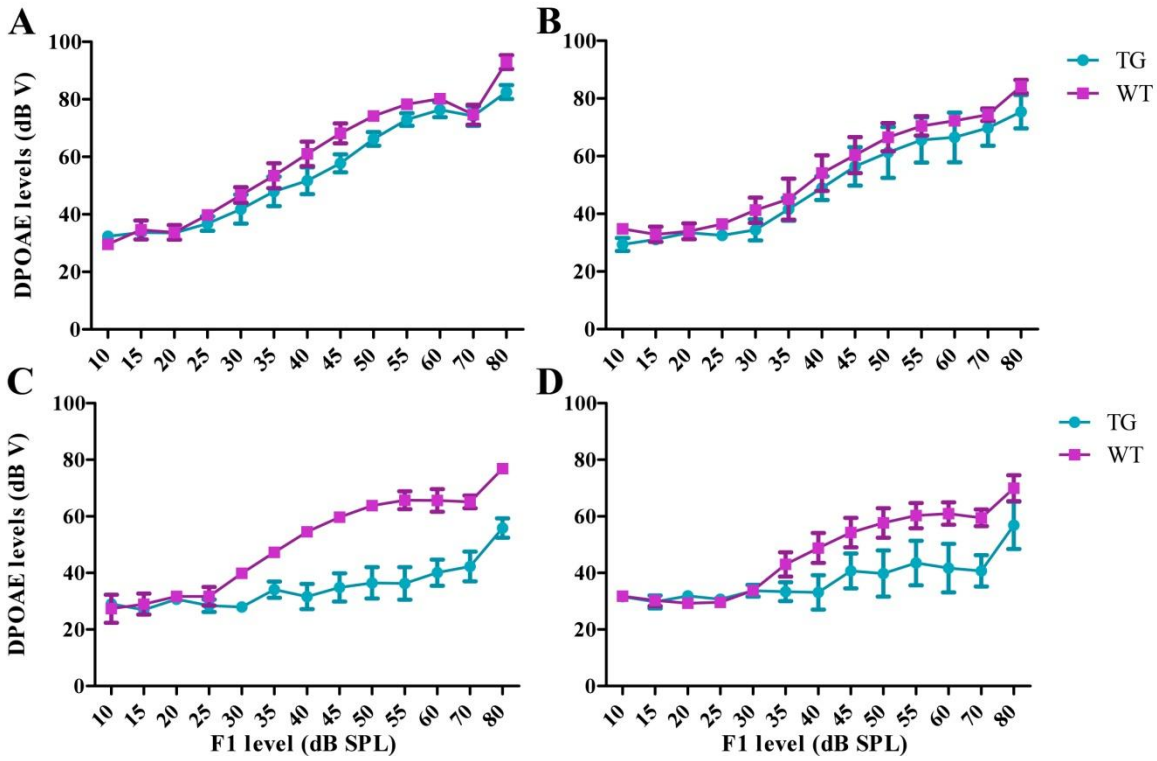

Figure 3-3. *Diap3*-overexpressing mice retain otoacoustic emissions at 12 kHz until at least 24 weeks of age. Mean DPOAE levels (and mean ± SEM) are shown. (A-B) At 12 kHz there was no significant difference between transgenic mice (blue circles) of line 771 (p=0.21; n=6) (A) or 924 (p=0.37; n=5) (B) and wild-type mice (purple squares, n=3 and 4, respectively). (C-D) At 24 kHz, in the same animals as in (A) and (B), differences between line 771 and wild-type littermates were statistically significant (p=0.0049), while those between line 924 and wild-type littermates were not (p=0.10). Statistical significance was determined by ANOVA.

The *Diap3* transgene is highly overexpressed in the cochleae of both transgenic mouse lines

qRT-PCR was performed on pooled cochleae of transgenic mice and wild-type littermates. The mean difference in threshold cycle (Ct) for *Diap3* (normalized to the Ct for a reference gene, *GusB*) between wild type and line 771 was 9.487 ± 3.257 (95% CI; p=0.006) (Figure 3-2A). The difference between wild type and line 924 was 10.153 ± 1.918 (95% CI; p=0.002) (Figure 3-4B). These differences correspond to fold changes of

~700 for line 771 and ~1100 for line 924 compared to wild-type littermates. Similar changes were also seen in heart tissue (see Appendix A).

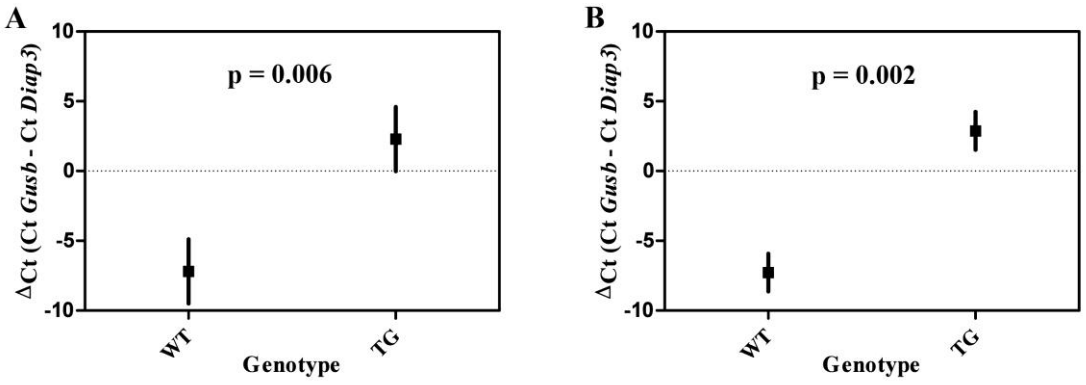

Figure 3-4. *Diap3* is highly overexpressed in cochlear tissue from line 771 and 924 mice as compared to wild-type littermates. Relative expression of *Diap3* was assessed using mRNA isolated from the cochleae of 2-3 transgenic and wild-type mice of 3 separate litters at 24 weeks of age. Quantitative RT-PCR demonstrated significant differences in *Diap3* expression between line 771 and wild-type littermates (A) and between line 924 and wild-type littermates (B). Mean threshold cycles (Ct) are indicated at the horizontal lines; vertical lines represent 95% confidence intervals. Threshold cycle differences were ~9-10, which correspond to expression levels approximately 700- to 1100-fold greater in transgenic mice than in wild-type littermates. Differences in expression between wild-type and transgenic mice were significantly significant for both lines (p=0.006 and 0.002 for lines 771 and 924, respectively), but differences between litters were not (p>0.05, ANOVA).

Diap3-overexpressing mice have normal numbers of spiral ganglion cells but decreased numbers of inner hair cell ribbons

We hypothesized that the change in ABR threshold might be due to a loss of type I SGNs, the large, myelinated afferent neurons that synapse on IHCs[97]. SGC counts of 24-week-old mice from line 771 and 924, however, suggest that there is no significant difference in numbers of type I neurons (Figure 3-5).

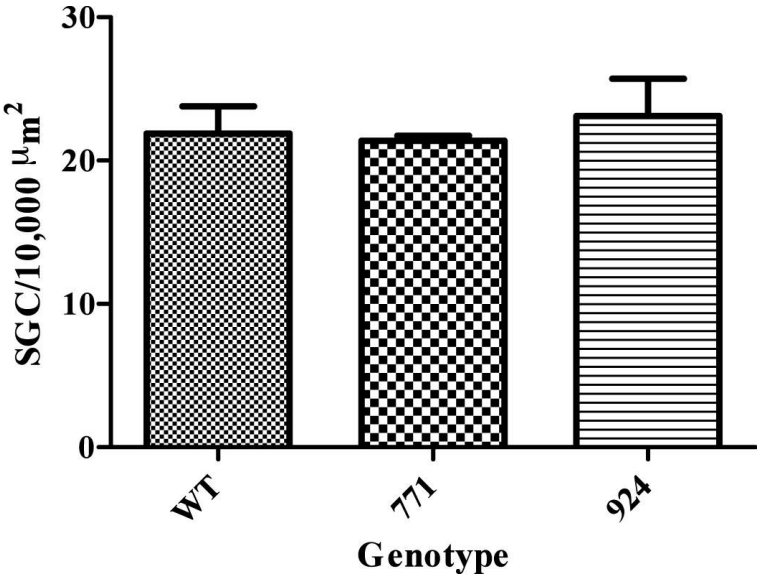

Figure 3-5. Elevated auditory thresholds in *Diap3*-overexpressing mice are not a result of spiral ganglion cell degeneration. Quantification of SGC density across all cochlear turns showed no significant differences between lines 771 (n=3) and 924 (n=4) and wild-type mice (n=4) at 24 weeks of age. Bars indicate mean ± SEM (p>0.05 for both comparisons, Student's t test).

We then wondered whether the elevated auditory thresholds were due to a defect at the IHC synapse, so we stained organ of Corti whole mounts using an antibody against CtBP2, which labels both the CtBP2 in nuclei and the Ribeye in ribbon synapses of IHCs[110]. This enabled us to count the number of both IHCs and ribeye-positive puncta from z-stack projections of confocal images. We found that the numbers of ribbon synapses per IHC were significantly reduced in lines 771 and 924 mice as compared to wild-type mice (Figure 3-6). Ribbon counts were reduced by 44% in line 771 and by 28% in line 924.

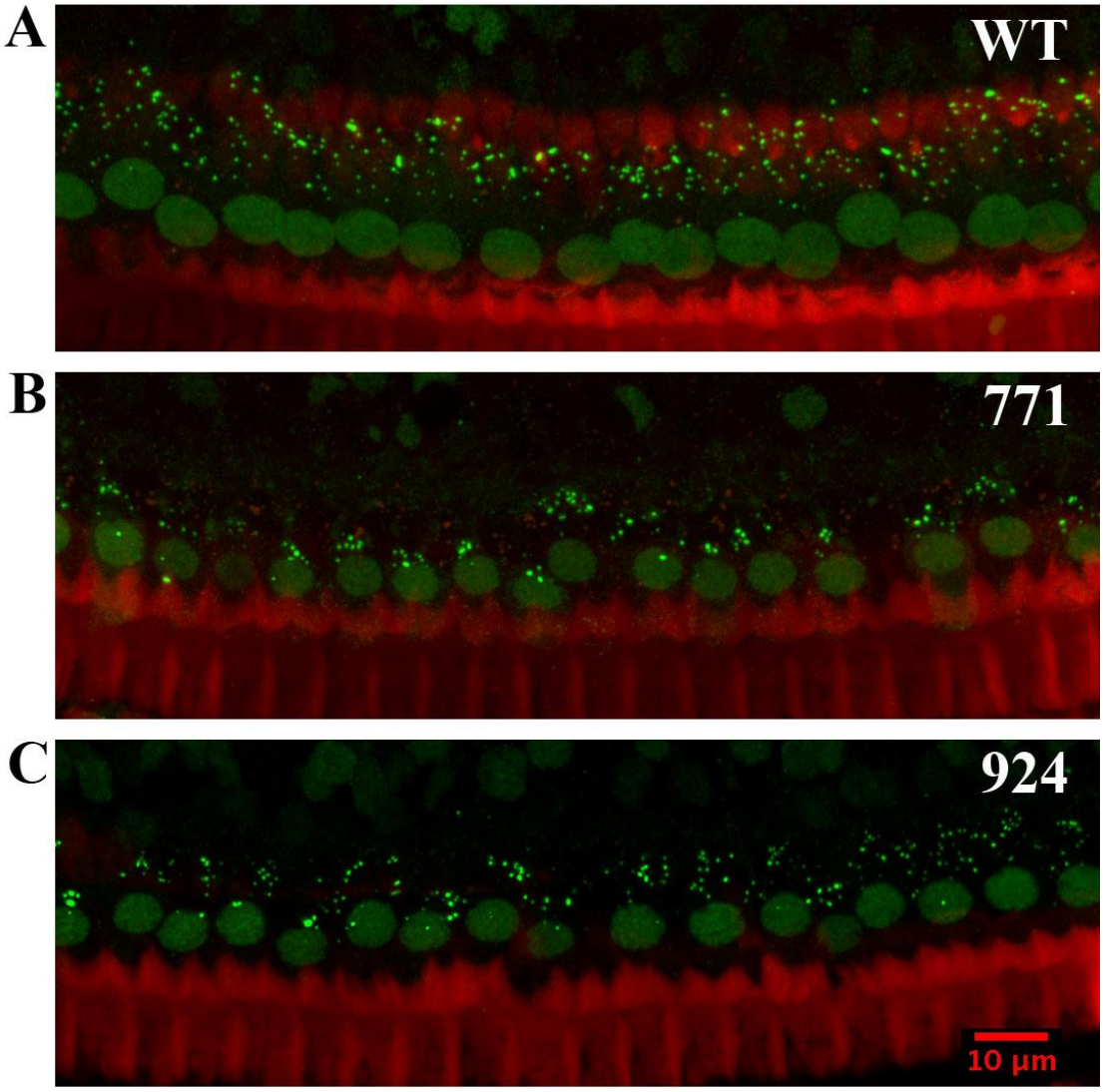
A
WT
B
771
C
924
10 µm

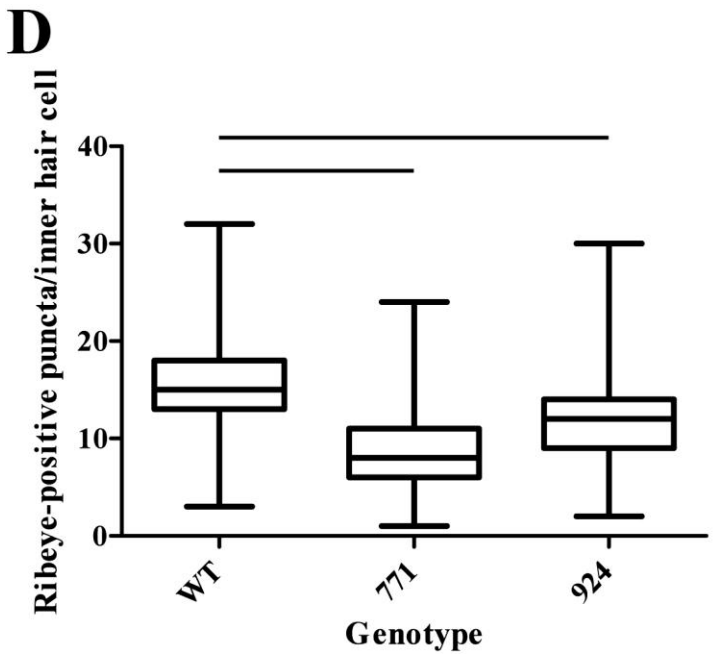

Figure 3-6. The number of ribbons in IHCs of *Diap3*-overexpressing mice is significantly reduced at 24 weeks of age. (A-C) Projected z-stacks of confocal images of IHCs from wild-type (A), line 771 (B), and line 924 (C) mice taken at similar cochlear locations. The differences in phalloidin staining between the wild-type and transgenic mice are due to the orientation of the planes of analysis. The transgenic mice appeared to have fewer ribbons than wild-type littermates (A). (D) Counts of ribbons in these lines confirmed the apparent difference. The mean for wild-type mice was 15.58 ± 0.1863 ribeye-positive puncta per IHC (mean ± SEM; n=4; 174 IHC); the mean for 771 is 8.675 ± 0.1996 (n=3 mice; 189 IHC); the mean for line 924 was 11.650 ± 0.2174 (n=5 mice; 150 IHC). Box plots indicate median, 25th, and 75th percentiles and minimum-maximum whiskers. Horizontal lines indicate p<0.0001.

The stereocilia and apical surfaces of inner hair cells are profoundly abnormal in *Diap3*-overexpressing mice

Phalloidin staining of organ of Corti whole mounts allowed us to visualize stereocilia at the apical surface of IHCs. OHC stereocilia are also labeled by phalloidin, and OHC hair bundles appeared normal (data not shown). At 8 weeks of age, when line 771 mice had elevated auditory thresholds but line 924 mice had auditory thresholds that were indistinguishable from wild-type littermates (Figure 3-2), IHC stereocilia in both lines appeared somewhat different from the stereocilia of wild-type mice (Figure 3-7A-C). While each IHC stereocilium of wild-type mice appeared to be individual and separate from its neighbors, many of the stereocilia of lines 771 and 924 appeared to be fused (Figure 3-7A-C). Furthermore, the stereocilia of line 771 mice appeared to be slightly longer than those of either wild-type or line 924 mice. By 16 weeks of age, both line 771 and 924 had elongated stereocilia that again appeared to be fused (Figure 3-7D-F). At 24 and 48 weeks, stereocilia continued to appear elongated and there were fewer per hair cell (Figure 3-7G-L) (not quantified). While most of the stereocilia of wild-type mice appeared uniform in thickness throughout the 48 weeks, many of the stereocilia of transgenic mice from both lines appeared to be thicker at the base than in the middle or tips of the stereocilia (Figure 3-7). This thickening at the base gave some of the stereocilia a fused appearance.

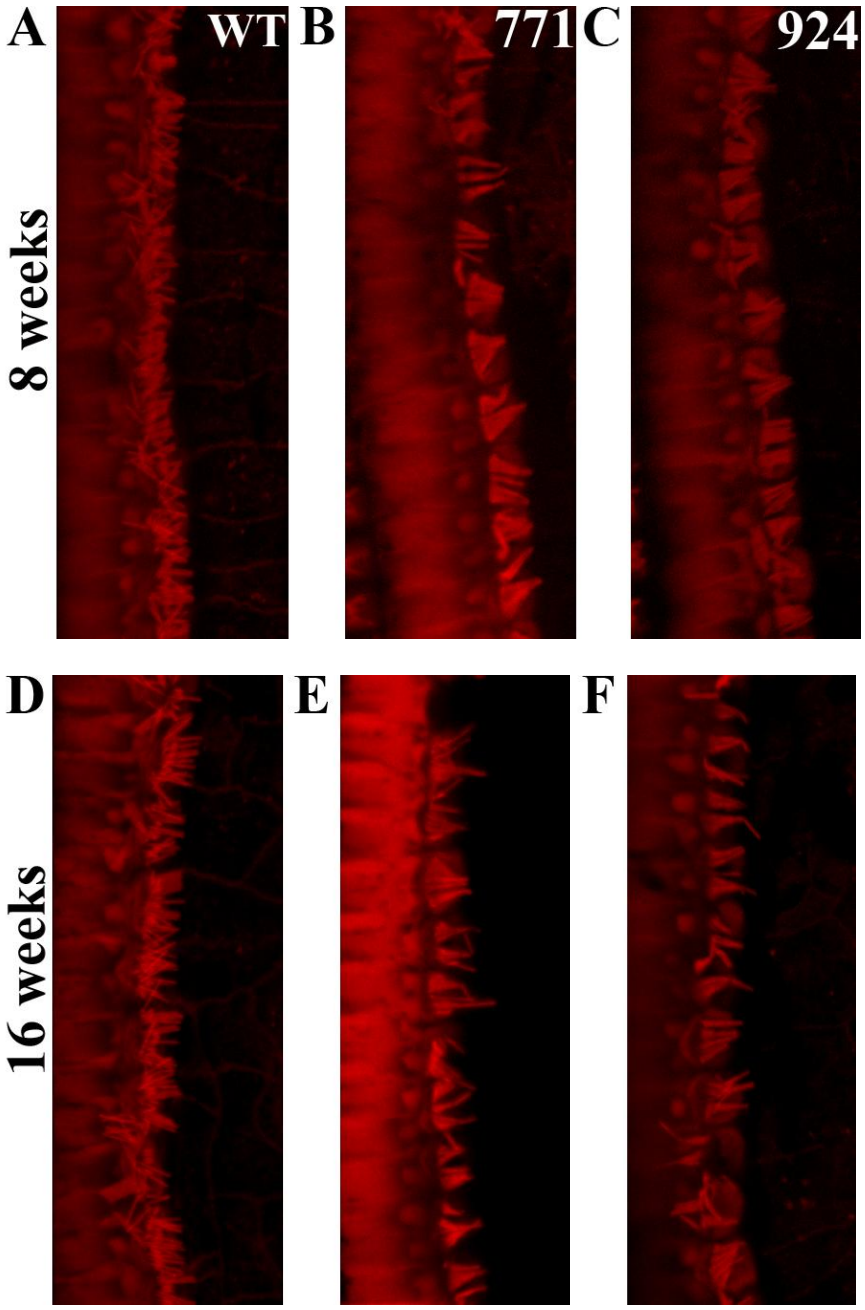
A
WT
B
771
C
924
8 weeks
D
E
F
16 weeks

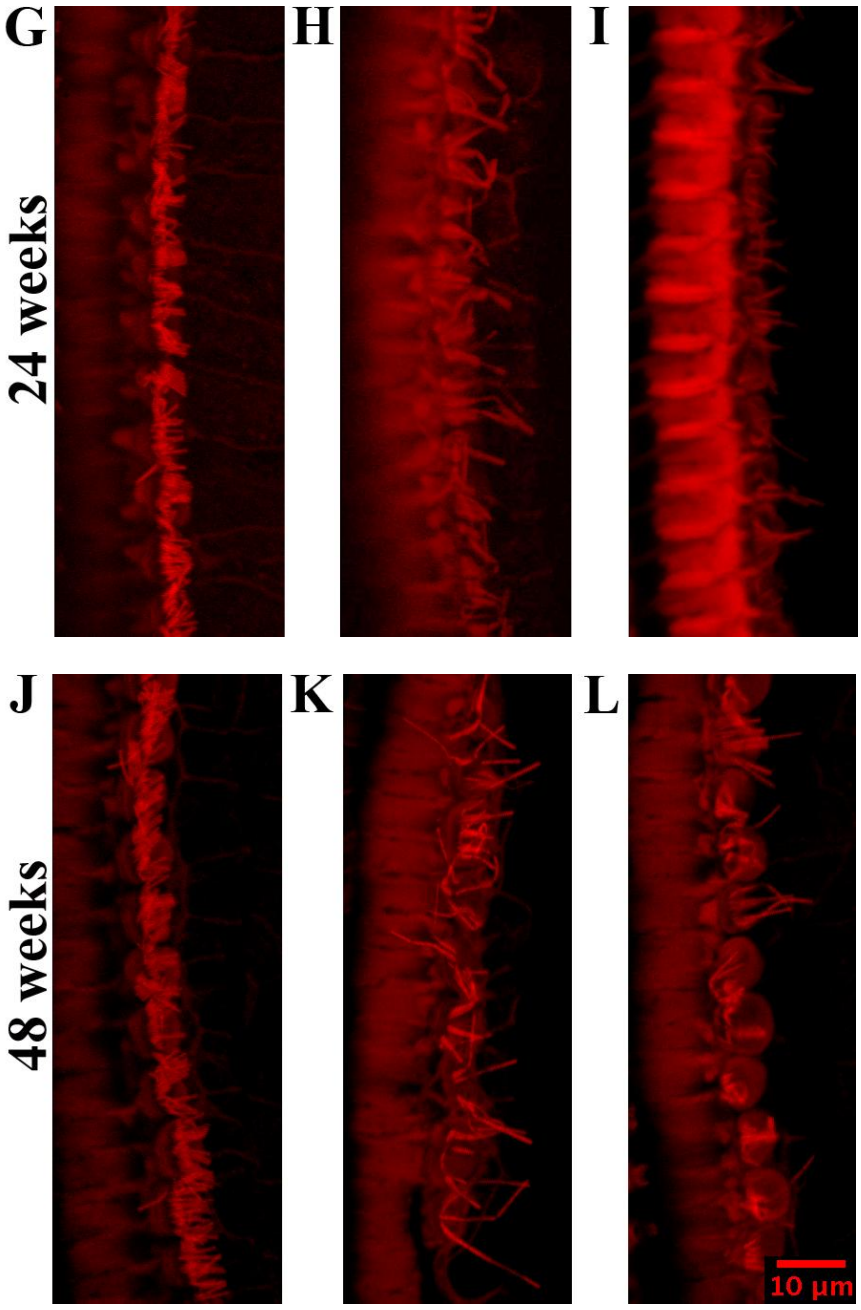

Figure 3-7. The stereocilia of *Diap3*-overexpressing mice change over time. Cochlear whole mounts from mice at 8 (A-C), 16 (D-F), 24 (G-I), and 48 (J-L) weeks of age were incubated with fluorophore-conjugated phalloidin to label F-actin. IHC stereocilia from wild-type mice (A,D,G,J) appeared slightly disorganized as a result of the fixation and mounting procedures, but they appeared to be freely standing individuals of approximately the same height and thickness from base to tip. (A-C) At 8 weeks of age, there were minor differences between wild-type (A), line 771 (B), and line 924 (C) mouse cochleae. Some of the stereocilia of transgenic mice at 8 and 16 weeks of age (B,C,E,F) appeared to be fused. At 24 weeks, there appeared to be fewer stereocilia in transgenic mice (H,I) than in wild-type mice (G), although this was not quantified. At 48

weeks, there appeared to be a further reduction in the number of stereocilia per hair cell, and the stereocilia appeared disorganized and elongated. (A-I) $n \geq 3$; (J) $n=2$; (K) $n=1$; (L) $n=2$. Scale bar in (L) applies to all images in (A-L).

To better visualize the graded rows of IHC and OHC stereocilia, we used SEM to image organ of Corti samples from 24-week-old mice (Figure 3-8). In these images, some of the OHC stereocilia from line 771, particularly those in the outermost row, appeared to have lost some of their structural integrity (Figure 3-8B). The OHC stereocilia from line 924, however, appeared indistinguishable from those of wild-type mice (Figure 3-8E and F). IHCs from both lines, however, appeared strikingly unusual. Their apical surfaces appeared to protrude from the reticular lamina, and the numbers of stereocilia per IHC were reduced from several dozen to approximately five. In addition, these few remaining IHC stereocilia were arranged in a single row rather than the expected three.

In summary, transgenic mice from line 771 exhibited a relatively mild 20 dB hearing loss at 12 kHz at 4 and 8 weeks of age that progressed to 40 dB at 16 weeks and 60 dB at 24 weeks at both 12 and 24 kHz. Line 924 showed no hearing loss at 4 and 8 weeks, but it progressed to 35 and 50 dB threshold shifts at 16 and 24 weeks, respectively. Transgenic mice from both lines retained otoacoustic emissions at time points and frequencies at which their auditory thresholds are significantly elevated. We have noted both a reduction in the number of ribbons in IHCs and profound changes to the IHC stereocilia in mice that overexpress *Diap3*.

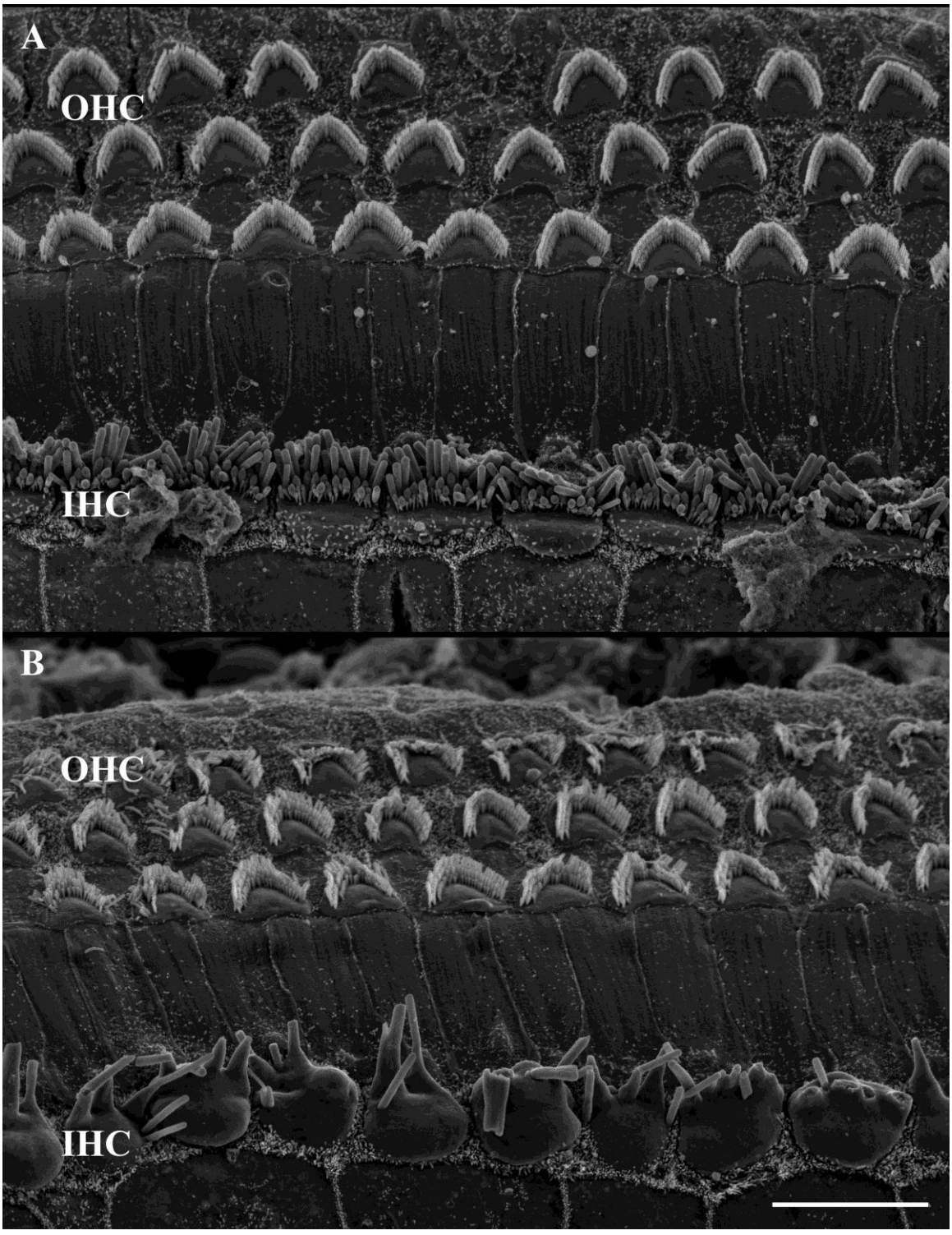
A
OHC
IHC
B
OHC
IHC

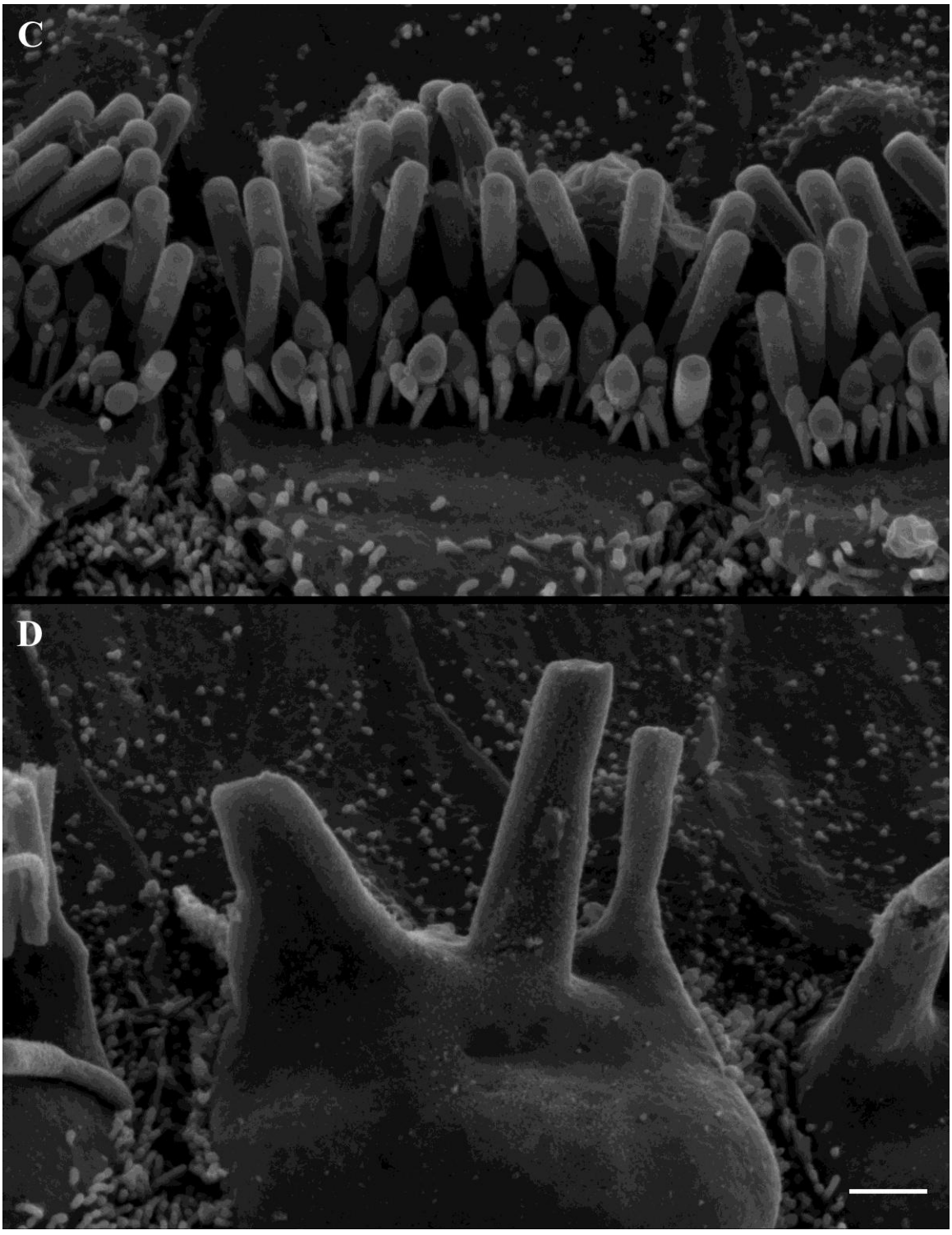
C
D

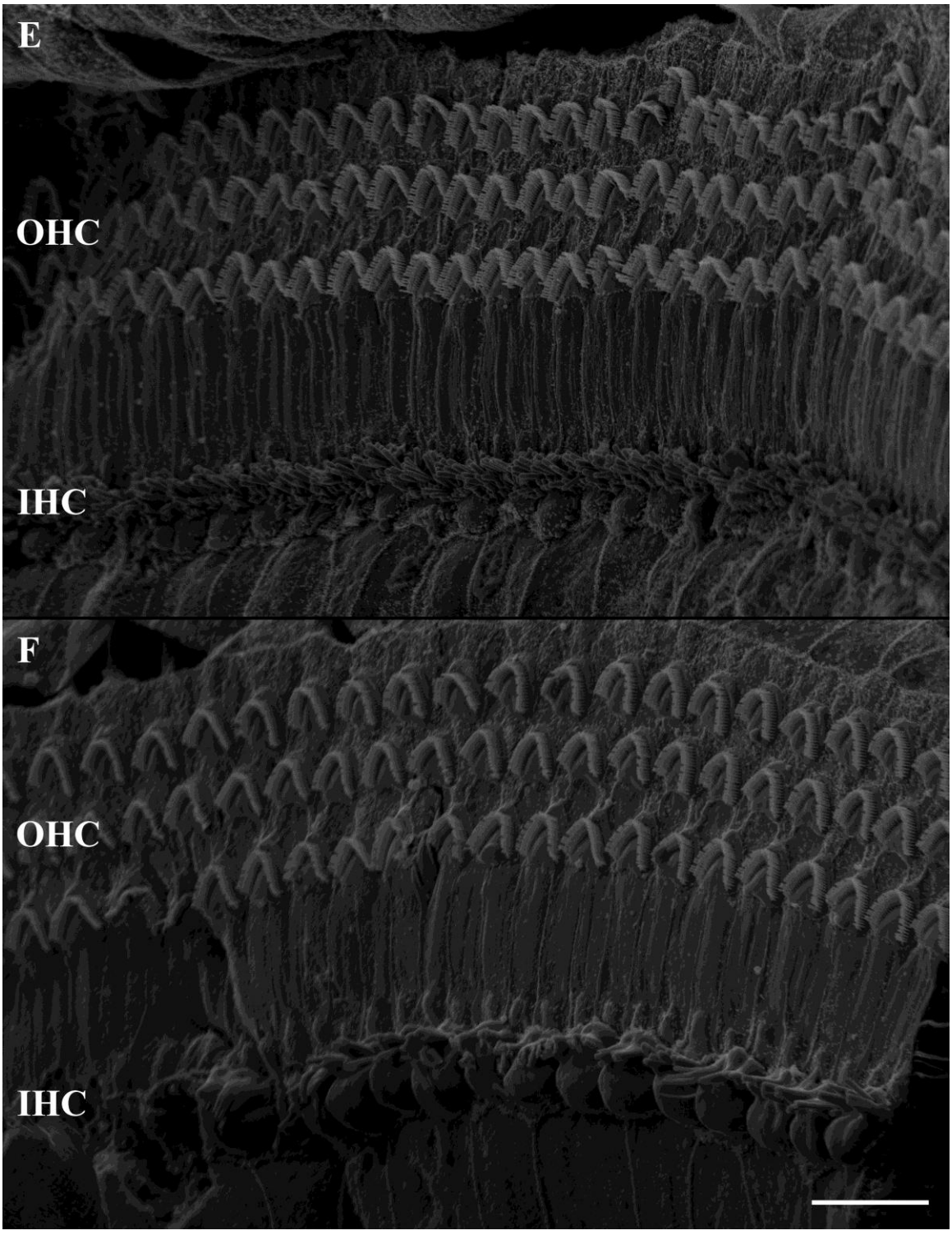
E
OHC
IHC
F
OHC
IHC

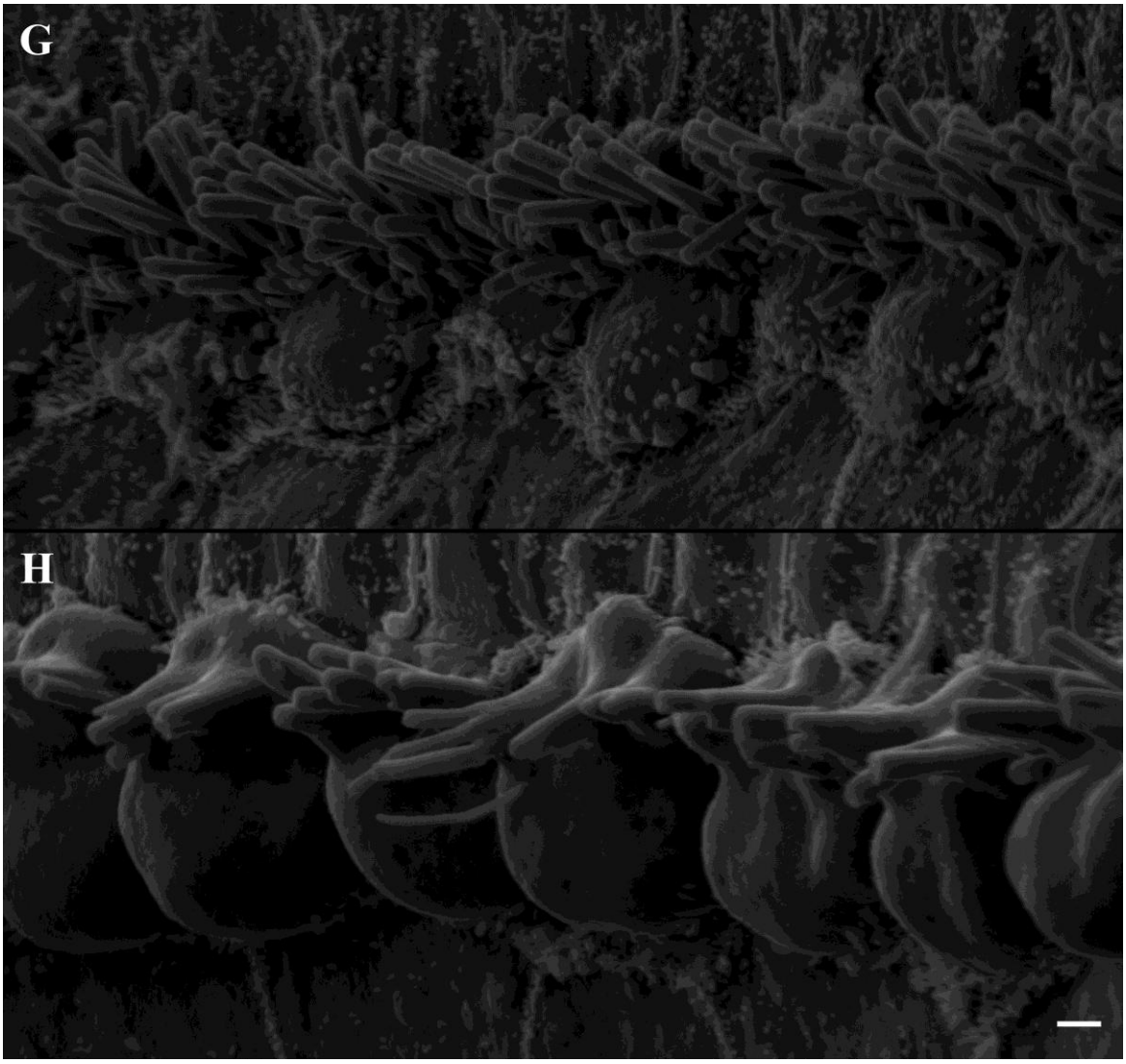

Figure 3-8. SEM images reveal dramatic differences in the stereocilia and apical surfaces of IHCs of *Diap3*-overexpressing mice compared to wild-type littermates at 24 weeks of age. Images show wild-type hair cells (A,C,E,G) juxtaposed to line 771 hair cells (B,D) or line 924 hair cells (F,H). Wild-type OHCs and IHCs (A) appeared orderly and organized. Note the missing OHC in the middle of the outermost row; occasional missing OHCs are not unusual in wild-type mice, especially at this age. Some of the IHC stereocilia appeared slightly splayed, but relatively normal. In the line 771 mouse (B), by contrast, quite a few OHC hair bundles were splayed or flattened. The IHC stereocilia, however, were highly unusual. Note that the apical surfaces appear distended and swollen, and the number of stereocilia is markedly reduced. At higher magnification the fused appearance of the line 771 stereocilia (D) becomes more obvious in comparison to the wild-type hair bundle (C). The phenotype of line 924 mice (F, H) was remarkably similar to that of line 771. Note that the polarity of the transgenic IHCs has not been altered, despite the drastic changes to their apical surfaces. Scale bars in B and F represent 10 μm and also apply to A and E, respectively. Scale bars in D and H represent 1 μm and also apply to C and G, respectively.

Discussion

We have developed two lines of transgenic mice that express high levels of *Diap3* in the cochlea. Both transgenic lines experience progressive increases in auditory theshold over similar, but not identical, time courses, and both lines produce OAEs at time points when ABRs are already significantly elevated. Despite severe hearing loss at 24 weeks of age, both lines have numbers of SGCs that are equivalent to those of wild-type mice. We demonstrate that the IHCs of these mice have decreased ribbons, and we document profound changes to their stereocilia and apical surfaces, while the OHCs appear relatively well preserved. Despite the supraphysiological levels of *Diap3* expression, these transgenic mice recapitulate the auditory phenotype associated with human progressive auditory neuropathy *AUNA1*. We suggest that these mice recapitulate aspects of the anatomical and molecular phenotypes as well. To our knowledge, this is the first genetic mouse model of an IHC-specific defect of the stereocilia.

We observe very similar phenotypes in two lines of transgenic mice that differ in the number of copies of transgene integrated and in the site of transgene integration. The effect of the *Diap3* transgene on the auditory system, therefore, is unlikely to be the result of integration effects. This is further supported by the phenotypic similarities of the mouse models to human *AUNA1* hearing loss.

Although 6 transgenic founders successfully transmitted the transgene to the next generation, offspring from only 3 of these lines developed hearing loss within 16 weeks of birth. Of the mice that did not develop hearing loss, it is possible that they may have developed significant hearing loss at later time points. Alternatively, it is possible that the transgene may have been silenced in one or more of these lines, as can occur when a transgene has integrated into a transcriptionally silent region of the genome[116]. Silencing

may also occur when large numbers of transgene constructs integrate as concatemers; although it is common for transgenes to concatemerize, increasing numbers of tandem constructs seem to increase the likelihood of transgene silencing[117]. There is more recent evidence, however, that the number of repeats may be irrelevant, and it is their orientation that is critical[118]. Inverted repeats (i.e. head to head or tail to tail) may be more likely to be silenced than direct repeats (i.e. tail to head)[118]. We did not assess expression levels in mice that did not demonstrate hearing loss by 16 weeks of age.

It has been shown that degeneration of as much as 50-60% of SGCs does not necessarily result in a change in auditory threshold[111]. In lines 771 and 924 we see a 44% and 28% decrease in ribbons, respectively, and although these decreases are statistically significant, we have not shown that they are biologically significant. We have not shown, for example, whether one population of cochlear nerve fibers is more significantly affected than another. If high-spontaneous, low-threshold fibers are more significantly affected than low-spontaneous, high-threshold fibers, decreases of 44 and 28% are likely to be biologically significant[119,120]. In addition, this study examines only the number of ribbons, not the number of complete synapses, which are comprised of pre-synaptic machinery apposed to post-synaptic machinery. It is possible, then, that the extent of loss of synaptic connections is vastly underestimated here because of additional decreases in functionality. For example, the ribbons in the IHCs of *Diap3*-overexpressing mice may not be anchored to the basal pole of the IHC, rendering the synapses incomplete. Alternatively, the ribbons may be anchored to the basal pole of the IHC, but the post-synaptic machinery may be deficient or absent. These issues can only be assessed by looking at pre- and post-synaptic components concomitantly, for example by staining for

both CtBP2/Ribeye and a post-synaptic component such as glutamate receptor subunits 2 and 3 (GluR2/3)[121], or by using transmission electron microscopy to visualize the pre- and post-synaptic densities.

The apical surfaces and stereocilia of the IHCs in the two lines of *Diap3*-overexpressing mice are grossly aberrant. The apical surfaces of transgenic IHCs appear substantially swollen and irregular in comparison to wild-type mice. Although some of the swelling at the apical surfaces may be due to the fixation procedure, which can result in greater distention in unhealthy cells than in healthy cells, it is unlikely to be the only cause. The apical surfaces of hair cells are made up largely of the cuticular plate, which anchors the roots of the stereocilia, and from which most cytoplasmic components are excluded[122]. The cuticular plate is composed of a matrix of actin filaments as well as unpolymerized actin and tubulin monomers[57]. The protrusions we observe in the SEM images of *Diap3*-overexpressing mice may be due to masses of excess tubulin, actin, or other excess proteins. Alternatively, the distention may be due to fluid retention. These possibilities will require further investigation.

In addition to the abnormalities of the IHC apical surfaces, we observe substantial differences between transgenic and wild-type IHC stereocilia. In transgenic IHCs, there is only a single row of stereocilia, which appear to be fused together. It seems unlikely that many of the mechanical processes for which the stereocilia of the IHCs are responsible could occur, and this is therefore the likely cause of hearing loss. MET channels, for example, have been localized to the lower end of the stereocilia tip links, and thus are only present on the two shorter rows of stereocilia[4]. Because these mice have normal or near normal auditory thresholds at early time points, it is expected that at one time they

have functional MET channels. Although it is unknown whether these stereocilia still possess MET channels by 24 weeks of age, it is unlikely that they would be functional in the remaining giant stereocilia. We did not observe tip links in our SEM images of transgenic mice, but we also did not observe them in our wild-type mice. This is likely to be the result of the tissue preparation procedure and the limitations of the resolution of existing equipment. The arrangement of the few remaining aberrant stereocilia, however, seems to preclude the possibility of tip links connecting adjacent rows. Without tip links, MET channels are ineffective[5].

Planar cell polarity is a necessary feature of the hair cells of the organ of Corti, required for development and maintenance of the precise orientation and position of their stereocilia[123]. Diaphanous-related formins have been implicated in the establishment of planar cell polarity[124], and we were thus interested to know whether the stereocilia maintained their orientation in relation to the hair cell and in relation to each other. Interestingly, our SEM images suggest that despite major disruptions in the morphology of the stereocilia, the polarity of the cells does not appear to be affected.

Based on the CAG promoter that we selected to drive expression of the *Diap3* transgene, we expect *Diap3* to be expressed ubiquitously[107]. If this is in fact the case, it is curious that OHCs and IHCs are not similarly affected. Perhaps *Diap3* is not expressed in OHCs, either endogenously or in these transgenic mice. It will be important to develop a robust and specific antibody to mDia2 in order to answer this question and others in the future. Another possibility is that the OHC stereocilia of transgenic mice will eventually fuse as in the IHCs. Based on the human phenotype, it is likely, although not certain, that these mice will lose their OAEs at some point in the future. If that is the case, it is

possible that OHCs are simply more resilient, or less sensitive, than IHCs are to overexpression of *Diap3*. It would be interesting to observe the appearance of transgenic IHCs and OHCs at both earlier and later time points to try to determine how the phenotype progresses. Alternatively, *Diap3* may be expressed in both OHCs and IHCs in wild-type mice, but the difference may be in the available pools of downstream binding partners in each cell type.

mDia2 interacts with both actin and microtubules. Both of these basic cytoskeletal elements are critical for the structure and integrity of stereocilia and/or the cuticular plate[125] as well as for synapse formation, organization, and regulation[55,56,126]. It is possible that dysregulation of *Diap3* may have functional effects both at the synapse and the stereocilia or cuticular plate. Alternatively, either the synaptic defect or the stereocilia defect could be secondary to the other. Based on the severity of the stereocilia phenotype, however, it is unlikely to be a secondary lesion. Another possibility is that either the stereocilia phenotype or the synapse phenotype is a consequence of the high overexpression of *Diap3*, and perhaps these effects would not be evident with more moderate overexpression, such as we would expect in the cochleae of humans with *AUNA1* hearing loss.

The two mouse models of *Diap3* overexpression that we generated recapitulate important aspects of human *AUNA1* deafness. Because the pattern of hearing loss onset and progression differs slightly between the two transgenic lines, each one will be a useful animal model. Line 771 experiences hearing loss at early time points, and it is therefore more amenable to electrophysiological techniques that are more easily performed early in the process of cochlear calcification. Line 924, on the other hand,

experiences a more delayed hearing loss onset, which is more similar to the onset of AUNA1 in humans and will be useful for testing preventative therapeutic interventions. In addition to uncovering the molecular mechanisms that underlie the deafness caused by *Diap3* overexpression, these transgenic mouse models will be useful for identifying molecular components and processes important for the maintenance of normal stereocilia structure and for normal hearing.

Acknowledgments

Additional experimental contributions: Thanks to the late Maggie Van Keuren in Thom Saunders's University of Michigan Transgenic Animal Model Core, who microinjected the eggs that became our mouse models. Jen Benson and Lisa Kabara in Dave Dolan's University of Michigan Auditory Physiology Core performed the ABR and DPOAE recordings. Ariane Kaniki performed the vascular perfusions for the plastic sections, Jong-Seung King embedded the cochleae in plastic, and Soo Duck Lee performed the SGN counts; all three are in Rick Altschuler's division of the University of Michigan Histology-Pathology Core that is part of the Auditory Anatomy Laboratory. Dorothy Sorenson of the University of Michigan Microscopy and Image Analysis Laboratory prepared samples for SEM and also generated the SEM images. I would like to thank Ariane Kanicki, Lisa Beyer, Rick Altschuler, and Yehoash Raphael for valuable lessons, suggestions, advice, and discussions.

This work was supported by National Institutes of Health Grants R01 DC007380 (to M.M.L.), F31 DC011428 (to C.J.S.), T32 DC000011 (to C.J.S.), and P30 DC005188

(in support of the University of Michigan Auditory Physiology and Histology-Pathology Cores), the University of Michigan Office of the Vice President for Research, and the University of Michigan Nathan Shock Aging Rodent Core.

Chapter 4

Potential downstream targets of *Diap3* in the mouse cochlea: an exploratory analysis

Introduction

Although much is known about the function of mDia2 (the protein product of *Diap3*) in cell systems and *in vitro*, its function in the inner ear has not been investigated. mDia2 is known to have a number of different binding partners and to participate in various cellular processes, but it is likely that more partners and functions will be discovered.

One of the benefits of generating a mouse model of a human disorder is the ability to investigate the downstream effects of a mutation in a particular tissue of interest by, for example, using unbiased, hypothesis-free, genome-wide analysis. Genome-wide screens of downstream effects can be performed at the level of mRNA (expression) or protein (proteomics). Expression analysis can reveal genes that are affected by dysregulation of a gene of interest, reveal pathways that the gene of interest might alter and thus that they might function within, and provide candidate genes for future investigation.

To try to ascertain what effects overexpression of *Diap3* might have on the molecular components of the cochlea, we used one of our mouse models to assess genome-wide expression levels by microarray analysis. In order to select the line of transgenic mouse from which to extract RNA, we primarily considered the progression of hearing loss. We reasoned that the line with later-onset hearing loss (line 924) might have fewer secondary changes that could mask the alterations we are interested in observing.

We identify several interesting candidates for molecules that may be affected by *Diap3* overexpression. The microarray experiments presented here are exploratory, designed to generate hypotheses that will be followed up on in the future.

Materials and methods

Mouse care

All mice were cared for in accordance with institutional animal care standards, and all experiments were approved by the University Committee on Use and Care of Animals (UCUCA).

Mouse cochleae gene expression analysis

Mice were euthanized in a saturated CO_2 chamber. Organs of Corti were removed and immediately submerged in Trizol (Invitrogen), and total RNA was isolated as per the manufacturer's instructions. Samples consisted of 4 transgenic 24-week-old mice from line 924 and 4 gender-matched wild-type littermates. Residual DNA was eliminated using TURBO DNA-free (Ambion) as per the manufacturer's instructions. Biotinylated cRNA was prepared from RNA using the Illumina TotalPrep RNA Amplification Kit (Ambion) as per the manufacturer's instructions. Biotinylated cRNA samples were hybridized to an Illumina MouseRef-8 v2.0 Expression BeadChip (Illumina, Inc., San Diego, CA, USA) per the manufacturer's instructions. This chip measures the amount of approximately 25,600 RefSeq transcripts covering more than 19,000 genes (www.illumina.com). The chip was scanned on an Illumina BeadArray Reader using BeadScan software, and data were downloaded to Illumina BeadStudio.

Data analysis and statistics

Raw expression data were exported from Illumina Beadstudio software, quantile-normalized, log2-transformed, and filtered for expression in R (www.R-project.org). Filtering was based on detection p-values, such that probes that have median expression ≤0.2 were defined as expressed (this corresponds to the median expression value of 5.9). Paired t-test and FDR correction were done using Significance Analysis of Microarray (SAM) (www-stat.stanford.edu/~tibs/SAM)[127].

Four probes fell below the typical false discovery rate (FDR) of 5%. In order to investigate enriched pathways, which require gene sets, we increased the cutoff to 30% FDR, with 62 probes passing the threshold. This list of 62 probes was further explored using Ingenuity pathway analysis software (Ingenuity Systems, www.ingenuity.com). The IPA Functional Analysis identified biological functions and disease states from the Ingenuity Knowledge Base that were most associated with the list of differentially expressed probes. IPA used a right-tailed Fisher's exact test to calculate a p-value that determined whether each biological function or disease state was associated with the data set by chance.

Results

Differentially expressed genes in the cochleae of *Diap3*-overexpressing mice versus wild-type littermates

Four probes—for the genes *Diap3*, *Aqp1*, *Dfnb59* (*Pjvk*), and *Kncn*—had FDR values below 5% (Figures 4-1 and 4-2). Increasing the cutoff to a 30% FDR, 62 probes representing 57 unique genes were identified as differentially expressed (Table 4-1).

Eight of the genes represented by the probes are involved in either human or mouse deafness (Figure 4-3; highlighted in Table 4-1).

Alteration of gene expression in molecular networks of *Diap3*-overexpressing mouse cochleae versus wild-type littermates

The IPA program identifies categories of disease states and networks in which the molecules of interest are involved. The top disease states that were identified based on the list of dysregulated genes included: Auditory Diseases (7 molecules; p-value range 2.2×10^{-8} to 0.009); Neurological Diseases (21 molecules; p-value range 2.2×10^{-8} to 0.004); and Genetic Disorders (15 molecules; p-value range 2.2×10^{-5} to 0.025).

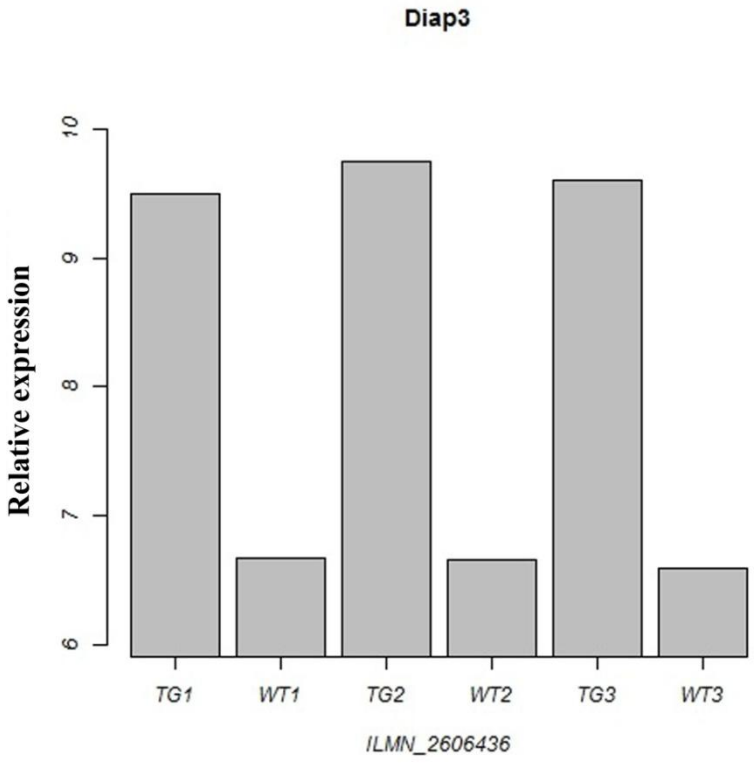

Figure 4-1. Relative expression of *Diap3* in line 924 cochlea compared to wild-type littermates. A bar plot shows the relative expression levels of *Diap3* in three gender- and age-matched pairs. TG, transgenic, WT, wild type. The origin of the y-axis is set at 5.9, the detection limit of the filtered probes. The Illumina probe ID is indicated.

Table 4-1. Probes most differentially expressed in *Diap3*-overexpressing mice versus paired, gender-matched wild-type littermates. Probes are arranged by *q*-value (FDR) in ascending order, then by average fold change in descending order. Genes highlighted in yellow have been implicated in human and/or mouse hearing loss.

Probe	Average fold change	*q*-value (%)
Diap3	7.923	0
Aqp1	-1.968	0
Dfnb59	-1.629	0
Kncn	-1.622	0
Lpl	-1.536	9.377
Dnajc5b	-2.164	13.396
Slc16a6	-1.523	13.396
Fabp3	1.886	17.861
Pip5kl1	1.826	17.861
Ibsp	1.816	17.861
LOC100047427	1.708	17.861
Nr1d1	1.672	17.861
1190003M12Rik	1.662	17.861
Cpxm1	1.576	17.861
Accn3	1.571	17.861
Dbp	1.558	17.861
Inmt	1.497	17.861
Cpne6	1.438	17.861
Ibsp	1.607	20.629
6430411K18Rik	1.515	20.629
Cyp2e1	1.401	20.629
Aqp1	-1.782	23.442
Krt23	-1.692	23.442
Sema3e	-1.625	23.442
Aqp1	-1.623	23.442
Gm129	1.605	23.442
Otof	-1.574	23.442
Plunc	-4.459	25.117
Slc17a8	-1.590	25.117
St13	-1.570	25.117
Ocm	-1.502	25.117

Probe	Average fold change	*q*-value (%)
AI595366	-1.488	25.117
Fgf12	-1.484	25.117
Slc5a3	-1.478	25.117
Arntl	-1.464	25.117
Apba1	-1.452	25.117
Hspa5	-1.441	25.117
Osbp2	-1.440	25.117
Zfh4	-1.426	25.117
Tmprss3	-1.426	25.117
Epha3	-1.417	25.117
Fam65c	-1.401	25.117
Ica1l	-1.385	25.117
Ubxn2a	-1.384	25.117
Sepp1	-1.375	25.117
Tspan12	-1.363	25.117
Myo7a	-1.349	25.117
Atp2a3	-1.338	25.117
Gtpbp8	-1.311	25.117
Stmn4	1.678	27.783
Zfp238	-1.396	27.783
Hadhb	-1.345	27.783
Trpm3	-1.341	27.783
Aldh6a1	-1.323	27.783
Creld2	-1.635	28.438
Lox	-1.450	28.438
Accn3	1.431	28.438
Ttc3	-1.368	28.438
4732418C07Rik	-1.365	28.438
Grhl2	-1.343	28.438
Tmprss9	-1.342	28.438
Mdfic	-1.338	28.438

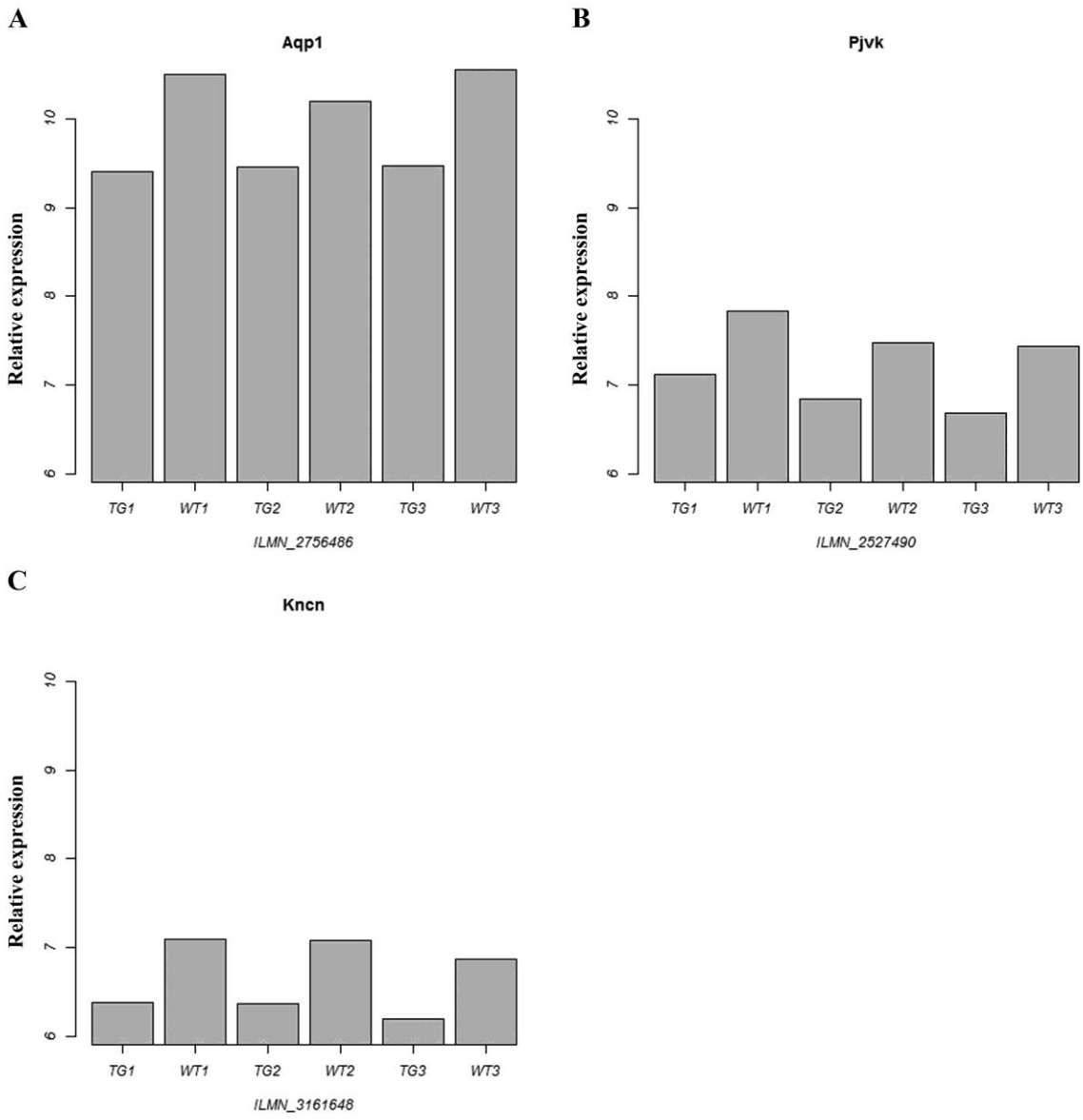

Figure 4-2. Relative expression of the three most dysregulated genes in *Diap3*-overexpressing mice compared to wild-type littermates. Bar plots show the relative expression levels of *Diap3* in three gender- and age-matched pairs. TG, transgenic, WT, wild type. Probes for *Aquaporin 1* (*Aqp1*) (A), *Pejvakin* (*Dfnb59* or *Pjvk*) (B), and *Kinocilin* (*Kncn*) (C). All three are down-regulated in transgenic mice as compared to wild-type littermates. The origin of the y-axis is set at 5.9, the detection limit of the filtered probes. The Illumina probe IDs are indicated.

The top molecular and cellular functions that were returned included: Cellular Function and Maintenance (15 molecules; p-value range 3.4×10^{-4} to 0.049); Carbohydrate Metabolism (8 molecules; p-value range 4.2×10^{-4} to 0.037); Molecular Transport (14 molecules; p-value range 4.2×10^{-4} to 0.046); Small Molecule Biochemistry (15 molecules; p-value range 4.2×10^{-4} to 0.046); and Energy Production (5 molecules; p-value range 0.001 to 0.040).

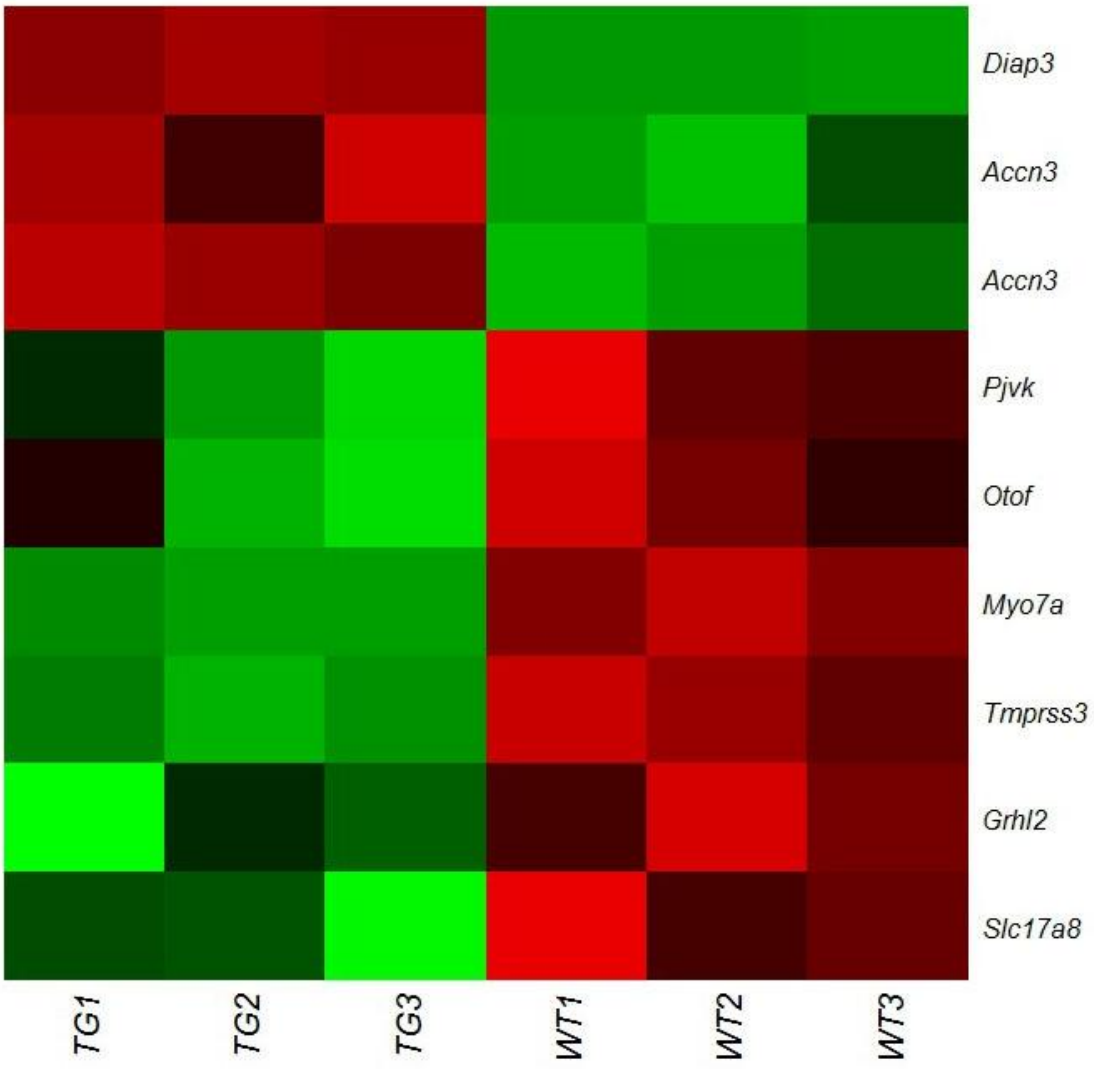

Figure 4-3. Heat map of differentially expressed deafness genes. Heat map represents relative difference in expression between line 924 mice and wild-type littermates. Each column represents a single sample. Each row represents a known deafness gene that fell below the 30% FDR. Red, increased; green, decreased.

Discussion

As expected, *Diap3* is up-regulated in line 924 mice compared to wild-type littermates. The 8-fold increase by expression array is substantially less than the ~1000-fold increase we see by qRT-PCR (Chapter 3), but microarray experiments are not intended to be quantitative. Furthermore, normalization and background correction methods decrease the relative differences between samples[128].

Using a 5% FDR cutoff, three genes in addition to *Diap3* are differentially expressed in *Diap3*-overexpressing mice compared to wild-type littermates. Unlike *Diap3*, however, all three of these genes—*Aqp1*, *Dfnb59*, and *Kncn*—are down-regulated. Of these three genes, one is known to be a human and mouse deafness gene. The other two have been shown to be expressed in the inner ear. Each of these genes is discussed further below.

According to the SAM, *Aqp1* is one of the three most down-regulated genes in *Diap3*-overexpressing mice, and this conclusion is reinforced by two additional *Aqp1* probes below the 30% FDR that indicate a 1.5- to 2-fold decrease in gene expression in *Diap3*-overexpressing mice compared to wild-type littermates (Table 4-1). *Aqp1* encodes aquaporin 1, one of a family of proteins that transports water in and out of cells[129]. Aquaporin 1 has been identified in a number of organs and tissues in the body, including the kidney, pancreas, and heart, in addition to photoreceptors and pain receptor cells[130]. More relevant for this discussion, aquaporin 1 has been shown to be localized to cells of the stria vascularis where it is presumed to have a role in water transport[131]. An *aquaporin 1* knockout mouse does not exhibit auditory dysfunction, although a knockout mouse of related family member *aquaporin 4* demonstrates elevated auditory thresholds[132]. Aquaporin 1 does not appear to be expressed in hair cells[131].

A second significantly downregulated gene, *Dfnb59*, encodes pejvakin, a protein of currently unknown function. Mutations in this gene are associated with both auditory neuropathy and sensory deafness in humans and mice[24-26]. While one group localized pejvakin to afferent SGNs[24], another localized the protein to IHCs and OHCs[25]. Because no function has been identified for the protein product, it is difficult to speculate how it might interact with mDia2.

Finally, a third significantly down-regulated gene is *Kncn*. The protein it encodes, kinocilin, is a little studied protein that, as its name suggests, is localized to the kinocilia of vestibular and auditory hair cells during development[133]. Kinocilin continues to be expressed in the kinocilia of vestibular hair cells into adulthood, but as the auditory hair cells lose their kinocilia, the protein is found only in the basal body and in a ring surrounding the cuticular plate of both the IHCs and OHCs[133]. It is also expressed in supporting cells of the cochlea, including the pillar cells and Deiters cells, as well as in the testis[133]. Based on its localization, the authors suggest that kinocilin may be involved in microtubule stabilization[133], a process in which mDia2 is known to be involved[41]. It is interesting to speculate that kinocilin and mDia2 may have a post-developmental role in stabilizing the IHC stereocilia either through direct interactions or through their interactions with microtubules.

In order to analyze multiple genes that might allow us to identify affected pathways, we selected a more liberal FDR cutoff of 30%. FDR corrects for multiple testing, and the higher the FDR cutoff, the higher the likelihood of false positives. An FDR threshold of 30% indicates that more than two thirds of the genes identified will be able to be validated, but 30% will be false positives. Pathway analysis calculates whether

a list of differentially expressed genes is enriched for those belonging to described pathways, and a single false positive gene will not lead to identification of an incorrect pathway. The decision to set the FDR cutoff at 30% was made somewhat *a priori*; we did not look at the individual genes that made up the list, only at the number of genes. The networks and biological functions suggested by these analyses will help to generate hypotheses for future investigation, but we recognize that at least some of them will likely be false leads.

The list of top disease states, which included Auditory Diseases, Neurological Diseases, and Genetic Disorders, served as confirmation that we were analyzing relevant molecules. There are a number of genes in the list of 57 that had intriguing real or potential connections to auditory function. Seven of the 57 (highlighted in Table 4-1) have been reported to be involved directly in human and/or mouse hearing loss.

Interestingly, *otof*, *slc17a8*, and *pjvk* have all been associated with forms of hearing loss in which OHCs may remain functional[22,24,59]. This suggests that the transgenic line and time point we selected were appropriate, because at later time points it is possible that the OHCs may also be affected. *Otof* and *slc17a8*, in particular, are each specifically associated with the exocytotic machinery at the base of the IHCs[22,59].

It is possible that overexpression of *Diap3* may not change the expression levels of downstream genes involved in *AUNA1* hearing loss, but instead may change localization or activity of one or more proteins. In this case, we would not expect a change in expression of the target genes. It is also possible that one or more genes in our list may be up- or down-regulated because of transgene insertion site effects and not because of overexpression of *Diap3*. This possibility can be explored by assessing

expression levels of those genes in the second transgenic mouse line, which is expected to have a different transgene insertion site. Alternatively, because the overexpression of *Diap3* in transgenic mice is supraphysiological, some of the differences in gene expression may be due to cellular processes involved in eliminating excess mDia2, and not related to the biological function of mDia2. If that is the case, some of these differences are likely to be physiologically irrelevant to individuals with *AUNA1* deafness.

This overview of the major salient findings of our expression analysis of *Diap3*-overexpressing mice and wild-type littermates has provided us with new hypotheses to test. Based on the list of dysregulated genes, one of the networks generated by the IPA software was Lipid Metabolism, Molecular Transport, and Small Molecule Biochemistry, and it will be interesting to try to determine whether *Diap3* overexpression is involved in one or more of these biological processes. The IPA-generated network includes 13 of the 57 most significantly dysregulated genes, including three of the top four. These top genes will be investigated by qRT-PCR and/or immunohistochemistry. It will also be interesting to consider whether *Diap3* overexpression might be involved in some of the forms of deafness indicated by the 7 dysregulated deafness genes. In addition, it may be informative to reanalyze the human expression data from LCLs from individuals with *AUNA1* and unaffected controls (Chapter 2). Comparing the results of the analyses from these two datasets may allow us to identify overlapping pathways or networks that would serve as a confirmation of the findings and which would again provide us with new directions for investigation.

Acknowledgements

Additional experimental contributions: Dr. Viktoriya Strumba normalized, log2-transformed, and filtered the microarray data and also provided the images of expression differences.

Chapter 5
Discussion and Future Directions

Summary

In this dissertation, I describe the identification of a mutation in a non-coding region of *DIAPH3* that segregates with *AUNA1* deafness, and we demonstrate that the 5' UTR mutation results in 2- to 3-fold overexpression in LCLs of affected individuals versus unaffected individuals. We confirm that this mutation is sufficient to drive 2- to 3-fold overexpression in a luciferase reporter system and show that expression of constitutively active *diaphanous* in *Drosophila* results in elevated sound evoked potentials. I describe the generation of a mouse model of *Diap3* overexpression and demonstrate that it experiences progressive hearing loss that initially presents with preserved OHC function. I show that IHC stereocilia in these transgenic mice are highly aberrant: they form a single row (compared to the three rows in wild-type mice) of disorganized and perhaps fused stereocilia that protrude from abnormally distended apical surfaces. In addition, I show that these transgenic mice have fewer ribbons at presynaptic sites of the IHCs. Finally, I identify potential downstream genes whose expression may be altered as a result of *Diap3* overexpression based on gene expression analysis of transgenic and wild-type mouse cochleae.

Clinical and scientific implications

Identification of a new deafness gene provides additional potential mutations for which to screen in genetic testing of newly identified probands. In addition to screening families with auditory neuropathy, it may also be worthwhile to screen hearing loss families with unidentified mutations. It has been suggested that there may be many more cases of auditory neuropathy than has been thought previously[134], and mutations in *DIAPH3* may be involved in some of them. In addition, it is possible that different mutations in *DIAPH3* may cause forms of hearing loss other than nonsyndromic auditory neuropathy. This has been shown to be the case, for example, for *PJVK*, in which mutations are associated with both sensory hearing loss and auditory neuropathy[24,26].

Development of a mouse model may also aid in the development of a rational therapeutic intervention. First, it will allow us to uncover the molecular mechanism responsible for *AUNA1* deafness, which in turn will enable researchers to identify targeted therapies. Second, the mouse model itself will be a good system on which to test any potential therapies identified. In delayed-onset hearing loss, there is a window of opportunity during which an intervention may be effective, and hearing loss may someday be able to be delayed or prevented.

These mouse models prompt additional scientific questions. The *Diap3* transgene, like the endogenous gene, is expected to be ubiquitously expressed, but unfortunately, without a specific and robust antibody for mDia2, localization of the protein to specific cells of the cochlea has not been possible. (The commercially available mDia2 antibodies that we evaluated were neither specific nor robust. *In situ* hybridization and/or development of an antibody will be informative next steps.) In our mouse models, IHCs appear to be affected to a much greater extent and/or prior to OHCs. If *Diap3* is in fact

overexpressed in both the OHCs and IHCs of transgenic mice, then it follows that OHCs might be more resistant, or IHCs more susceptible, to the changes induced by *Diap3* overexpression. Perhaps, as is thought to occur in SGC degeneration that is secondary to IHC loss, important neurotrophic factors may be lost[135]. Or perhaps more maintenance is required in IHCs than in OHCs, and perhaps the timing may reflect the activity of the many more afferents that synapse on IHCs than OHCs[97].

We identified a significant decrease in ribbons of *Diap3*-overexpressing mice. It is possible that changes at the apical surface of the IHC cause a reduction in ribbons at the base or vice versa, but such interactions have not been documented before. We cannot rule out the possibility that there is an unidentified defect in the terminal dendrites of the nerve in addition to the defects observed in the IHC. Finally, it is possible that both observed defects (and also a hypothetical defect of the dendrites) could occur independently. *Diap3* may be important both for stereocilia structure and for synaptic function. This is in fact the case for myosin VI, for example, in which mouse mutants demonstrate both stereocilia disarray and deficits in exocytosis at the IHC synapse that have been shown to be independent of the role of myosin VI in stereocilia[136,137]. Yet another possibility is that both of the IHC defects we have identified are the result of the high level of overexpression we observe in the cochleae of our transgenic mice. A more moderate 2- to 3-fold overexpression, as we see in the LCLs of humans with *AUNA1*, might demonstrate that neither of these defects is physiologically relevant and that the deficit in humans is in fact much subtler than what we have observed in our transgenic mice.

At early time points, *Diap3*-overexpressing mice have auditory thresholds that are normal or only mildly elevated compared to wild-type littermates, which suggests that auditory structures develop relatively normally. If mDia2 is involved in maintenance rather than development of auditory structures, one might wonder which actin nucleators and filament elongators are involved in auditory system development. Perhaps different splice isoforms of *Diap3* are required for development than are needed for post-development stages. Alternatively, perhaps expression of binding partners changes during development. These will be interesting questions to pursue. The fact that the identified mutations in both *DIAPH1* and *DIAPH3* result in postlingual hearing loss may suggest that neither one is necessary for development, but that is not necessarily the case. It has been shown, for example, that only one actin gene is required during auditory system development (either gamma- or beta-), but, surprisingly, both are required for maintenance of hearing[138,139].

The causes for the delays in hereditary delayed-onset hearing loss have never been fully identified. While there are many steps at which the developmental program can be interrupted, the mechanisms behind post-development hearing loss are less clearly defined. There may be, for example, mutations in molecules that are specifically and actively involved in maintenance but not in developmental functions. Alternatively, a deficit may result from inappropriate accumulation of pathological or even wild-type molecules. These hypotheses are not mutually exclusive, and *Diap3* may be an active participant in maintenance at the same time that inappropriate accumulation of mDia2 may be harmful to cellular function.

It is often suggested that inherited delayed onset hearing loss may have parallels to age-related hearing loss, and therefore it is natural to speculate that genes responsible for inherited delayed onset hearing loss might also have a role in age-related hearing loss. Based on histological data, it is generally thought that presbycusis has three primary sources of defect: loss of stria vascularis integrity, spiral ganglion degeneration, and sensory hair cell loss[140]. Based on our results, the primary defect caused by *Diap3* overexpression seems to affect the IHC stereocilia exclusively. This phenotype does not correspond to any known histological features of presbycusis, which suggests that *Diap3* overexpression is an unlikely primary contributor to age-related hearing loss.

Ultimately, we do not know how the 5' UTR mutation we have identified might affect *DIAPH3* expression in the human ear of individuals with *AUNA1* hearing loss. It is possible, for instance, that *DIAPH3* is expressed in the cochleae of *AUNA1* patients at levels significantly higher than the 2- to 3-fold overexpression we see in lymphoblastoid cell lines. A knock-in mouse model of the human 5' UTR mutation might allow us to answer this question with more certainty, although it is also possible that such a mouse would not develop hearing loss at all. Some human pathologies transferred to mouse models develop on an absolute timescale rather than proportionally to lifespan[141].

There have been other mouse models of IHC-specific dysfunction. The IHCs only of the Bronx Waltzer, for example, degenerate during development[142]. There are also a number of mouse models in which stereocilia of both IHCs and OHCs are affected. To our knowledge, however, this is the first mouse model to demonstrate a specific pathology of the stereocilia of the IHCs. Elucidation of the mechanisms that cause this

pathology will contribute to the identification of additional important components of the molecular machinery of auditory function.

Future directions

As with most scientific endeavors, these mouse models have generated more questions than they have answered. As mentioned earlier, studies on the localization of the protein product of *Diap3* in wild-type mice have not yet been performed. Development of specific and robust antibodies to mDia2 will be important in order to localize this protein both to specific cell types and to specific subcellular compartments in both wild-type and transgenic mice.

Our mouse microarray results were compelling, and appropriate follow-up will help to confirm and validate some of our findings. In addition to using qRT-PCR to test expression levels of our top findings, it will also be interesting to stain cochlear whole mounts with antibodies against kinocilin, pejvakin, and aquaporin 1, the three most dysregulated genes in our microarray analysis. We also plan to reanalyze our human LCL microarray results in order to compare them to our mouse data. Ideally, we will identify biological functions or perhaps even specific molecules that overlap between mice and humans. Two of our top three down-regulated molecules, however, are not likely to be expressed in lymphocytes; kinocilin and pejvakin have been associated primarily with cochlear expression[24,133]. Regardless, we may not observe overlaps between the mouse and human analyses, both because the comparison will be between LCLs and cochlear tissue, and because humans, unlike inbred mouse strains, are not genetically identical.

We identified dramatic differences in the apical surfaces and stereocilia of IHCs of *Diap3*-overexpressing mice compared to wild-type littermates at 24 weeks of age. As

these data were collected at only a single time point during the course of a progressive disorder, they open up a number of additional questions. When does the IHC pathology begin? Do the IHC stereocilia of transgenic mice appear normal prior to onset of hearing loss, or are they mildly aberrant even while these mice still have normal hearing? Presumably, since hearing in *Diap3*-overexpressing mice was normal or near normal at one time, MET channels were present and functional; were there were multiple rows of stereocilia at one point in time? Do the apical bulges precede the apparent fusion of the stereocilia or vice versa? Do IHCs eventually begin to degenerate and die? When and how do OHCs become affected? SEM images taken at both earlier and later time points will enable us to answer many of these questions.

As suggested earlier, a more targeted mouse model—a knock-in mouse with the human 5' UTR mutation—might prove to be very useful. It would provide a *Diap3*-overexpressing mouse that might be expected to be more physiologically similar to *AUNA1* hearing loss than our current models. We cannot, however, predict how the 5' UTR mutation might affect expression of *Diap3* in a mouse or how this might affect hearing. In particular, a lower level of overexpression might change the timeline for hearing loss onset, as discussed above.

In conclusion, we have developed unique transgenic mouse models of *Diap3* overexpression that recapitulate the human AUNA1 auditory neuropathy phenotype of progressive, delayed-onset hearing loss with preservation of outer hair cell function. To our knowledge, these are the first mouse models to demonstrate IHC-specific stereocilia defects. These models will be useful in uncovering new molecular mechanisms of IHC structure and function in pathological and normal hearing.

Appendix A

Cardiac phenotype in transgenic mice from lines 771 and 924

Introduction

Protein function in the heart is often investigated using mouse models with transgene overexpression driven by heart-specific promoters. Beneficial outcomes of transgene overexpression are often ascribed to expression of the trangene, and likewise, detrimental effects are often assumed to be due to expression of the transgene. In a letter to the editor of Nature Medicine in 2000, however, Huang et al. describe an experiment that demonstrates that overexpression of a gene encoding green fluorescent protein (GFP) results in dilated cardiomyopathy in FVB/N transgenic mice in a dose-dependent manner[143]. This was a surprising finding since GFP has generally been considered a benign protein that can be expressed in most cells with no adverse consequences[144]. Similarly, Buerger et al. showed in 2006 that transgenic mice that highly overexpress Cre-recombinase also suffer from cardiomyopathy, while low expressors have no evidence of heart defects[145].

As we bred our *Diap3*-overexpressing mouse lines, we observed that a small but noticeable proportion of transgenic mice from line 771 unexpectedly died at early ages, at approximately 3 to 4 months. In two instances of premature death, the University of Michigan Unit for Laboratory Animal Medicine (ULAM) performed necropsies and identified the primary cause of death as dilated cardiomyopathy, with liver lesions that may have been secondary to the heart lesion. We sought to determine whether this

cardiac phenotype might be due to overexpression of the *Diap3* transgene or whether the phenotype was similar to what is seen in overexpression of GFP. Based on our findings, although the phenotype is remarkably similar to that found in GFP-overexpressing mice, we cannot yet exclude the possibility that the *Diap3* transgene is the cause of the cardiac phenotype in our transgenic mice.

Materials and methods

Mouse care

All mice were cared for in accordance with institutional animal care standards, and all experiments were approved by the University Committee on Use and Care of Animals (UCUCA).

Necropsies

Necropsies were performed by the University of Michigan Unit for Laboratory Animal Medicine.

Preparation of cardiac tissue for staining

Mice were deeply anesthetized with sodium pentobarbital, and tissues were fixed by vascular perfusion with 4% paraformaldehyde (PFA). Hearts were post-fixed in 4% PFA overnight, then transferred to a 30% sucrose solution for cryoprotection. The sucrose solution was allowed to infiltrate the hearts by incubating at 4°C on a rocker until the hearts sank. Alternatively, mice were deeply anesthetized with ketamine/xylazine. Body weight was recorded. Hearts were removed, their weights recorded, and then they were embedded in Tissue-Tek Optimum Cutting Temperature Compound (Sakura

Finetek USA, Torrance CA) and frozen in a container of isopentane submerged in liquid nitrogen. Eight µm sections were sliced on a cryostat.

Quantitative reverse transcription PCR (qRT-PCR)

cDNA from heart tissue was prepared and qRT-PCR was performed as described for cochlear tissue in Chapter 3.

Hematoxylin and Eosin (H&E) staining

Cryosections were incubated in Harris hematoxylin (EMD Millipore) for 5-10 minutes, washed, then counterstained with eosin Y (EMD Millipore, Billerica, MA). Stained specimens were dehydrated in a series of baths of increasing concentrations of ethanol from 80-100%, then rinsed in xylene. Sections were coverslipped with Permount Mounting Medium (Thermo Fisher Scientific).

Picrosirius Red staining

Cryosections were incubated in picrosirius red solution (0.1% Sirius Red/ 0.1% Fast Green in picric acid) for 30 minutes, washed, and dehydrated in a series of baths of increasing concentrations of ethanol from 80-100%. Slides were rinsed in xylene, then coverslipped as above.

Results

A number of mice from line 771 die prematurely. Necropsies of two animals from this line suggested that the primary cause of death was dilated cardiomyopathy, with lesions of the liver that may be secondary to the cardiomyopathy. In addition, prior to systemic perfusion for cochlear tissue fixation, we noted that as the chest cavities of mice from lines 771 and 924 were opened to prepare them for vascular perfusion, the hearts of

the transgenic mice were markedly enlarged compared to wild-type littermates. In fact, it was possible for observers who were blind to genotype to identify transgenic mice based only on the size and appearance of hearts from both lines 771 and 924 (Figure A1-A and data not shown). In line 771 this correlated to an increase in heart mass, as measured by the ratio of heart weight to body weight (p=0.02, Figure A-1B). Although we observed enlarged hearts in line 924 mice as well, there was no statistically significant difference in heart mass (p=0.28, data not shown).

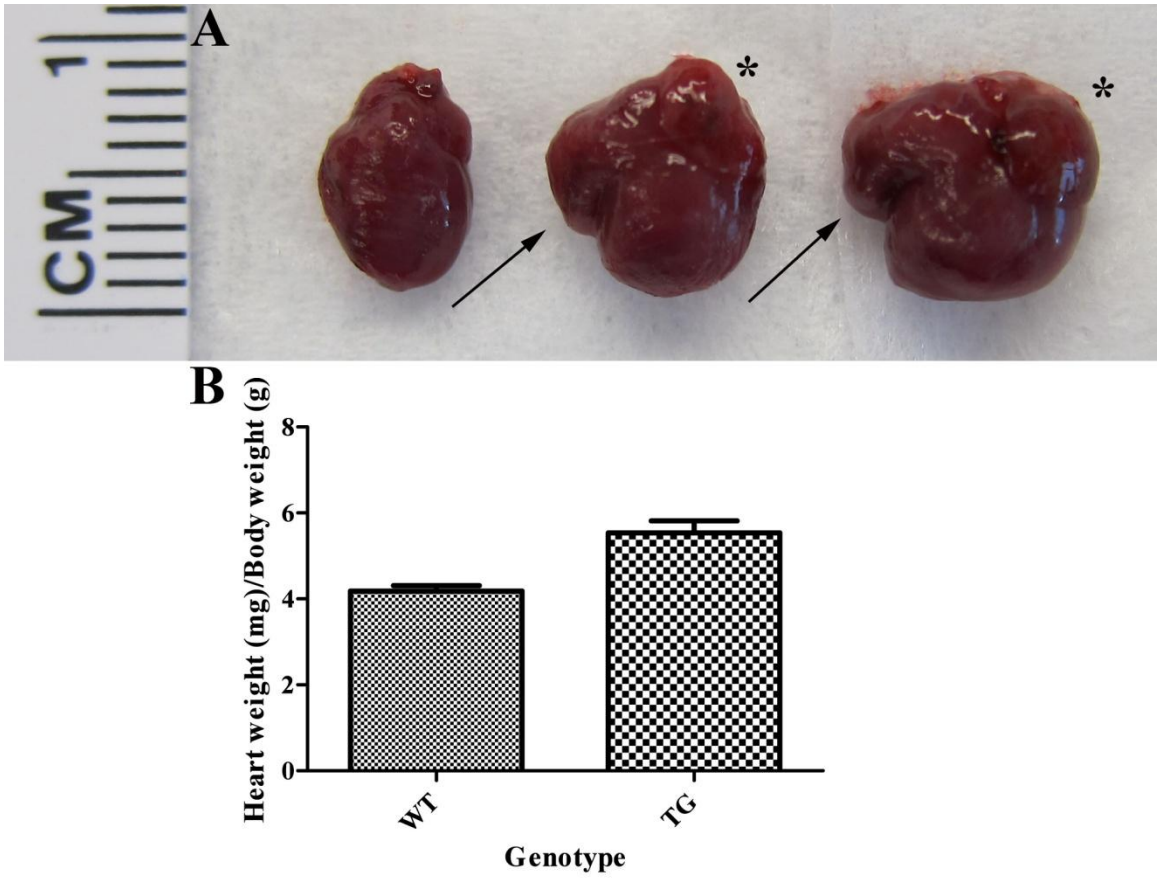

Figure A- 1. Hearts from line 771 mice are significantly enlarged compared to wild-type littermates. (A) The right ventricles of two line 771 mice (middle, right) are enlarged to the point that they protrude and appear to form a second apex (arrows). The left atria (asterisks) are also visibly larger than those of a wild-type littermate (left). All hearts are shown in the same orientation. (B) Heart mass is significantly increased in line

771 as measured by the ratio of heart mass to body mass. Bars represent mean ± SEM. The mean heart mass to body mass ratio for line 771 is 5.54 ± 0.28 (mean ± SEM, n=4) and for wild-type mice is 4.19 ± 0.12 (n=4). The difference is statistically significant (p=0.0045; Student's t test).

Heart-specific overexpression of transgenes that are generally considered to be benign can result in dilated cardiomyopathy, and the greater the overexpression, the more severe the cardiac phenotype[143]. To assess the level of overexpression of *Diap3* in the two lines of transgenic mice, we used qRT-PCR on RNA from cardiac tissue of lines 771 and 924 and wild-type littermates. The mean difference in threshold cycle (Ct) for *Diap3* (normalized to the Ct for a reference gene, *GusB*) between transgenic and wild-type mice was 10.57 ± 2.27 (95% CI) for line 771 (p=0.0002), and 10.14 ± 2.54 (95% CI) for line 924 (p=0.0002) (Figure A-2). These differences correspond to overexpression of approximately 1100-fold in *Diap3*-overexpressing mice compared to wild-type littermates, similar to what is observed in the inner ears (Chapter 3).

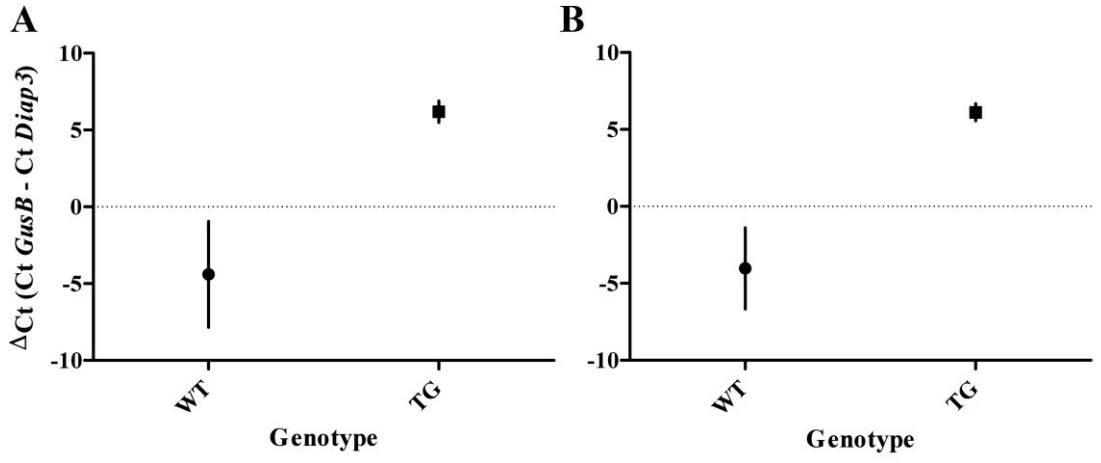

Figure A- 2. The *Diap3* transgene is highly overexpressed in heart tissue of mice from lines 771 and 924 as compared to wild-type littermates. Relative expression of *Diap3* was assessed using mRNA isolated from the hearts of 3 transgenic and 3 wild-type mice at 24 weeks of age. Quantitative RT-PCR demonstrates significant differences in *Diap3* expression between line 771 and wild-type littermates (A) and between line 924

and wild-type littermates (B). Mean Cts are indicated at the horizontal lines; vertical lines represent 95% confidence intervals. The difference in Cts is approximately 10 for each line, which corresponds to expression levels of approximately 1100-fold greater in transgenic mice than in wild-type littermates. Differences in expression between wild-type and transgenic mice were significantly significant for both lines (p=0.0002 and 0.0002 for lines 771 and 924, respectively, Student's t test).

In order to visualize the basic cellular structure of the cardiac tissue, we stained cryosections of heart tissue from lines 771 and 924 to try to identify the cause of cardiac disease in these mice. H&E staining revealed what appeared to be substantial myocyte disarray (Figure A-3). Myocyte disarray is sometimes considered to be indicative of fibrotic processes, but this assessment can be highly dependent on the plane of the observed tissue section[146]. To determine whether the apparent myocyte disarray in lines 771 and 924 might in fact be due to fibrosis, we used picrosirius red staining to identify collagen deposition. Picrosirius red staining of cardiac tissue from *Diap3*-overexpressing mice revealed considerable collagen deposition compared to tissue sections taken at a similar plane from wild-type littermates (Figure A-4) (not quantified).

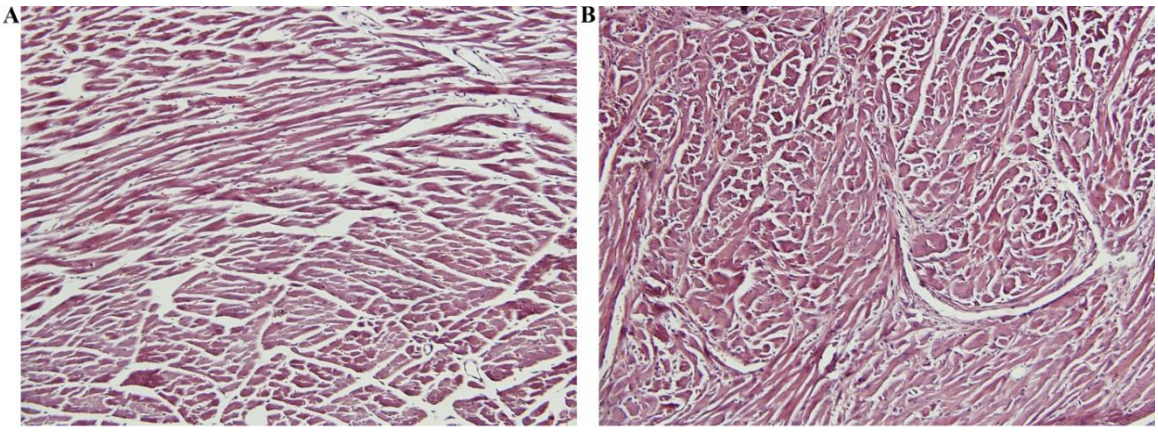

Figure A- 3. H&E staining suggests that transgenic hearts may exhibit myocyte disarray in comparison to wild-type littermates. (A) A wild-type heart demonstrates the expected pattern of myocytes in which there are large swaths of myocytes running in a single direction adjacent to large swaths of myocytes running in an orthogonal

direction. Note that in (A) the myocytes are arrayed in approximately 3 separate swaths running in two different directions. One of the swaths bisects the image almost horizontally. In line 771 mice (B), the myocyte patches are much smaller and therefore appear more closely interleaved. Note that the myoctyes appear to form a swirling pattern.

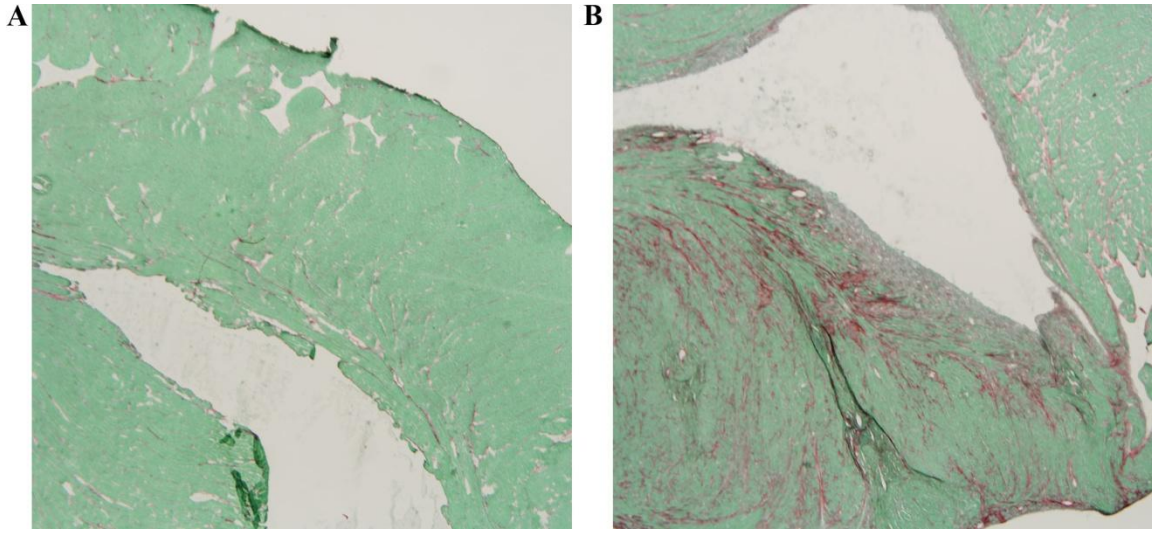

Figure A- 4. The hearts of transgenic mice demonstrate a substantial increase in fibrosis compared to wild-type littermates. These two cardiac cryosections, taken from approximately the same region of the heart, are stained with picrosirius red, which labels collagen in red. (A) Hearts from wild-type mice exhibit very little collagen staining. (B) Staining of hearts from line 771 mice reveals substantial areas of collagen deposition, indicative of fibrosis.

Discussion

We have identified a cardiac phenotype in *Diap3*-overexpressing transgenic mice that is often expressed as dilated cardiomyopathy, and we confirm this diagnosis by identifying substantial regions of fibrosis in the heart tissue. In addition, we show that *Diap3* is highly overexpressed in the hearts of both lines, but line 771 seems to be more severely affected (based on the number of premature deaths and the significant change in heart mass). Because expression is roughly equivalent in both lines, it is likely that the differences in cardiac phenotype are due to transgene overexpression, and not specifically to *Diap3* overexpression. We cannot, however, rule out the possibility that *Diap3* itself causes the cardiac phenotype.

It has been shown that overexpression of GFP in the heart muscle can result in dilated cardiomyopathy[143]. As our qRT-PCR data show, expression levels of *Diap3* in the hearts of transgenic mice from lines 771 and 924 are on the order of hundreds- to thousands-fold greater than in wild-type littermates. It is quite possible that this level of overexpression, independent of the function of the transgene, is sufficient to cause a dilated cardiomyopathy similar to that caused by highly overexpressed GFP.

Although specific investigation has not been performed, to our knowledge, individuals with *AUNA1* auditory neuropathy do not report an incidence of cardiac disease that is different from that of the general population. The levels of *Diap3* in our mouse models are much higher than in the LCLs of humans with *AUNA1* auditory neuropathy. The cardiac phenotype we describe here, even if due to the effects of *Diap3* itself, is not necessarily physiologically relevant to humans with *AUNA1* deafness. A knock-in mouse model of the human 5' UTR mutation in the endogenous *Diap3* gene would more closely approximate the expression levels of *DIAPH3* seen in individuals with *AUNA1* deafness and might help address the question of whether heart function is compromised by *Diap3* overexpresseion or whether the cardiac phenotype in these mice is independent of the function of the particular transgene.

Acknowledgements

I would like to thank Dr. Daniel Michele and his lab manager Ashley Archambeau—Dr. Michele for valuable discussions and suggestions and for allowing me to work in his lab, and Ashley for teaching me how to fix, freeze, section, and stain

hearts. Thanks also to Dr. Lucy Kennedy for performing the necropsies on our transgenic mice.

Appendix B

Diap3 transgene integration into the X chromosome (line 946)

Introduction

When developing transgenic mouse models, it is hoped that the microinjected transgene construct will integrate into an intergenic region that is also transcriptionally active, in order to avoid disrupting an endogenous gene and to improve the chances that the transgene will not be silenced, respectively. Occasionally, however, integration results in unintended consequences by inserting into an endogenous gene, effectively disrupting the gene and disabling expression from that allele. Often there may be no dire consequences because one working copy of the gene may be all that is needed. Sometimes, however, haploinsuffiency may result in a severe phenotype. Alternatively, integration into a gene on the X or Y chromosome would result in knocking out of the only copy of the gene. If this gene is functionally important, offspring will experience problems with development or viability or will display a phenotype. In addition, hybrid proteins may be translated from endogenous and exogenous gene fragments. Finally, transgene insertion may also lead to changes in expression of an endogenous gene, such as in cases in which the endogenous gene uses the transgenic promoter, or alternatively, in cases in which the insertion site disrupts an endogenous promoter[147]. An analysis of 153 transgene insertions suggests that approximately 7% of transgenesis events interrupt important endogenous gene function, although this is likely to be an underestimate

because of embryonic lethality and because some of the phenotypes may be too subtle to detect easily[148].

During the development of lines of *Diap3*-overexpressing mice, we initially noted that the offspring of line FVB-Tg(CAG-Diap3)946Lesp (referred to here as 946) were born in non-Mendelian ratios. Very few transgenic males were genotyped at two weeks of age, and many of those that were born died within the first 4 weeks of life. We hypothesized that the *Diap3* transgene had integrated into the X chromosome into a region that altered expression of a gene important for long-term viability.

Materials and Methods

Mouse care

All mice were cared for in accordance with institutional animal care standards, and all experiments were approved by the University Committee on Use and Care of Animals (UCUCA).

Measures of hearing

Auditory Brainstem Response and Distortion Product Otoacoustic Emissions were performed as described in Chapter 3.

Immunohistochemistry

Immunohistochemical analyses were performed as described in Chapter 3.

Florescence in situ hybridization

Florescence in situ hybridization mapping was performed by SeeDNA Biotech, Inc. (Windsor, Ontario, Canada).

Results

Line 946 manifests a more severe hearing phenotype and a variable vestibular phenotype, as well as variable loss of inner and outer hair cells by four weeks of age

Transgenic mice from line 946 manifest a severe hearing loss of earlier onset than lines 771 and 924. At 4 weeks of age, these mice demonstrate a 50 dB threshold shift at 12 kHz ($p=0.012$), a 60 dB shift at 24 kHz ($p=0.001$), and a 30 dB shift at 48 kHz ($p<0.001$) (Figure B-1A) compared to wild-type littermates. There was no change in auditory thresholds between 4 and 8 weeks of age for line 946 or wild-type mice (Figure B-1B and data not shown). However, approximately 20% of transgenic females from this line have auditory thresholds that are similar to wild-type females (Figure B-1C). At 4 weeks of age, hearing impaired transgenic mice also have poor OAEs (Figure B-1D).

A proportion of the hearing-impaired 946 females initially exhibit a vestibular phenotype, primarily circling. These behaviors are not noted in transgenic females with auditory thresholds that are similar to wild-type littermates, and not all transgenic females with poor auditory thresholds exhibit the vestibular phenotype. Organ of Corti whole mounts of affected transgenic mice show many regions of significant loss of both IHCs and OHCs (Figure B-2).

X-linked integration of the transgene results in distortion of transgene transmission in line 946

Transgenic offspring of line 946 are born in non-Mendelian ratios, with fewer transgenic males than expected. Only 30% of offspring are transgenic (32/108), with 40% of all female mice carrying the transgene, while only 20% of males are transgenic.

While few transgenic male offspring from this line survive past 4 weeks of age, it was possible to analyze the distribution of progeny from the mating of a surviving transgenic male to a wild-type female littermate. This pairing produced 18 wild-type males and 12 transgenic females, with no transgenic males or wild-type females, a result that is significantly different from that expected by chance (p<0.0001, Fisher exact test). Fluorescence in situ hybridization (FISH) confirmed that the transgene was integrated into XF3-XF4, a 14 Mb region on the X chromosome. This region, from 145 Mb to 159.5 Mb, contains approximately 100 known genes and almost 150 predicted genes.

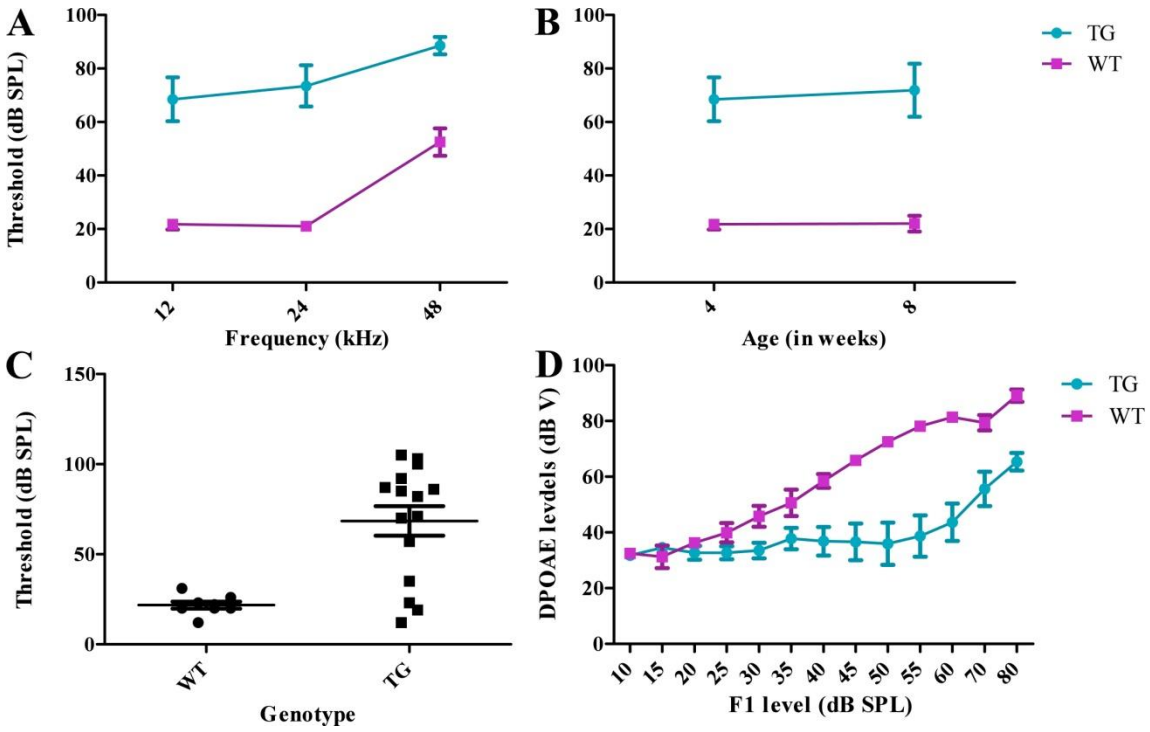

Figure B- 1. Mice from line 946 experience significant hearing loss compared to wild-type littermates. (A) Mean ABR thresholds (and mean ± SEM) demonstrate significant hearing loss at 4 weeks of age across all frequencies tested. (B) There is no significant change in ABR thresholds between 4 and 8 weeks of age (12 kHz is shown, but 24 kHz ABR thresholds are also stable). (C) Approximately 20% of transgenic females from this line have auditory thresholds that are similar to wild-type females (again, although data points for 12 kHz ABRs are shown, this is also true for 24 kHz).

(D) At 4 weeks of age, hearing impaired transgenic mice from line 946 have significantly reduced DPOAEs (p=0.0091, ANOVA).

Figure B- 2. Line 946 mice demonstrate a substantial loss of inner and outer hair cells as revealed by phalloidin staining. The cochlear phenotype in this line varies

widely. A wild-type mouse is shown in (A). The IHCs and OHCs are orderly and regular. Note a single missing OHC in the outermost row in the bottom right corner. The hair cells of a transgenic female are shown in (B). There are a number of missing OHCs, as well as multiple missing IHCs (asterisks). Note the spiked appearance of the apparently elongated IHC stereocilia. The hair cells of a transgenic male are shown in (C). No OHCs are identifiable. There appear to be few remaining IHC stereocilia (identified with asterisks).

As with other phenotypic characteristics of mice from line 946, heart mass was inconsistent. Some 946 mice had hearts that appeared grossly enlarged, while others had hearts that appeared very similar to wild-type mice. In support of this observation, there is no significant difference in heart weight to body weight ratio between wild-type and transgenic mice of line 946, most likely due to the wide range of values in transgenic mice ($p>0.05$, Student's *t* test, data not shown).

Discussion

Loss of hearing in line 946 was not fully penetrant, but transgenic mice with hearing impairment often demonstrated a more severe hearing loss than did lines 771 or 924. We determined that the transgene in line 946 was incorporated into the X chromosome, which explains the transgene transmission distortion we observe among offspring of line 946, and among offspring sired by a surviving transgenic male. Approximately 25 to 30% of transgenic females from line 946 had auditory thresholds that were indistinguishable from wild-type littermates. We hypothesize that the incomplete penetrance of the auditory phenotype among transgenic females is due to X-inactivation of the transgene. In combination with the reduced numbers of transgenic offspring, our results suggest that a gene important for viability, and perhaps also for auditory system development, is affected by the transgene insertion.

Interestingly, a number of transgenic males born in subsequent generations survived longer than one to two months. This survival may be due to inactivation of the transgene over several generations, which would suggest that the phenotypes we observe in this transgenic line are due to activity of the transgene, and not to inactivation of an endogenous gene. might be explained by transgene-mediated altered expression of an endogenous gene[149].

Ultimately, because of the difficulties in maintaining this line, the phenotypic variability in both females and males, and the confounding of overexpression of *Diap3* with a possible effect on an endogenous gene, we concluded that this mouse was a poor model for either *AUNA1* hearing loss or for the phenotype(s) that may have been caused by insertional mutation.

Acknowledgments

Additional experimental contributions: As in Chapter 3, thanks to the late Maggie Van Keuren in Thom Saunders's University of Michigan Transgenic Animal Model Core, who microinjected the eggs that became our mouse models. Jen Benson and Lisa Kabara in Dave Dolan's University of Michigan Auditory Physiology Core performed the ABR and DPOAE recordings. I would also like to thank Ariane Kanicki, Lisa Beyer, Rick Altschuler, and Yehoash Raphael for valuable lessons, suggestions, advice, and discussions.

References

1. CORTI and his research. *N Engl J Med* **246**, 428-9 (1952).
2. Pickles, J.O., Comis, S.D. & Osborne, M.P. Cross-links between stereocilia in the guinea pig organ of Corti, and their possible relation to sensory transduction. *Hear Res* **15**, 103-12 (1984).
3. Corey, D.P. & Hudspeth, A.J. Kinetics of the receptor current in bullfrog saccular hair cells. *J Neurosci* **3**, 962-76 (1983).
4. Beurg, M., Fettiplace, R., Nam, J.H. & Ricci, A.J. Localization of inner hair cell mechanotransducer channels using high-speed calcium imaging. *Nat Neurosci* **12**, 553-8 (2009).
5. Assad, J.A., Shepherd, G.M. & Corey, D.P. Tip-link integrity and mechanical transduction in vertebrate hair cells. *Neuron* **7**, 985-94 (1991).
6. Kelley, M.W. Regulation of cell fate in the sensory epithelia of the inner ear. *Nat Rev Neurosci* **7**, 837-49 (2006).
7. Spoendlin, H. Innervation densities of the cochlea. *Acta Otolaryngol* **73**, 235-48 (1972).
8. Spoendlin, H. & Schrott, A. The spiral ganglion and the innervation of the human organ of Corti. *Acta Otolaryngol* **105**, 403-10 (1988).
9. Dallos, P. *et al.* Prestin-based outer hair cell motility is necessary for mammalian cochlear amplification. *Neuron* **58**, 333-9 (2008).
10. Matthews, G. & Fuchs, P. The diverse roles of ribbon synapses in sensory neurotransmission. *Nat Rev Neurosci* **11**, 812-22 (2010).
11. Fettiplace, R. & Hackney, C.M. The sensory and motor roles of auditory hair cells. *Nat Rev Neurosci* **7**, 19-29 (2006).
12. Peng, A.W., Salles, F.T., Pan, B. & Ricci, A.J. Integrating the biophysical and molecular mechanisms of auditory hair cell mechanotransduction. *Nat Commun* **2**, 523 (2011).
13. Ries, P.W. Prevalence and characteristics of persons with hearing trouble: United States, 1990-91. *Vital Health Stat 10*, 1-75 (1994).
14. Mehra, S., Eavey, R.D. & Keamy, D.G., Jr. The epidemiology of hearing impairment in the United States: newborns, children, and adolescents. *Otolaryngol Head Neck Surg* **140**, 461-72 (2009).
15. Morton, N.E. Genetic epidemiology of hearing impairment. *Ann N Y Acad Sci* **630**, 16-31 (1991).
16. Kochhar, A., Hildebrand, M.S. & Smith, R.J. Clinical aspects of hereditary hearing loss. *Genet Med* **9**, 393-408 (2007).
17. Roizen, N.J. Etiology of hearing loss in children. Nongenetic causes. *Pediatr Clin North Am* **46**, 49-64, x (1999).

18. Van Eyken, E., Van Camp, G. & Van Laer, L. The complexity of age-related hearing impairment: contributing environmental and genetic factors. *Audiol Neurootol* **12**, 345-58 (2007).
19. Starr, A., Picton, T.W., Sininger, Y., Hood, L.J. & Berlin, C.I. Auditory neuropathy. *Brain* **119 (Pt 3)**, 741-53 (1996).
20. Kemp, D.T. Stimulated acoustic emissions from within the human auditory system. *J Acoust Soc Am* **64**, 1386-91 (1978).
21. Manchaiah, V.K., Zhao, F., Danesh, A.A. & Duprey, R. The genetic basis of auditory neuropathy spectrum disorder (ANSD). *Int J Pediatr Otorhinolaryngol* **75**, 151-8 (2011).
22. Roux, I. *et al.* Otoferlin, defective in a human deafness form, is essential for exocytosis at the auditory ribbon synapse. *Cell* **127**, 277-89 (2006).
23. Johnson, C.P. & Chapman, E.R. Otoferlin is a calcium sensor that directly regulates SNARE-mediated membrane fusion. *J Cell Biol* **191**, 187-97 (2010).
24. Delmaghani, S. *et al.* Mutations in the gene encoding pejvakin, a newly identified protein of the afferent auditory pathway, cause DFNB59 auditory neuropathy. *Nat Genet* **38**, 770-8 (2006).
25. Schwander, M. *et al.* A forward genetics screen in mice identifies recessive deafness traits and reveals that pejvakin is essential for outer hair cell function. *J Neurosci* **27**, 2163-75 (2007).
26. Hashemzadeh Chaleshtori, M. *et al.* Novel mutations in the pejvakin gene are associated with autosomal recessive non-syndromic hearing loss in Iranian families. *Clin Genet* **72**, 261-3 (2007).
27. Starr, A. *et al.* A dominantly inherited progressive deafness affecting distal auditory nerve and hair cells. *J Assoc Res Otolaryngol* **5**, 411-26 (2004).
28. Kim, T.B. *et al.* A gene responsible for autosomal dominant auditory neuropathy (AUNA1) maps to 13q14-21. *J Med Genet* **41**, 872-6 (2004).
29. Wilson, B.S. & Dorman, M.F. Cochlear implants: current designs and future possibilities. *J Rehabil Res Dev* **45**, 695-730 (2008).
30. Pfingst, B.E. *et al.* Cochlear infrastructure for electrical hearing. *Hear Res* **281**, 65-73 (2011).
31. Shepherd, R.K. & Javel, E. Electrical stimulation of the auditory nerve. I. Correlation of physiological responses with cochlear status. *Hear Res* **108**, 112-44 (1997).
32. Lynch, E.D. *et al.* Nonsyndromic deafness DFNA1 associated with mutation of a human homolog of the Drosophila gene diaphanous. *Science* **278**, 1315-8 (1997).
33. Peng, J. *et al.* Myeloproliferative defects following targeting of the Drf1 gene encoding the mammalian diaphanous related formin mDia1. *Cancer Res* **67**, 7565-71 (2007).
34. Bione, S. *et al.* A human homologue of the Drosophila melanogaster diaphanous gene is disrupted in a patient with premature ovarian failure: evidence for conserved function in oogenesis and implications for human sterility. *Am J Hum Genet* **62**, 533-41 (1998).
35. Vorstman, J.A. *et al.* A double hit implicates DIAPH3 as an autism risk gene. *Mol Psychiatry* **16**, 442-51 (2011).

36. Castrillon, D.H. *et al.* Toward a molecular genetic analysis of spermatogenesis in Drosophila melanogaster: characterization of male-sterile mutants generated by single P element mutagenesis. *Genetics* **135**, 489-505 (1993).
37. Castrillon, D.H. & Wasserman, S.A. Diaphanous is required for cytokinesis in Drosophila and shares domains of similarity with the products of the limb deformity gene. *Development* **120**, 3367-77 (1994).
38. Li, F. & Higgs, H.N. The mouse Formin mDia1 is a potent actin nucleation factor regulated by autoinhibition. *Curr Biol* **13**, 1335-40 (2003).
39. Pring, M., Evangelista, M., Boone, C., Yang, C. & Zigmond, S.H. Mechanism of formin-induced nucleation of actin filaments. *Biochemistry* **42**, 486-96 (2003).
40. Zigmond, S.H. *et al.* Formin leaky cap allows elongation in the presence of tight capping proteins. *Curr Biol* **13**, 1820-3 (2003).
41. Bartolini, F. *et al.* The formin mDia2 stabilizes microtubules independently of its actin nucleation activity. *J Cell Biol* **181**, 523-36 (2008).
42. DeWard, A.D. & Alberts, A.S. Ubiquitin-mediated degradation of the formin mDia2 upon completion of cell division. *J Biol Chem* **284**, 20061-9 (2009).
43. Watanabe, S. *et al.* mDia2 induces the actin scaffold for the contractile ring and stabilizes its position during cytokinesis in NIH 3T3 cells. *Mol Biol Cell* **19**, 2328-38 (2008).
44. Wallar, B.J., Deward, A.D., Resau, J.H. & Alberts, A.S. RhoB and the mammalian Diaphanous-related formin mDia2 in endosome trafficking. *Exp Cell Res* **313**, 560-71 (2007).
45. Gupton, S.L., Eisenmann, K., Alberts, A.S. & Waterman-Storer, C.M. mDia2 regulates actin and focal adhesion dynamics and organization in the lamella for efficient epithelial cell migration. *J Cell Sci* **120**, 3475-87 (2007).
46. Yang, C. *et al.* Novel roles of formin mDia2 in lamellipodia and filopodia formation in motile cells. *PLoS Biol* **5**, e317 (2007).
47. Otomo, T., Otomo, C., Tomchick, D.R., Machius, M. & Rosen, M.K. Structural basis of Rho GTPase-mediated activation of the formin mDia1. *Mol Cell* **18**, 273-81 (2005).
48. Higgs, H.N. Formin proteins: a domain-based approach. *Trends Biochem Sci* **30**, 342-53 (2005).
49. Campellone, K.G. & Welch, M.D. A nucleator arms race: cellular control of actin assembly. *Nat Rev Mol Cell Biol* **11**, 237-51 (2010).
50. Chang, F., Drubin, D. & Nurse, P. cdc12p, a protein required for cytokinesis in fission yeast, is a component of the cell division ring and interacts with profilin. *J Cell Biol* **137**, 169-82 (1997).
51. Paul, A.S. & Pollard, T.D. The role of the FH1 domain and profilin in formin-mediated actin-filament elongation and nucleation. *Curr Biol* **18**, 9-19 (2008).
52. Neidt, E.M., Scott, B.J. & Kovar, D.R. Formin differentially utilizes profilin isoforms to rapidly assemble actin filaments. *J Biol Chem* **284**, 673-84 (2009).
53. Higashida, C. *et al.* Actin polymerization-driven molecular movement of mDia1 in living cells. *Science* **303**, 2007-10 (2004).
54. Paul, A.S. & Pollard, T.D. Review of the mechanism of processive actin filament elongation by formins. *Cell Motil Cytoskeleton* **66**, 606-17 (2009).

55. Cingolani, L.A. & Goda, Y. Actin in action: the interplay between the actin cytoskeleton and synaptic efficacy. *Nat Rev Neurosci* **9**, 344-56 (2008).
56. Dent, E.W., Merriam, E.B. & Hu, X. The dynamic cytoskeleton: backbone of dendritic spine plasticity. *Curr Opin Neurobiol* **21**, 175-81 (2011).
57. Flock, A., Cheung, H.C., Flock, B. & Utter, G. Three sets of actin filaments in sensory cells of the inner ear. Identification and functional orientation determined by gel electrophoresis, immunofluorescence and electron microscopy. *J Neurocytol* **10**, 133-47 (1981).
58. Muller, U. & Littlewood-Evans, A. Mechanisms that regulate mechanosensory hair cell differentiation. *Trends Cell Biol* **11**, 334-42 (2001).
59. Ruel, J. *et al.* Impairment of SLC17A8 encoding vesicular glutamate transporter-3, VGLUT3, underlies nonsyndromic deafness DFNA25 and inner hair cell dysfunction in null mice. *Am J Hum Genet* **83**, 278-92 (2008).
60. Deol, M.S. The inner ear in Bronx waltzer mice. *Acta Otolaryngol* **92**, 331-6 (1981).
61. Liberman, M.C., Tartaglini, E., Fleming, J.C. & Neufeld, E.J. Deletion of SLC19A2, the high affinity thiamine transporter, causes selective inner hair cell loss and an auditory neuropathy phenotype. *J Assoc Res Otolaryngol* **7**, 211-7 (2006).
62. Wake, M., Takeno, S., Ibrahim, D. & Harrison, R. Selective inner hair cell ototoxicity induced by carboplatin. *Laryngoscope* **104**, 488-93 (1994).
63. Schmiedt, R.A., Okamura, H.O., Lang, H. & Schulte, B.A. Ouabain application to the round window of the gerbil cochlea: a model of auditory neuropathy and apoptosis. *J Assoc Res Otolaryngol* **3**, 223-33 (2002).
64. Lang, H., Schulte, B.A. & Schmiedt, R.A. Ouabain induces apoptotic cell death in type I spiral ganglion neurons, but not type II neurons. *J Assoc Res Otolaryngol* **6**, 63-74 (2005).
65. Bellen, H.J., Tong, C. & Tsuda, H. 100 years of Drosophila research and its impact on vertebrate neuroscience: a history lesson for the future. *Nat Rev Neurosci* **11**, 514-22 (2010).
66. Bier, E. Drosophila, the golden bug, emerges as a tool for human genetics. *Nat Rev Genet* **6**, 9-23 (2005).
67. Muqit, M.M. & Feany, M.B. Modelling neurodegenerative diseases in Drosophila: a fruitful approach? *Nat Rev Neurosci* **3**, 237-43 (2002).
68. Cosetti, M. *et al.* Unique transgenic animal model for hereditary hearing loss. *Ann Otol Rhinol Laryngol* **117**, 827-33 (2008).
69. Todi, S.V., Franke, J.D., Kiehart, D.P. & Eberl, D.F. Myosin VIIA defects, which underlie the Usher 1B syndrome in humans, lead to deafness in Drosophila. *Curr Biol* **15**, 862-8 (2005).
70. Caldwell, J.C. & Eberl, D.F. Towards a molecular understanding of Drosophila hearing. *J Neurobiol* **53**, 172-89 (2002).
71. Kernan, M.J. Mechanotransduction and auditory transduction in Drosophila. *Pflugers Arch* **454**, 703-20 (2007).
72. Eberl, D.F. & Boekhoff-Falk, G. Development of Johnston's organ in Drosophila. *Int J Dev Biol* **51**, 679-87 (2007).

73. Boekhoff-Falk, G. Hearing in Drosophila: development of Johnston's organ and emerging parallels to vertebrate ear development. *Dev Dyn* **232**, 550-8 (2005).
74. Wallar, B.J. & Alberts, A.S. The formins: active scaffolds that remodel the cytoskeleton. *Trends Cell Biol* **13**, 435-46 (2003).
75. Katoh, K., Misawa, K., Kuma, K. & Miyata, T. MAFFT: a novel method for rapid multiple sequence alignment based on fast Fourier transform. *Nucleic Acids Res* **30**, 3059-66 (2002).
76. Staus, D.P., Blaker, A.L., Taylor, J.M. & Mack, C.P. Diaphanous 1 and 2 regulate smooth muscle cell differentiation by activating the myocardin-related transcription factors. *Arterioscler Thromb Vasc Biol* **27**, 478-86 (2007).
77. Prestridge, D.S. Predicting Pol II promoter sequences using transcription factor binding sites. *J Mol Biol* **249**, 923-32 (1995).
78. Grati, F.R. *et al.* Pure monosomy and pure trisomy of 13q21.2-31.1 consequent to a familial insertional translocation: exclusion of PCDH9 as the responsible gene for autosomal dominant auditory neuropathy (AUNA1). *Am J Med Genet A* **149A**, 906-13 (2009).
79. Letovsky, J. & Dynan, W.S. Measurement of the binding of transcription factor Sp1 to a single GC box recognition sequence. *Nucleic Acids Res* **17**, 2639-53 (1989).
80. Brand, A.H. & Perrimon, N. Targeted gene expression as a means of altering cell fates and generating dominant phenotypes. *Development* **118**, 401-15 (1993).
81. Somogyi, K. & Rorth, P. Evidence for tension-based regulation of Drosophila MAL and SRF during invasive cell migration. *Dev Cell* **7**, 85-93 (2004).
82. Kamikouchi, A., Shimada, T. & Ito, K. Comprehensive classification of the auditory sensory projections in the brain of the fruit fly Drosophila melanogaster. *J Comp Neurol* **499**, 317-56 (2006).
83. Sharma, Y., Cheung, U., Larsen, E.W. & Eberl, D.F. PPTGAL, a convenient Gal4 P-element vector for testing expression of enhancer fragments in drosophila. *Genesis* **34**, 115-8 (2002).
84. Kaczynski, J., Cook, T. & Urrutia, R. Sp1- and Kruppel-like transcription factors. *Genome Biol* **4**, 206 (2003).
85. Sgourou, A. *et al.* Thalassaemia mutations within the 5'UTR of the human beta-globin gene disrupt transcription. *Br J Haematol* **124**, 828-35 (2004).
86. Hudder, A. & Werner, R. Analysis of a Charcot-Marie-Tooth disease mutation reveals an essential internal ribosome entry site element in the connexin-32 gene. *J Biol Chem* **275**, 34586-91 (2000).
87. DeWard, A.D., Eisenmann, K.M., Matheson, S.F. & Alberts, A.S. The role of formins in human disease. *Biochim Biophys Acta* **1803**, 226-33 (2010).
88. Wilkie, A.O. The molecular basis of genetic dominance. *J Med Genet* **31**, 89-98 (1994).
89. Hilgert, N. *et al.* A splice-site mutation and overexpression of MYO6 cause a similar phenotype in two families with autosomal dominant hearing loss. *Eur J Hum Genet* **16**, 593-602 (2008).
90. Di Vizio, D. *et al.* Oncosome formation in prostate cancer: association with a region of frequent chromosomal deletion in metastatic disease. *Cancer Res* **69**, 5601-9 (2009).

91. Geiger, B., Spatz, J.P. & Bershadsky, A.D. Environmental sensing through focal adhesions. *Nat Rev Mol Cell Biol* **10**, 21-33 (2009).
92. Lai, S.L. *et al.* Diaphanous-related formin 2 and profilin I are required for gastrulation cell movements. *PLoS One* **3**, e3439 (2008).
93. Chesarone, M.A., DuPage, A.G. & Goode, B.L. Unleashing formins to remodel the actin and microtubule cytoskeletons. *Nat Rev Mol Cell Biol* **11**, 62-74 (2010).
94. Pawson, C., Eaton, B.A. & Davis, G.W. Formin-dependent synaptic growth: evidence that Dlar signals via Diaphanous to modulate synaptic actin and dynamic pioneer microtubules. *J Neurosci* **28**, 11111-23 (2008).
95. Kollmar, R. Who does the hair cell's 'do? Rho GTPases and hair-bundle morphogenesis. *Curr Opin Neurobiol* **9**, 394-8 (1999).
96. Lin, H.W., Schneider, M.E. & Kachar, B. When size matters: the dynamic regulation of stereocilia lengths. *Curr Opin Cell Biol* **17**, 55-61 (2005).
97. Spoendlin, H. Anatomy of cochlear innervation. *Am J Otolaryngol* **6**, 453-67 (1985).
98. Hotulainen, P. *et al.* Defining mechanisms of actin polymerization and depolymerization during dendritic spine morphogenesis. *J Cell Biol* **185**, 323-39 (2009).
99. Kamikouchi, A. *et al.* The neural basis of Drosophila gravity-sensing and hearing. *Nature* **458**, 165-71 (2009).
100. Yorozu, S. *et al.* Distinct sensory representations of wind and near-field sound in the Drosophila brain. *Nature* **458**, 201-5 (2009).
101. Varga, R. *et al.* Non-syndromic recessive auditory neuropathy is the result of mutations in the otoferlin (OTOF) gene. *J Med Genet* **40**, 45-50 (2003).
102. Yasunaga, S. *et al.* A mutation in OTOF, encoding otoferlin, a FER-1-like protein, causes DFNB9, a nonsyndromic form of deafness. *Nat Genet* **21**, 363-9 (1999).
103. Rodriguez-Ballesteros, M. *et al.* A multicenter study on the prevalence and spectrum of mutations in the otoferlin gene (OTOF) in subjects with nonsyndromic hearing impairment and auditory neuropathy. *Hum Mutat* **29**, 823-31 (2008).
104. Romanos, J. *et al.* Novel OTOF mutations in Brazilian patients with auditory neuropathy. *J Hum Genet* **54**, 382-5 (2009).
105. Starr, A. *et al.* Cochlear receptor (microphonic and summating potentials, otoacoustic emissions) and auditory pathway (auditory brain stem potentials) activity in auditory neuropathy. *Ear Hear* **22**, 91-9 (2001).
106. Schoen, C.J. *et al.* Increased activity of Diaphanous homolog 3 (DIAPH3)/diaphanous causes hearing defects in humans with auditory neuropathy and in Drosophila. *Proc Natl Acad Sci U S A* **107**, 13396-401 (2010).
107. Niwa, H., Yamamura, K. & Miyazaki, J. Efficient selection for high-expression transfectants with a novel eukaryotic vector. *Gene* **108**, 193-9 (1991).
108. Livak, K.J. & Schmittgen, T.D. Analysis of relative gene expression data using real-time quantitative PCR and the 2(-Delta Delta C(T)) Method. *Methods* **25**, 402-8 (2001).
109. Muller, M. & Smolders, J.W. Shift in the cochlear place-frequency map after noise damage in the mouse. *Neuroreport* **16**, 1183-7 (2005).

110. Schmitz, F., Konigstorfer, A. & Sudhof, T.C. RIBEYE, a component of synaptic ribbons: a protein's journey through evolution provides insight into synaptic ribbon function. *Neuron* **28**, 857-72 (2000).
111. Kujawa, S.G. & Liberman, M.C. Adding insult to injury: cochlear nerve degeneration after "temporary" noise-induced hearing loss. *J Neurosci* **29**, 14077-85 (2009).
112. Stamataki, S., Francis, H.W., Lehar, M., May, B.J. & Ryugo, D.K. Synaptic alterations at inner hair cells precede spiral ganglion cell loss in aging C57BL/6J mice. *Hear Res* **221**, 104-18 (2006).
113. Osborne, M.P. & Comis, S.D. Preparation of inner ear sensory hair bundles for high resolution scanning electron microscopy. *Scanning Microsc* **5**, 555-64 (1991).
114. Zheng, Q.Y., Johnson, K.R. & Erway, L.C. Assessment of hearing in 80 inbred strains of mice by ABR threshold analyses. *Hear Res* **130**, 94-107 (1999).
115. Taketo, M. *et al.* FVB/N: an inbred mouse strain preferable for transgenic analyses. *Proc Natl Acad Sci U S A* **88**, 2065-9 (1991).
116. Robertson, G. *et al.* Position-dependent variegation of globin transgene expression in mice. *Proc Natl Acad Sci U S A* **92**, 5371-5 (1995).
117. Garrick, D., Fiering, S., Martin, D.I. & Whitelaw, E. Repeat-induced gene silencing in mammals. *Nat Genet* **18**, 56-9 (1998).
118. Calero-Nieto, F.J., Bert, A.G. & Cockerill, P.N. Transcription-dependent silencing of inducible convergent transgenes in transgenic mice. *Epigenetics Chromatin* **3**, 3 (2010).
119. Liberman, M.C. Auditory-nerve response from cats raised in a low-noise chamber. *J Acoust Soc Am* **63**, 442-55 (1978).
120. Costalupes, J.A., Young, E.D. & Gibson, D.J. Effects of continuous noise backgrounds on rate response of auditory nerve fibers in cat. *J Neurophysiol* **51**, 1326-44 (1984).
121. Matsubara, A., Laake, J.H., Davanger, S., Usami, S. & Ottersen, O.P. Organization of AMPA receptor subunits at a glutamate synapse: a quantitative immunogold analysis of hair cell synapses in the rat organ of Corti. *J Neurosci* **16**, 4457-67 (1996).
122. Liberman, M.C. Chronic ultrastructural changes in acoustic trauma: serial-section reconstruction of stereocilia and cuticular plates. *Hear Res* **26**, 65-88 (1987).
123. Kelly, M. & Chen, P. Shaping the mammalian auditory sensory organ by the planar cell polarity pathway. *Int J Dev Biol* **51**, 535-47 (2007).
124. Liu, R., Linardopoulou, E.V., Osborn, G.E. & Parkhurst, S.M. Formins in development: orchestrating body plan origami. *Biochim Biophys Acta* **1803**, 207-25 (2010).
125. Jaeger, R.G., Fex, J. & Kachar, B. Structural basis for mechanical transduction in the frog vestibular sensory apparatus: II. The role of microtubules in the organization of the cuticular plate. *Hear Res* **77**, 207-15 (1994).
126. Hoogenraad, C.C. & Akhmanova, A. Dendritic spine plasticity: new regulatory roles of dynamic microtubules. *Neuroscientist* **16**, 650-61 (2010).

127. Tusher, V.G., Tibshirani, R. & Chu, G. Significance analysis of microarrays applied to the ionizing radiation response. *Proc Natl Acad Sci U S A* **98**, 5116-21 (2001).
128. Schmid, R. *et al.* Comparison of normalization methods for Illumina BeadChip HumanHT-12 v3. *BMC Genomics* **11**, 349 (2010).
129. Verkman, A.S. Aquaporins at a glance. *J Cell Sci* **124**, 2107-12 (2011).
130. Yool, A.J. Functional domains of aquaporin-1: keys to physiology, and targets for drug discovery. *Curr Pharm Des* **13**, 3212-21 (2007).
131. Sawada, S. *et al.* Aquaporin-1 (AQP1) is expressed in the stria vascularis of rat cochlea. *Hear Res* **181**, 15-9 (2003).
132. Li, J. & Verkman, A.S. Impaired hearing in mice lacking aquaporin-4 water channels. *J Biol Chem* **276**, 31233-7 (2001).
133. Leibovici, M. *et al.* Initial characterization of kinocilin, a protein of the hair cell kinocilium. *Hear Res* **203**, 144-53 (2005).
134. Vlastarakos, P.V., Nikolopoulos, T.P., Tavoulari, E., Papacharalambous, G. & Korres, S. Auditory neuropathy: endocochlear lesion or temporal processing impairment? Implications for diagnosis and management. *Int J Pediatr Otorhinolaryngol* **72**, 1135-50 (2008).
135. Shibata, S.B., Budenz, C.L., Bowling, S.A., Pfingst, B.E. & Raphael, Y. Nerve maintenance and regeneration in the damaged cochlea. *Hear Res* **281**, 56-64 (2011).
136. Self, T. *et al.* Role of myosin VI in the differentiation of cochlear hair cells. *Dev Biol* **214**, 331-41 (1999).
137. Roux, I. *et al.* Myosin VI is required for the proper maturation and function of inner hair cell ribbon synapses. *Hum Mol Genet* **18**, 4615-28 (2009).
138. Belyantseva, I.A. *et al.* Gamma-actin is required for cytoskeletal maintenance but not development. *Proc Natl Acad Sci U S A* **106**, 9703-8 (2009).
139. Perrin, B.J., Sonnemann, K.J. & Ervasti, J.M. beta-actin and gamma-actin are each dispensable for auditory hair cell development but required for Stereocilia maintenance. *PLoS Genet* **6**, e1001158 (2010).
140. Fetoni, A.R., Picciotti, P.M., Paludetti, G. & Troiani, D. Pathogenesis of presbycusis in animal models: a review. *Exp Gerontol* **46**, 413-25 (2011).
141. Erickson, R.P. Why isn't a mouse more like a man? *Trends Genet* **5**, 1-3 (1989).
142. Cheong, M.A. & Steel, K.P. Early development and degeneration of vestibular hair cells in bronx waltzer mutant mice. *Hear Res* **164**, 179-89 (2002).
143. Huang, W.Y., Aramburu, J., Douglas, P.S. & Izumo, S. Transgenic expression of green fluorescence protein can cause dilated cardiomyopathy. *Nat Med* **6**, 482-3 (2000).
144. Okabe, M., Ikawa, M., Kominami, K., Nakanishi, T. & Nishimune, Y. 'Green mice' as a source of ubiquitous green cells. *FEBS Lett* **407**, 313-9 (1997).
145. Buerger, A. *et al.* Dilated cardiomyopathy resulting from high-level myocardial expression of Cre-recombinase. *J Card Fail* **12**, 392-8 (2006).
146. Becker, A.E. & Caruso, G. Myocardial disarray. A critical review. *Br Heart J* **47**, 527-38 (1982).
147. Stefan, M. *et al.* Genetic mapping of putative Chrna7 and Luzp2 neuronal transcriptional enhancers due to impact of a transgene-insertion and 6.8 Mb

deletion in a mouse model of Prader-Willi and Angelman syndromes. *BMC Genomics* **6**, 157 (2005).
148. Palmiter, R.D. & Brinster, R.L. Germ-line transformation of mice. *Annu Rev Genet* **20**, 465-99 (1986).
149. Qin, Y. *et al.* Long-range activation of Sox9 in Odd Sex (Ods) mice. *Hum Mol Genet* **13**, 1213-8 (2004).